OPTIMIZATION OF NEXT GENERATION SOLAR-POWERED RADIO ACCESS NETWORKS

by

Turgay Pamuklu

B.S., Electronics Engineering, Istanbul Technical University, 2005

M.S., Computer Engineering, Istanbul Technical University, 2010

Submitted to the Institute for Graduate Studies in
Science and Engineering in partial fulfillment of
the requirements for the degree of
Doctor of Philosophy

Graduate Program in Computer Engineering

Boğaziçi University

2020

OPTIMIZATION OF NEXT GENERATION SOLAR-POWERED RADIO ACCESS NETWORKS

APPROVED BY:

DATE OF APPROVAL: 08.06.2020

ACKNOWLEDGEMENTS

I would like to express my sincere appreciation to my thesis supervisor, Cem Ersoy, who encouraged me in every step of my Ph.D. journey. His teachings lead me to deal with challenges like a professional. Without his wisdom and friendship, I could not carry this burden.

I especially thank Çiçek Çavdar; this work would not have been possible without her guidance. I would also like to express my deepest gratitude to my core jury members Mutlu Koca and Can Özturan, for their invaluable contributions over the years. I am also grateful to Gülfem Alptekin and Özlem Durmaz İncel for their participation in my thesis committee.

I wish to thank all members of CMPE family, especially colleagues from BM46 and BM47, with whom I shared ideas and experiences, and have become good friends with. Research and support facilities are essential for successful graduation. TETAM provides me this support, and I thank my whole heart to the founders of this crucial research center, especially Ufuk Çağlayan.

I wish to acknowledge the support and great love of my family and my lifelong friends. I would especially like to thank Ezgim and my brothers Turgut and Tuncay for sharing the many joyful and candid moments of my Ph.D. journey with me.

This thesis has been supported by the Turkish Directorate of Strategy and Budget under the TAM Project number 2007K12-873.

ABSTRACT

OPTIMIZATION OF NEXT GENERATION SOLAR-POWERED RADIO ACCESS NETWORKS

Due to the incontrovertible effects of global warming, society grows its sustainability awareness regularly, and governments start to change their energy policies to promote green energy sources. However, mobile network technologies have not been ready for new sustainable solutions. Besides, the high data demand in the next-generation radio access networks encourages mobile network operators to investigate cost-efficient solutions. Therefore, this thesis addresses the energy and cost optimization problems of a radio access network that uses the solar panels as an alternative energy source. We investigate several design problems from deployment and operation of solar-powered base stations in the third generation mobile communication networks to integrate the renewable energy sources into the function splitting, and Radio over Ethernet approaches in the fifth-generation centralized radio access networks. The proposed architectures are novel for their generations and offer remarkable guidance to the service providers to choose the proper size of renewable energy source equipment and how to operate this equipment to get the best energy and cost-efficiency. Besides, we provide both mixed-integer linear programming and heuristic solutions for different scales of problems. Also, we use real-world solar data and experiment with several instances to prove that our solutions can be implemented in the networks with different circumstances. Therefore, the operators can improve their profits and economic feasibility in their projected mobile communication networks while our proposed solutions reduce the energy consumptions and the carbon emission rates by promoting the use of renewable energy sources.

ÖZET

YENİ NESİL GÜNEŞ ENERJİLİ RADYO ERİŞİM AĞLARININ OPTİMİZASYONU

Global ısınmanın yadsınamaz etkileri, toplumun gün geçtikçe sürdürülebilirlik konusunda farkındalığını artırmakta ve hükümetlerin yeşil enerji politikalarını desteklemesini sağlamaktadır. Öte yandan mobil ağ teknolojileri için önerilen çözümler sürdürülebilirlik açısından yetersiz kalmaktadır. Bunun yanında, gelecek nesil radyo erişim ağlarının yüksek veri ihtiyacı mobil servis sağlayıcılarının maliyetlerini arttırmakta ve bu sağlayıcıları ekonomik çözüm arayışına itmektedir. Bu tezde, tüm bu ihtiyaçlara karşılık vermek için, güneş panellerinin alternatif enerji olarak kullanıldığı radyo erişim ağlarının enerji ve maliyet optimizasyonu problemlerine odaklanıldı. Bu problemler, üçüncü nesil mobil haberleşme teknolojilerindeki solar enerji beslemeli baz istasyonlarının kurulum ve operasyon aşamalarından, beşinci nesil merkezi mobil erişim ağlarındaki fonksiyon paylaştırma ve Ethernet üzerinden radyo yaklaşımlarıyla solar enerji kaynaklarının entegrasyonuna kadar geniş bir spektrumda yer almaktadır. Çözüm için önerilen mimariler nesillerine göre yenilikçi yaklaşımlar olup, mobil servis sağlayıcılarına enerji ve maliyet giderlerini azaltmaları için en uygun boyuttaki yenilenebilir enerji ekipmanlarını seçmelerini ve bunları işletmelerini sağlamaktadır. Bunun yanında çözümlerde gerçek güneş enerjisi verisi kullanılması ve birçok değişken koşulun test edilmesi, bu çözümlerin birbirinden farklı ağ ortamlarında kullanılmasına olanak vermektedir. Böylece, bu çözümler yenilenebilir enerji kaynaklarını kullanarak mobil ağlardaki enerji tüketimi ve karbon emisyon oranlarını azaltırken, bir yandan da servis sağlayıcıların karlarını arttırarak bu sistemlerin ekonomik uygulanabilirliğini sağlamaktadır.

TABLE OF CONTENTS

ACKNOWLEDGEMENTS iii
ABSTRACT iv
ÖZET v
LIST OF FIGURES ix
LIST OF TABLES xiii
LIST OF SYMBOLS xiv
LIST OF ACRONYMS/ABBREVIATIONS xvii
1. INTRODUCTION 1
1.1. Contributions 3
1.2. Thesis Outline 4
2. STATE OF THE ART 6
2.1. Energy-Efficient Base Station Deployment Strategies 6
2.2. Energy-Efficient Base Station Operating Methods 7
2.3. Studies on Renewable Energy Powered Base Stations 7
2.4. Function Splitting Methods in Centralized Radio Access Networks . . . 9
2.5. Radio Over Ethernet Meets Centralized Radio Access Networks 11
2.6. Embedding Renewable Energy in Centralized Radio Access Networks . 12
2.7. Total Cost of Ownership Oriented Approaches in Solar Powered Radio Access Networks 12
3. RENEWABLE ENERGY AWARE BASE STATION DEPLOYMENT IN A HETEROGENEOUS RADIO ACCESS NETWORK 14
3.1. Introduction 14
3.2. Green Base Station Deployment Problem 14
3.3. Methods for Energy-Efficient Deployment 18
3.4. Computational Experiments 21
3.5. Discussion 23
4. REDUCING THE TOTAL COST OWNERSHIP OF A THIRD GENERATION RADIO ACCESS NETWORK 24

4.1. Introduction 24
4.2. System Description 25
4.2.1. Traffic Model 26
4.2.2. Channel Model 28
4.2.3. Base Station Energy Consumption Model 30
4.2.4. Renewable Energy System Model 31
4.2.4.1. Solar Panel Model 32
4.2.4.2. Battery Model 33
4.3. Cost Optimization Problem of a HEBRAN 34
4.3.1. Problem Formulation 35
4.3.2. The Complexity Analysis 37
4.4. Proposed Algorithms for the Optimal Design and Operation of a HEBRAN 38
4.4.1. HEBRAN Framework 39
4.4.2. Sizing of Solar Panels and Batteries 41
4.4.3. Base Station Switch On/Off Algorithms 42
4.5. Computational Experiments 47
4.6. Discussion 56
5. REDUCING OPERATIONAL EXPENDITURE OF A HYBRID CLOUD RADIO ACCESS NETWORK 58
5.1. Introduction 58
5.2. Green Hybrid Cloud Radio Access Network Model 59
5.3. Green-Aware Function Splitting Optimization Problem 62
5.4. A Heuristic Approach for Green Energy-Aware Function Splitting Optimization Problem 65
5.5. Case Study and Results 71
5.6. Discussion 77
6. GROVE: RADIO OVER ETHERNET IMPLEMENTATION IN RADIO ACCESS NETWORKS 78
6.1. Introduction 78
6.2. GROVE System Model 79
6.3. Minimizing the Operational Expenditures in GROVE Model 82

6.3.1. Problem Formulation 82
6.3.2. Problem Linearization 85
6.3.3. Complexity Analysis 86
6.4. Computational Experiments 86
6.4.1. Evaluation Settings 86
6.4.2. Performance of Operational Expenditure Minimization 88
6.4.3. Network Scalability Analysis 91
6.4.4. Economic Feasibility Analysis 92
6.5. Discussion 95
7. CONCLUSION 97
REFERENCES 100

LIST OF FIGURES

Figure 3.1. User distribution in a time interval. 15

Figure 3.2. Step 1: Greedy algorithm for choosing the locations of new micro BSs. 19

Figure 3.3. Step 2: Aggregation of BSs at the non-adjacent time intervals. . . 19

Figure 3.4. Step 3: CoM algorithm to decrease the number of BSs. 20

Figure 3.5. Increase in ASE with the transmission power. 22

Figure 3.6. Amount of on-grid energy consumption for extra ASE. 23

Figure 4.1. HEBRAN system model. 24

Figure 4.2. Five different data traffic patterns in a day period. 26

Figure 4.3. The traffic rate of our covered sector in a day period. 27

Figure 4.4. The traffic rate of our covered sector in a week period. 29

Figure 4.5. HEBRAN energy model. 30

Figure 4.6. Distribution of harvested solar radiation in a day period. 31

Figure 4.7. Distribution of harvested solar radiation in a year period. 32

Figure 4.8. HEBRAN solution framework. 39

Figure 4.9. Sizing Algorithms: Main algorithm. 40

Figure 4.10. Sizing Algorithms: ISSP algorithm. 42

Figure 4.11. Sizing Algorithms: ISB algorithm. 43

Figure 4.12. BS switch on/off algorithms: Battery-aware algorithm. 44

Figure 4.13. BS switch on/off algorithms: Hybrid algorithm. 46

Figure 4.14. Assignment decisions of hybrid algorithm. 47

Figure 4.15. The distribution of BSs in different traffic rates. 48

Figure 4.16. Solar radiation and traffic rates impact on online algorithms. . . . 50

Figure 4.17. Comparison of online algorithms in different configurations. 51

Figure 4.18. Instance based comparison of traffic aware and hybrid algorithms. 51

Figure 4.19. Comparison of online algorithms in a day period. 52

Figure 4.20. Comparison of online algorithms in a year period 52

Figure 4.21. Comparison of the TCO with Gurobi solution. 54

Figure 4.22. Instance based comparison of the TCO with Gurobi solution. . . . 54

Figure 4.23. Comparison of the TCO in different solar radiations. 55

Figure 4.24. Comparison of the TCO in different traffic rates. 55

Figure 5.1. Green hybrid C-RAN system model. 58

Figure 5.2. Splitting options of green hybrid C-RAN system. 60

Figure 5.3. Green hybrid C-RAN energy model. 62

Figure 5.4. Heuristic: Main algorithm. 65

Figure 5.5. Heuristic: Initial user assignment to ECs. 66

Figure 5.6. Heuristic: Cost-efficient RES usage in a cloud. 67

Figure 5.7. Heuristic: User offloading decision from ECs to CC. 68

Figure 5.8. Heuristic: User offloading operation from ECs to CC. 69

Figure 5.9. Heuristic: User migration decision between the ECs and CC. . . . 70

Figure 5.10. Comparing the performance of the methods. 72

Figure 5.11. Average remaining energy in the batteries of ECs and CC. 73

Figure 5.12. Number of active DUs in each cloud in a day period. 74

Figure 5.13. Distribution of renewable energy consumption in a year period. . . 75

Figure 5.14. Distribution of the sold energy in a year period. 76

Figure 5.15. The Cost of a pure grid and a renewable system in lifetime period. 77

Figure 6.1. GROVE: Green Radio over Ethernet system architecture. 80

Figure 6.2. Function Splitting Options in GROVE System Model. 82

Figure 6.3. The Use case network topology. 87

Figure 6.4. Operational costs in different traffic loads and solar radiations. . . 88

Figure 6.5. Remaining energy in ECs and CC in a year period. 89

Figure 6.6. Number of active DUs in a day period in CC and ECs 90

Figure 6.7. Unstored energy in ECs and CC in a day period. 90

Figure 6.8. Remaining energy in the CC and ECs in a day period. 91

Figure 6.9. Analysis of network scalability: Topologies. 92

Figure 6.10. Analysis of network scalability: OpEx and memory consumptions. 93

Figure 6.11. Analysis of RoC 93

LIST OF TABLES

Table 3.1. BS deployment problem experiment parameters. 21

Table 3.2. BS deployment channel model parameters. 21

Table 3.3. Energy consumptions of full and split combinations. 21

Table 4.1. HEBRAN test configurations. 48

Table 4.2. HEBRAN experiment parameters. 48

Table 4.3. HEBRAN channel model parameters. 49

Table 5.1. Green hybrid C-RAN experiment parameters. 71

Table 6.1. GROVE experiment parameters. 88

LIST OF SYMBOLS

$\mathcal{A}$	area spectral efficiency
$\mathcal{A}_{min}$	minimum area spectral efficiency threshold
a_{dt}	whether DU d is active
b_{it}^{SITE}	remaining renewable energy (SITE is BS, EC or CC)
BW_i	bandwidth allocated to the BS i
$c \in \mathcal{C}$	set of remote radio heads
c^E	energy price ($/kWh)
c^S	unit cost of a solar panel ($/kWh)
c^B	unit cost of a battery ($/2.5kWh)
$d \in \mathcal{D}^{SITE}$	set of Digital Units
$dist_0$	referenced distance for path loss calculation
$dist_{ij}$	distance between i and j
$e \in \mathcal{E}$	set of edges in GROVE Model, $e = (x, y) \in \mathcal{V}^2$
E_i^{BS}	total energy consumption of BS i (kWh)
E_i^{BSD}	dynamic energy consumption of BS i (kWh)
E_i^{BSG}	grid energy consumption of BS i (kWh)
E_i^{BSS}	static energy consumption of BS i (kWh)
E_t^{CC}	total energy consumption of a CC
E^{CCD}	energy consumption of a DU in CC
E^{CCS}	static energy consumption of a CC
E_{rt}^{EC}	total energy consumption of a EC
E^{ECD}	energy consumption of a DU in EC
E^{ECS}	static energy consumption of a EC
$f \in \mathcal{F}$	set of URFs
$f_z(t)$	daily traffic profile
G_t^{reg}	regeneration ratio of renewable energy
G_t^{SITE}	generated renewable energy in a time interval

$H_j^z(.)(t)$	precalculated function which maps the j^{th} location to the z^{th} traffic profile
$i \in \mathcal{I}$	set of BSs
$j \in \mathcal{J}$	set of user locations
l_{rte}	transmission flows to EC r on edge e
L_{ij}	path loss between BS i and location j
L^{EXP}	path loss exponent
L^{REF}	referenced path loss
L^{SHA}	shadowing effect in path loss calculation
MC	Maintenance Cost
m_{jdft}	whether URF f of user j is hosted in DU d
$n_{(t)}$	noise for traffic profile
p_{rt}^{SITE}	amount of sold energy
P_{ij}^{rx}	received power at location j from BS i (kW)
P_{min}^{rx}	minimum received power threshold
P_i^{tx}	transmission power of BS i (kW)
Pr_j	normalized rate of users in location j
$r \in \mathcal{R}$	set of ECs
S_{ij}^{BS}	service rate of BS i to location j
s_{it}^{BS}	green energy consumption ratio in BS i
s_{rt}^{CC}	green energy consumption in CC r
s_{rt}^{EC}	green energy consumption in EC r
$t \in \mathcal{T}$	set of discrete time intervals
u^B	unit capacity of a battery ($2.5kWh$)
U_{jt}^{BS}	data traffic demand of location j
U_{jt}^{EC}	traffic load ratio
$v \in \mathcal{V}$	set of nodes in GROVE Model
w_{it}	BS on/off decision ($w_{it} \in \{0, 1\}$)
z_{ijt}	user - BS assigning decision ($z_{ijt} \in \{0, 1\}$)
α_i^{SITE}	solar panel size

β_i^{SITE}	battery size
δ_{jt}	delay threshold of user j
Γ_{ij}	SNR/SINR from BS i to location j
κ	peak hour traffic value
$\lambda(j,t)$	mean arrival rate of the location j
Λ^{SITE}	DU function capacity
$\mu(j,t)$	mean requested data size of the location j
ν	abruptness of the traffic profile
ω_{ej}	bandwidth usage of j on edge e
Ω_e	bandwidth capacity of edge (link) e
Ψ	sold energy penalty ratio
ρ	utilization bound of a BS
σ^2	Gaussian Noise
φ	a random value between $3\pi/4$ and $7\pi/4$

LIST OF ACRONYMS/ABBREVIATIONS

5G	Fifth-Generation
ASE	Area Spectral efficiency
BBU	Baseband Unit
BS	Base Station
CapEx	Capital Expenditure
CC	Center Cloud
CO_2	Carbon Dioxide
CoM	Center of Mass
CoMP	Coordinated Multi-Point
CPU	Central Processing Unit
C-RAN	Centralized/Cloud-Radio Access Network
CRF	Cell Related Function
DU	Digital Unit
EC	Edge Cloud
eNB	User-Evolved-Node-B
EPDK	Republic of Turkey Energy Market Regulatory Authorities
FEC	Forward Error Correction
GOPS	Giga Operations per Second
GROVE	Green Radio over Ethernet
HEBRAN	Hybrid Energy Based Radio Access Network
Hz	Hertz
ISB	Increasing size of batteries algorithm
ISSP	Increasing size of solar panels algorithm
IEEE	Institute of Electrical and Electronics Engineers
ITU-R	International Telecommunication Union Radiocommunication Sector
km	kilometer
kWh	kilowatt-hour

MAC	Medium Access Control
MILP	Mixed-Integer Linear Programming
MNO	Mobile Network Operator
NLOS	Non-line-of-sight
NP-Hard	Non-Deterministic Polynomial-Time Hard
OpEx	Operational Expenditure
PDCP	Packet Data Convergence Protocol
PRB	Physical Resource Blocks
QAM	Quadrature Amplitude Modulation
QoS	Quality of Service
RAM	Random-Access Memory
RAN	Radio Access Network
RES	Renewable Energy Sources
RLC	Radio Link Control
RoC	Return of Capital
RoE	Radio over Ethernet
RRH	Remote Radio Head
sec	second
SNR	Signal Noise Ratio
TCO	Total Cost of Ownership
TRY	Turkish Lira
URF	User Related Function
W	Watt

1. INTRODUCTION

Global warming is an inevitable physical phenomenon, and a lot of evidence shows that reasons for global warming in the last century are highly originated by humankind. For example, carbon dioxide (CO_2) is the most critical greenhouse gas causing global warming and is closely related to using fossil fuels by humans [1]. Doubling rates of CO_2 raises the temperature almost 6 $^{\circ}C$ which results in that our planet's temperature has approximately increased by 2 $^{\circ}C$ due to fossil fuels [2]. The effect of increasing temperature has already been started to show in some areas of our planet, which would get worse if we could not stop this inevitable climate change [3]. The other drawback of fossil fuels is that they will assume to deplete in the next sixty years except for the hard coal and lignite resources. Nuclear power is not an alternative energy source because uranium will be depleted in the next fifty years [2].

Another significant disadvantage of using fossil fuels comes from increasing energy costs. The prices of on-grid energy may increase dramatically in the following years because power plants usually depend on fossil fuel resources [4]. Therefore economic and environmental problems lead to a renewed interest in related research to reduce the consumption of fossil fuels and on-grid electricity in many different areas. The radio access network (RAN) researchers are not an exception; they are also motivated to explore energy-efficient solutions to reduce on-grid energy consumption.

While developing energy-efficient mobile equipment is studied well to increase the battery performance, the base stations (BSs) are consuming 60-80% of the energy of the cellular networks [5]. Thus, the studies should aim to optimize BSs for the overall energy efficiency of a RAN. Meanwhile, the mobile network operators (MNOs) are the most responsible stakeholders for the BS technological development and they are for-profit organizations. For that reason, the proposed solutions to develop energy-efficient BSs should also be cost-efficient [6].

There are many different approaches to develop cost-efficient solutions for cellular networks. Some researchers focus on deployment and planning optimizations to reduce the capital expenditure (CapEx) of an MNO. Others aim energy-efficient operation of BSs such as well-known switch on/off technique to reduce the operational expenditure (OpEx). Meanwhile, adopting renewable energy powered BSs is also one of the promising methods for the next generation RANs for energy efficiency [7]. Moreover, the pricing trends of solar panels and lithium-ion batteries provide extra support for using renewable energy sources (RESs) in a RAN [8, 9]. However, a system-wide solution needs to merge all of these approaches to reduce the total cost of ownership (TCO) of an MNO for economic feasibility.

The high data demand for future fifth-generation mobile communication (5G) networks also promotes cost-efficient research for the BSs. Centralized/Cloud-Radio Access Network (C-RAN) is a well-known architecture for this goal. This architecture has several benefits, such as energy-efficiency and ease of maintenance due to the centralization of the baseband units (BBUs) in a centralized cloud (CC). Thus, an MNO reduces its OpEx, which increases annually as a result of the increasing amount of BSs [10]. On the other hand, increasing end-to-end delay and high-bandwidth requirement in optical fronthaul links between remote radio heads (RRHs) and CC make this architecture infeasible and uneconomical and calls for novel solutions [11]. One of the solutions introduces the edge-cloud (EC) layers before the CC layer to keep resources closer to the RRHs. Then, split the BBU functions between the CC and ECs to reduce the fronthaul bandwidth requirement and to relax the stringent end-to-end delay requirements. Briefly, this method is a tradeoff between energy-efficiency and reducing the delay and bandwidth requirements by choosing the weight of centralization [12].

Another next-generation strategy for energy-efficiency is the Radio over Ethernet (RoE), in which the radio traffic between an EC and the CC is encapsulated in Ethernet frames on a multihop mesh network topology [13]. This approach is more cost-efficient by using the advantage of aggregating the traffic of different ECs in the same network lines. Moreover, this network topology may also be integrated with the backhaul

network for additional cost-efficiency [14]. On the other hand, the RoE approach complicates the function splitting problem; thus, extra efforts and joint optimization methods are needed to provide cost-efficient solutions [15].

1.1. Contributions

In this thesis, we focus on energy and cost optimization problems of solar-powered BSs. We investigate several design problems from the deployment and operation of BSs in a packet-switched network to energy-efficient function splitting, and RoE approaches in a 5G C-RAN. The contributions and novelties of this thesis are detailed as follows:

(i) A Novel BS deployment methodology that promotes the usage of RES in a cellular network is described briefly.

(ii) We provide a system-wide solution to reduce the TCO of a packet-switched cellular network, which is called hybrid energy based radio access network (HEBRAN).

(iii) The CC, ECs, and BSs in our network models have two energy sources complementing each other. The RES reduces the electrical grid energy consumption, and the electrical grid provides the energy demand in the case of the lack of insufficient renewable energy. This thesis is a guide for using these two types of energy sources together with an economic perspective.

(iv) Our findings confirm that using RES for RANs in an urban region is as efficient as using them in a rural area. We provide several cost-feasibility studies that may encourage the MNOs to consider the RES systems in their projected plans.

(v) One of our studies merges the RES and the hybrid C-RAN architecture. Then we propose a joint approach that is more economical than the examples in the current literature. This study is one of the pioneer examples in this research area.

(vi) Our Green Radio OVer Ethernet (GROVE) model is a novel concept that improves the economic aspect of a hybrid C-RAN architecture for an MNO. Therefore, our solutions provide not only green solutions that reduce the carbon emission rates but also present cost-effective experimental results that encourage an MNO to implement them in future projects.

(vii) We provide both mixed-integer linear programming (MILP) and heuristic solutions. One solution may perform better than the other, which depends on the size of the problem. Thus, an MNO prefers any one of the solutions by considering its corresponding network size.

(viii) The real-world solar data from four different geographical areas are used in the experiments. We performed these experiments for a year to see the effect of seasonal changes. Thus, we demonstrate the performance of our methods in different locations with significantly different solar radiation patterns.

(ix) We provide the results of different instances, such as traffic rate, to show the effect of various factors on our proposed solutions. Consequently, it is proved that these solutions can be implemented in the networks with different circumstances.

(x) Our cost feasibility analyses for different architectures offer guidance to the MNOs to choose the proper size of solar panels and the batteries in their networks to reduce their CapEx and OpEx.

1.2. Thesis Outline

Chapter 2 provides an overview of the existing literature on solutions targeting the energy and cost efficiency for RANs.

Chapter 3 describes a deployment problem, in which an MNO chooses the optimum places to deploy BSs by considering the RESs. Furthermore, we evaluate the performance of the transmission power changes of BSs on the area spectral efficiency (ASE).

Chapter 4 details another problem in which the BSs are already deployed in an urban area as a given topology. Then, we focus on finding the proper size of solar panels and the batteries in this system. We also focus on the operating problem of this topology and try to promote the use of solar energy to reduce the electrical grid energy consumption.

Chapter 5 introduces a new type of green RAN architecture called C-RAN. Then, the chapter addresses a cost-efficiency problem for this next-generation network. We provide both MILP and heuristic solutions, in which we use RESs to improve the cost-efficiency in this architecture.

Chapter 6 enhances the problem in the previous chapter with the addition of packet-switching network optimization. Thus, we propose a more economical network topology for C-RAN. Then, we linearize the quadratic constraints of this more complex topology and present encouraging solutions for MNOs to implement RESs systems in their next-generation RANs.

Chapter 7 concludes the thesis with an overall discussion of the contributions.

2. STATE OF THE ART

In this chapter, we present an overview of the existing approaches for energy and cost-efficient solutions for RAN.

2.1. Energy-Efficient Base Station Deployment Strategies

To decrease energy consumption, one of the proposed solutions is improving BS deployment strategies. Therefore, acceptable performance in the form of spectral efficiency and coverage can be provided by consuming less energy [16]. To decrease energy consumption by a deployment strategy, Badic et al. emphasize the effects of cell size on energy consumption [17]. They stated that bringing the BS closer to users increases energy efficiency. Then they create a case study to calculate the effect of cell sizes, which is a classical hexagonal deployment. Firstly, they calculate the energy consumption of a BS with a $1km$ range. Then they start to reduce this range and add new BSs which cover the holes between the old BSs. They found that the performance gets better with a short-range between the BS and users, which indicates that small cell deployment is preferable for energy efficiency. On the other hand, they do not consider the embodied energy, which is a very significant value of the total BS energy consumption [5].

In the paper of the Richter et al., micro BSs are deployed at the edges of macrocells, where the received signal strength is at the lowest value [16]. Therefore they can increase ASE value as much as possible. Moreover, with their solutions, the macrocell transmission power can be reduced to increase energy efficiency. Son et al. proposed a novel deployment strategy for the peak-time usage where microcells are used to incrementally increase spectral efficiency and coverage beyond the initial deployment of macrocells [18]. They use a greedy algorithm that adding micro BSs (microcells) in an order which considers the amount of increasing ASE. They stop adding microcells when they reach the desired ASE value. Therefore they provide acceptable performance with

a minimum number of microcells that contribute less carbon emission rates.

2.2. Energy-Efficient Base Station Operating Methods

A considerable amount of these studies focus on providing a more energy-efficient operating method for the BSs when they aim to achieve reducing the energy consumption in a RAN. They have two meaningful motivations: the BSs in a RAN form the primary source (60-80%) of the energy consumption [5], and they are under-utilized during most of their operating time. Improvement efforts usually take advantage of data traffic changes in time [19]. Some of the researchers adapt the transmission power of the BSs by the traffic variation, called cell-breathing. For example, Yigitel et al. propose the FastWISE algorithm, in which they increase the power level of the BSs in their network step by step to provide the minimum coverage constraint [20]. The most crucial part is that they perform this operation for different time intervals of a day to benefit from traffic variations in a day.

Another approach prefers selectively switching off the BSs according to the traffic fluctuations. For example, Yildiz et al. propose a price-based algorithm for assigning the users to the BSs [21]. In this algorithm, they serve the users with fewer BSs than the classic nearest BS assignment algorithm. Therefore they can reduce the overall energy consumption in their network. Zhang et al. highlight the importance of the spatial differences of the user traffic demands [22]. They proposed two BS clustering algorithms, which also consider the spatial changes to reduce the number of active BS in their experimental network.

2.3. Studies on Renewable Energy Powered Base Stations

Although using RESs in a RAN is a new concept, there has been a significant amount of studies focusing on the problems of this new kind of network. In one of the early research, Carreno et al. analyze a single BS system that can change its coverage area with the amount of renewable energy in this BS [23]. The critical results in this

study show a cross-correlation between user satisfaction and the ratio of the renewable energy used in this BS. Fan et al. prove that the amount of harvested renewable energy at a BSs should be considered while the users are assigned to this BS [24]. Therefore, the total on-grid energy consumption in a RAN can be reduced more than the standard best SINR assignment method.

Some studies focus on cost-effective energy sharing between the BSs by using the smart-grid architecture. Chen et al. present one of the first energy sharing applications in which two BSs share their harvested energy among each other with a resistive loss [25]. Farooq et al. provide a cost optimization methodology for the direct power line construction between the BSs while these BSs can share their excessive renewable energy by using a smart-grid interface [26]. They are also interested in how to operate these two different connection lines together in a cost-effective way. Sheng et al. introduce a grid energy minimization problem for a network in which BSs may perform energy transmissions among each other. Then they provide centralized and distributed algorithms to solve this NP-Hard problem [27]. Ahmed et al. show that energy sharing is a non-convex problem and linearizes this problem to solve it with the interior point method [28]. Lastly, Lee et al. introduce a ski rental pricing method to solve their BS on/off scheduling problem and reduce the total cost of their studied network [29].

Chiang et al. minimize a multi-objective function which combines the on-grid energy consumption and user satisfaction according to their demand [30]. For this purpose, they implement Lyapunov optimization to handle temporal-coupling due to their renewable energy storage system property, and then they proposed an algorithm for a feasible optimal solution.

Zhang et al. consider renewable energy usage to the millimeter-wave-based ultra-dense networks [31]. They propose a load-aware algorithm for user and BS assignment by considering the energy harvesting of BSs. In another study, they use game theory for this assignment and the power allocation problem. Besides, their pricing mechanism deals with both cross-tier and co-tier interferences between the BSs and favors the

energy harvesting revenue [32]. In another study, researchers use the pricing method for the fairness between the BSs while they distribute the excessive harvested renewable energy between these BSs [33]. Han et al. demonstrate that operating a system with hybrid energy sources is an NP-hard problem, and they decompose this problem into two subproblems to handle the complexity. In the first subproblem, they aim to optimize the allocation of green energy (which is generated by a solar panel) to each time interval for each BS. In the second subproblem, they change the transmission power of the BSs in each time interval by considering the allocated green energy from the first subproblem. Therefore they use the generated green energy more efficiently to reduce the overall energy consumption [34].

2.4. Function Splitting Methods in Centralized Radio Access Networks

One of the key performance metrics of a C-RAN architecture is the multiplexing gain that comes from centralizing the BBU functions in a CC. Thus, we can get rid of the unnecessary energy consumption of underutilized BBUs originate from low traffic loads. Checko et al. advance the multiplexing gain analysis by investigating it for function splitting approaches [35]. They form their proposed architecture in two ways: an N-dimensional Markovian process model and a discrete event simulation model. Then, for each model, they provide the impact of different splitting decisions on the quantitative multiplexing gain results, in terms of energy and cost minimization. Wang et al. introduce a new approach to the function splitting concept, in which some of the functions are processed in an EC as an alternative to the CC [36]. In this architecture, the ECs may serve more than one RRHs to increase the Quality of Service (QoS). They call this architecture "Hybrid C-RAN", and their objective is jointly minimizing the total energy consumption in the network and the bandwidth of the midhaul, which provides the connections between the CC and ECs. Also, in an additional study, they focus on the end-to-end latency of this type of architecture by adding it as a constraint in their problem [37]. Then, they enhance their studies by analyzing the effect of traffic load on their findings [38].

Some studies prefer to model the function splitting problem as a graph, in which the BBU functions are represented as nodes, and the connections between these nodes are shown as weighted edges. Mharsi et al. choose the weight of the edges as the latency requirement. The start nodes of their graph are the antennas, and the end node is the CC. Thus, they perform the splitting decisions for all data flows between the antennas and the core node in their studied network. They have a multi-objective function that jointly minimizes the sum of the end-to-end latencies and the total number of Central Processing Units (CPUs) used in their proposed network [39]. Meanwhile, Liu et al. choose more than one metric for the weight of the edges, which are the computational costs and the fronthaul link costs. Then they characterize the tradeoff between these two parameters while choosing the delay as a constraint in their problem formulation [40].

Shehata et al. focus on static function splitting options. They investigate the effect of these options on reducing the energy consumption and the needed Giga Operations per Second (GOPS) in the network. They detail the difference between the local BBU architecture and BBU pool in C-RAN. They also explain the layers that processed in these BBUs and the impact of several split options between these layers. Their analytical model starts with User-Evolved-Node-B (eNB) assignment according to the highest received signal strength indication at the user side. Next, they schedule the physical resource blocks (PRBs) among the users. Then, they provide a detailed energy consumption model of BBUs in a classical distributed-RAN and a C-RAN. Their experiments demonstrate the incrementation of the system performance in each split option for different geographical type areas [41]. Harutyunyan et al. suggest a virtual network embedding (VNE) approach in their papers for the purpose of finding the optimum place for splitting the BBU functions. In their first study, they formulate a problem in which they jointly minimize the interference and the fronthaul bandwidth [42]. In their second study, they combine the problem of choosing the optimum places for the BBU functions with minimizing the number of using millimeter-wave wireless fronthaul links in this VNE model [43].

2.5. Radio Over Ethernet Meets Centralized Radio Access Networks

RoE approach reduces not only the operating costs but also the planning costs of an MNO. Thus, several recent studies implement this approach to the function splitting problem to improve the feasibility of their proposed models. Garcia-Saavedra et al. present a decision-making engine, called Wizhaul, that jointly choose the flow paths and the weight of the function centralization in a CC. By using this engine, they provide solutions for both network planning and operating phases [15]. In another recent paper, they also implement the multi-access edge computing design in their problem models. These studies are promising guides to integrate the RoE with the function splitting to improve the edge computing performance in a C-RAN [10, 44]. Meanwhile, they provide a detailed analysis of the crosshaul approach in a separate study. This approach combines the fronthaul and backhaul networks as a joint packet-based network to reduce the network costs further [14].

Chang et al. focus on three inter-related problems in an RoE network. The first problem aims to packetize the BBU processed data in Ethernet frames according to choosing the function splitting decisions. The second one deals with the scheduling of these frames, and the last one ensures a HARQ-based timing constraint while providing the first and second problems [45]. In their next paper, they specify a detailed key performance analysis of several indicators, such as the network throughput and user satisfaction [46]. Ojaghi et al. highlight the importance of network slicing to improve throughput. They combine it with RoE connections and target to optimize the computational cost and the throughput of the whole network [47]. Diez et al. aim to minimize the total end-to-end latency in their packet-based network by providing a connection for each RRH. They compare their solution with the fixed split and fixed scheduling approaches [48].

2.6. Embedding Renewable Energy in Centralized Radio Access Networks

Using RESs as an alternative to the on-grid energy in a C-RAN architecture is another promising approach to reduce the OpEx of an MNO. Alameer et al. present a RES queuing model in a C-RAN architecture. They deploy RES in each RRHs and BBUs and focus on minimizing the overall energy consumption by considering the QoS [49]. Guo et al. focus on a similar problem, in which they represent the system as an MINLP problem. They propose a two-phase heuristic to reduce the brown energy consumption [50].

Although the function splitting is a new concept, Temesgene et al. integrates the RESs in this concept and provide a detailed energy consumption analysis in this system. They propose a solution for an offline problem to reduce the on-grid energy consumption [51]. In their next study, they enhance this study and provide a solution for an online problem that dynamically changes the splitting decisions according to the traffic load and the harvested energy [52]. Meanwhile, Wang et al. propose a novel model to maximize the throughput of the network by solving the function splitting problem with RESs [53]. On the contrary, Ko et al. choose the throughput as a constraint in their problem. Then they target to reduce the overall on-grid energy consumption in the network by using RESs [54].

2.7. Total Cost of Ownership Oriented Approaches in Solar Powered Radio Access Networks

There are relatively few TCO researches in the area of RAN with RES. In one of the earliest studies, Zheng et al. formulate an optimization problem in which they try to minimize the TCO. Their TCO includes the total installation, connection, and electrical grid costs. They consider both effective renewable energy usage and balancing the energy between the BSs [55]. In a broader study, Han et al. focus on a heterogeneous network where small-cell BSes are powered by on-grid energy, and macro-cell BSes are powered by both on-grid and renewable energy. In this network, they aim to try to

minimize the solar panel and battery sizes at the macro-cell BSes as much as possible while achieving a sufficient QoS for the users [56]. In their other work, Han et al. propose a similar solution, but they offload the traffic from the pure renewable energy-powered small-cell BSes to the pure on-grid energy-powered macro-cell BSs [57].

Wang et al. contribute a TCO study for the function splitting approach in a C-RAN architecture. First, they calculate the GOPS and needed midhaul bandwidth values for each function splitting option. Then, they propose a TCO minimization problem, which includes not only CapEx items such as equipment, civil work costs, but also OpEx items such as maintenance and electrical bills. Their findings show that function splitting C-RAN is more economical than the classical Distributed RAN [58].

3. RENEWABLE ENERGY AWARE BASE STATION DEPLOYMENT IN A HETEROGENEOUS RADIO ACCESS NETWORK

3.1. Introduction

The main subject of this chapter is the energy-efficient deployment of micro BSs with RES. Thus, we have to investigate both heterogeneous deployments of BSs and to use of RESs in a RAN. First, we deploy the micro BSs on an area where an MNO already deploys macro BSs; then, we try to use the RESs on the BSs efficiently to reduce the on-grid electricity and carbon emission rates. Finally, we modify the transmission power of micro BSs to increase the ASE. Results justify that the solution proposed in this chapter reduces the carbon emission rates and decreasing the expenditures of an MNO significantly while sustaining acceptable performance in the form of ASE and coverage.

The remainder of this chapter is organized as follows. In Section 3.2, we define the problem, constraints, and objective function. In Section 3.3, we explain our methods for energy-efficient deployment. In Section 3.4, we provide the simulation setup and the results of our methods, and in Section 3.5, we conclude the chapter. This study was also presented in the IEEE GreenCom conference [59].

3.2. Green Base Station Deployment Problem

In this section, we define a problem for decreasing the energy consumption of a RAN by efficiently deploying BSs considering the coverage and ASE. We represent the deployment area as a collection of discrete locations with different user densities, as shown in Figure 3.1. These densities may change during the different time intervals of the day. The set of these locations and the set of deployed BSs are defined as $j \in \mathcal{J}$ and $i \in \mathcal{I}$, respectively.

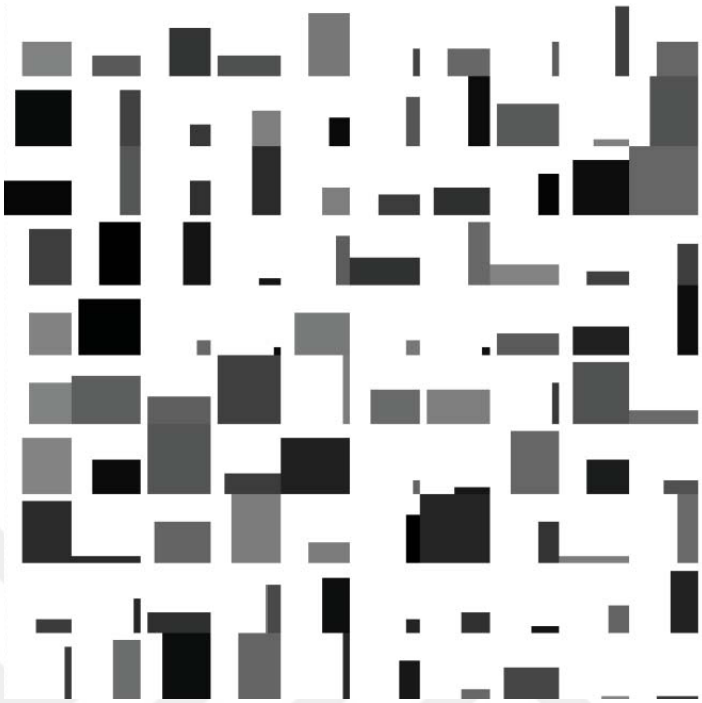


Figure 3.1. User distribution in a time interval.

We use a simplified path-loss model to calculate the received power, which is required to calculate our coverage and QoS constraints. The received power in a user location in the path-loss model is defined in Equation 3.1. In this formula, P_{ij}^{rx} is the received signal power at location j from BS i, and P_i^{tx} is the transmission power of BS i. We will change this transmission power to increase the ASE. $dist_{ij}$ is the distance between BS i and location j, which depends on the deployment strategy. For the simplicity of calculations, we ignore the shadowing effect (L^{SHA}). Path loss exponent L^{EXP} depends on the different area types such as urban, rural, or indoor. Finally, $dist_0$ and L^{REF} are the reference distance and the reference path loss, respectively. We use the ITU path loss model for the urban Non-line-of-sight (NLOS) area, which is found in [60].

As a QoS constraint, we have to find the ASE for each BS and location pair. Thus, first, we should calculate the signal to interference (SINR) by Equation 3.2, where $\Gamma_{i'j}$ is the SINR value in location j, $P_{i'j}^{rx}$ is the highest received signal at this location which is propagated from BS i', $Interference$ is the sum of the received signals from other BSs except BS i', and σ^2 is the noise power. Then, the service rate (spectral

efficiency) of a BS, $S_{i'j}^{BS}$, can be easily calculated with SINR and allocated bandwidth ($BW_{i'}$) values in Equation 3.3. Finally, ASE can be expressed by Equation 3.4, where $\mathcal{A}$ denotes ASE, and Pr_j denotes the normalized rate of users in location j.

$$P_{ij}^{rx} = L^{REF} * L^{SHA} * P_i^{tx} * \left\{ \frac{dist_{ij}}{dist_0} \right\}^{-L^{EXP}} \tag{3.1}$$

$$\Gamma_{i'j} = \frac{P_{i'j}^{rx}}{Interference + \sigma^2} \tag{3.2}$$

$$S_{i'j}^{BS} = BW_{i'} \log_2(1 + \Gamma_{i'j}) \tag{3.3}$$

$$\mathcal{A} = \frac{\sum\limits_{j \in \mathcal{J}} S_{i'j}^{BS} * Pr_j}{\mid \mathcal{J} \mid} \tag{3.4}$$

Our objective function is to minimize the overall energy consumption of the BSs, shown in Formula 3.5. P_i^{tx} is the transmission power of BS i, E_i^{BSD} is the coefficient accounts for energy consumption that scales with the transmission power, and E_i^{BSS} is the energy consumption that is independent of the transmission power [16]. E_i^{BSD} and E_i^{BSS} values may change with different BS types because they might have different hardware or design like different amplifier circuits or cooling systems.

Minimize:

$$\sum_{i \in \mathcal{I}} \left\{ E_i^{BSS} + E_i^{BSD} * P_i^{tx} \right\} \tag{3.5}$$

Subject to:

$$P_{i'j}^{rx} \geq P_{min}^{rx}, \quad \forall j \in \mathcal{J} \tag{3.6}$$

$$\mathcal{A} \geq \mathcal{A}_{min} \tag{3.7}$$

The first constraint represents the coverage requirement (Inequality 3.6). An MNO should provide at least P_{min}^{rx} received power at all locations of the urban area for

a minimum communication rate. The second constraint is aimed at an overall urban area criterion, which is called ASE. As a result of pricing policies, increasing ASE does not only improve the data communication QoS of an MNO but also increases the provider's income [18]. Thus, we have to provide a minimum ASE (A_{min}) in a RAN, shown in Inequality 3.6. To solve the first problem described above, we should choose the deployment places (the set of I) of the BSs to provide a minimum received signal for each location and a minimum spectral efficiency in the overall area. The objective is to satisfy these constraints with the minimum overall energy consumption.

The second problem involves the use of RES for these BSs effectively. These BSs can produce their own energy from a RES such as sunlight or wind. That means zero carbon emissions, which is an excellent solution for a green network. However, a RES has a limited energy regeneration rate, and it may not be enough to operate a BS for the whole day [61]. Therefore, these BSs should also be connected to the electricity grid. This on-grid energy consumption, E_i^{BSG}, is calculated by Equation 3.8, where G_t^{reg} is the regeneration rate of renewable energy in a time interval. Therefore, we should try to spread the individual energy consumption of a BS in time. Hence, the BS can store more energy for its operations, and its need for on-grid energy consumption reduces dramatically.

$$E_i^{BSG} = \sum_{t \in \mathcal{T}} \left\{ E_i^{BSS} + E_i^{BSD} * P_i^{tx} \right\} * (1 - G_t^{reg}), \quad \forall i \in \mathcal{I} \tag{3.8}$$

The third problem is the decision of the transmission power level (P_i^{tx}) of the BSs. We should change a BS transmission power according to the number of mobile users served by this BS. Therefore, the overall energy consumption (also carbon emission) can be reduced with fewer BSs. On the other hand, as mentioned before, we should provide a minimum received power for all locations of the area ($j \in \mathcal{J}$). Therefore, we need to use some BSs like an umbrella that covers the whole area [62].

3.3. Methods for Energy-Efficient Deployment

In our solution, we use two types of BS. The first one is the macro BS, which provides higher transmission power, which means a larger coverage area. The second one is the micro BS, which has a smaller coverage area but lower power consumption [63]. We use macro BSs as an umbrella to satisfy our first constraint, the coverage of the whole area. On the other hand, micro BSs are very useful to increase the ASE with relatively lower power consumption. In Figure 3.1, we represent a sample user distribution for a time interval. The user distribution may be altered at different times of the day [5]. For example, a business area may be at peak user density between 09:00-17:00 hours, and an entertainment area may be at peak user density at 19:00-23:00 hours. Therefore, we divide a day into several time intervals with different user distributions then solve a separate optimization problem for each time interval for deploying the micro BSs to increase the ASE. In fact, all micro BSs for all time intervals will be deployed. However, those not utilized in a particular time interval will not be operational for saving energy.

For further energy savings, the transmission power of micro BSs can be reconfigured easily, which provides us another tool to optimize the energy consumption for the chosen BS locations. However, this is an NP-hard problem [64]. When the solution area gets bigger, which is typical in a metropolitan area, finding the optimum solution is very hard. Therefore we divide this problem into smaller subproblems, and we first focus on the selection of the BS locations in which the BSs operate with their maximum power. We will present our solution for reconfiguring the transmission powers at the end of this section. We use a greedy algorithm in which the main idea is adding a new micro BS on the location, which provides the most increase in the ASE value (Figure 3.2). These BSs are iteratively added, while ASE is lower than the minimum ASE threshold. We run this algorithm for each time interval, and each of these time intervals has a different user distribution. Therefore, we have $\mid \mathcal{T} \mid$ different micro BSs deployment schemes ($\mathcal{I}_t$) at the end of the first step, where $\mid \mathcal{T} \mid$ is the number of time intervals.

initial: $\mathcal{I}_t = \emptyset, \mathcal{J}^{CAN} = \mathcal{J}, \mathcal{A} = 0$
while $\mathcal{A} \leq \mathcal{A}_{min}$ **do**
  $j^{MAX} = \emptyset$
  for all $j \in J^{CAN}$ **do**
    $\mathcal{I}^{CAN} = \mathcal{I}_t \bigcup j$
    Calculate $\mathcal{A}_{I^{CAN}}$
    if $\mathcal{A}_{I^{CAN}} > \mathcal{A}$ **then**
      $\mathcal{A} = \mathcal{A}_{I^{CAN}}$
      $j^{MAX} = j$
    end if
  end for
  $\mathcal{I}_t = \mathcal{I}_t \bigcup j^{MAX}$
  $J^{CAN} = J^{CAN} \setminus j^{MAX}$
end while
return $\mathcal{I}_t$

Figure 3.2. Step 1: Greedy algorithm for choosing the locations of new micro BSs.

In the second step, we focus on the renewable energy capacity of these micro BSs and come up with a novel solution. As mentioned before, these BSs may not have enough regeneration rates. If we operate these BSs only at non-adjacent time intervals, these BSs require lesser on-grid electricity. Therefore, we combine $\mathcal{T}/2$ BS sets ($\mathcal{I}_t$) at each user distribution, as shown in Figure 3.3. In this algorithm, $\mathcal{I}_t$ is the deployment scheme of the time interval t. Hence, at the end of step 2, we reduce the number of deployment schemes from $\mathcal{T}$ to 2, which are $\mathcal{I}_{odd}$ and $\mathcal{I}_{even}$.

initial: $\mathcal{I}_{odd} = \emptyset, \mathcal{I}_{even} = \emptyset$
for all $t \in \mathcal{T}$ **do**
  if $t \mod 2 = 0$ **then**
    $\mathcal{I}_{even} = \mathcal{I}_{even} \bigcup \mathcal{I}_t$
  else
    $\mathcal{I}_{odd} = \mathcal{I}_{odd} \bigcup \mathcal{I}_t$
  end if
end for
return $\mathcal{I}_{odd}, \mathcal{I}_{even}$

Figure 3.3. Step 2: Aggregation of BSs at the non-adjacent time intervals.

The second step optimizes the renewable energy usage ability of the BSs. On the other hand, aggregating the BSs from different time intervals increases the number of BSs in deployment schemes ($\mathcal{I}_{odd}$ and $\mathcal{I}_{even}$) and the overall energy consumption. Therefore, we need to remove some BSs by considering the minimum ASE value. We implement the center of mass (CoM) optimization algorithm for each deployment

scheme, as shown in Figure 3.4 [65]. The traffic rates and the user distributions of different time intervals do not have any effect on this algorithm; we only need to consider the distances between the BSs. Because all the time intervals in the same scheme have the same BS deployment, we run this algorithm only for two schemes, $\mathcal{I}_{odd}$ and $\mathcal{I}_{even}$, which are denoted as $\mathcal{I}_{sch}$ in Figure 3.4. In the while loop, first, we find the two BSs in $\mathcal{I}_{sch}$, which are the nearest to each other ($nearestBSs$). Then we find the middle point of these two BSs and add it to $\mathcal{I}_{sch}$. Finally, we remove $nearestBSs$ from $\mathcal{I}_{sch}$. We run this loop until we reach the ASE value.

```
1:  while A > A_min do
2:      nearestDist = ∞
3:      nearestBSs = ∅
4:      for all x ∈ I_sch do
5:          for all y ∈ I_sch \ x do
6:              if distance(x, y) < nearestDist then
7:                  nearestDist = distance(x, y)
8:                  nearestBSs = x ⋃ y
9:              end if
10:         end for
11:     end for
12:     I_sch = I_sch ⋃ MidPoint(nearestBSs)
13:     I_sch = I_sch \ nearestBSs
14: end while
15: return I_sch
```

Figure 3.4. Step 3: CoM algorithm to decrease the number of BSs.

At the end of Step 3, we have two deployment schemes that work at non-adjacent time intervals with the minimum constraint restrictions. However, BSs may have excess renewable energy. Therefore, we also investigate adjusting the transmission power of these BSs at these time intervals to use RES more effectively. This operation is called cell zooming that is adaptively changing the transmission power of BSs according to the user distribution [66]. This step provides extra ASE, which means increasing the QoS and income of an MNO. We will give the comparison chart for this step in the next section.

Table 3.1. BS deployment problem experiment parameters.

Parameter	Unit	Macro BS	Micro BS
P_i^{tx}	W	24	4
E_i^{BSS}	W	354.44	71.5
E_i^{BSD}	–	21.45	7.84

3.4. Computational Experiments

Our deployment area size is $3x3\ km^2$, with one macro BS, which provides an umbrella role for coverage. The energy consumption parameters of BSs, given in Table 3.1, is provided from [16]. We use the ITU path loss channel model for urban micro BSs [60]. The other parameters used in the experiments are given in Table 3.2. For simplicity, interferences between BSs are ignored.

Table 3.2. BS deployment channel model parameters.

Parameter	Unit	Value
L^{EXP}	–	4
L^{REF}	W	24
$dist_0$	$meter$	1
σ^2	dBm	-144
P_{min}^{rx}	dBm	-90
$\mathcal{A}_{min}$	$bit/sec/Hz/km^2$	12

Table 3.3. Energy consumptions of full and split combinations.

G_t^{reg}	Energy source	Full comb.	Split comb.
0	On-grid	3189	2109
0	Renewable	0	0
0.3	On-grid	1924	843
0.3	Renewable	1265	1265
0.5	On-grid	1080	0
0.5	Renewable	2109	2109

In the first set of experiments, we compare our non-adjacent time interval combination and full-time interval combination to calculate the performance of our algorithm. In the full combination, we can satisfy the constraints with 31 micro BSs. In the split

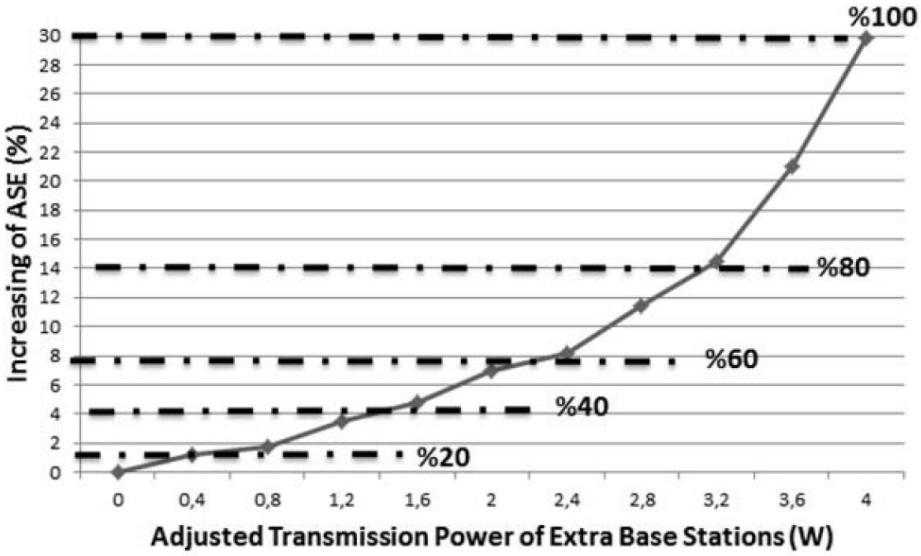


Figure 3.5. Increase in ASE with the transmission power.

version, which we propose as a new solution, we can satisfy the constraints with 17 BSs in one deployment scheme and 24 BSs in the other one. In Table 3.3, we present the energy consumptions of these two solutions. When G_t^{reg} is selected[1] as 0.5, zero on-grid energy consumption can be achieved if the BSs are operated 50% of the time. Therefore, the split combination solution provides zero carbon emission rates with a regeneration rate of 0.5. Moreover, the on-grid energy consumption is lower than the full combination at smaller regeneration rate scenarios and even at zero regeneration rates. The reason is that in the split combination, BSs are deployed for the more specific user distributions. However, this solution needs the deployment of extra 10 BSs which increases the deployment costs [67].

In the second set of experiments, we focus on the transmission power (P_i^{tx}) adjustment to provide a higher ASE. The results are shown in Figure 3.5. The dedicated BSs for the specific time interval remains with the same transmission power. The transmission powers of other BSs, which were in the sleep mode (zero transmission power) in the first set of experiments, are increased from $0W$ to $4W$ to increase the ASE value. For example, we can provide 8% more ASE with $2.5W$ transmission power incrementation. In addition, this figure also shows the zero carbon emission bound with

[1]For simplicity, we assume G_t^{reg} is the same value for every time interval in this study.

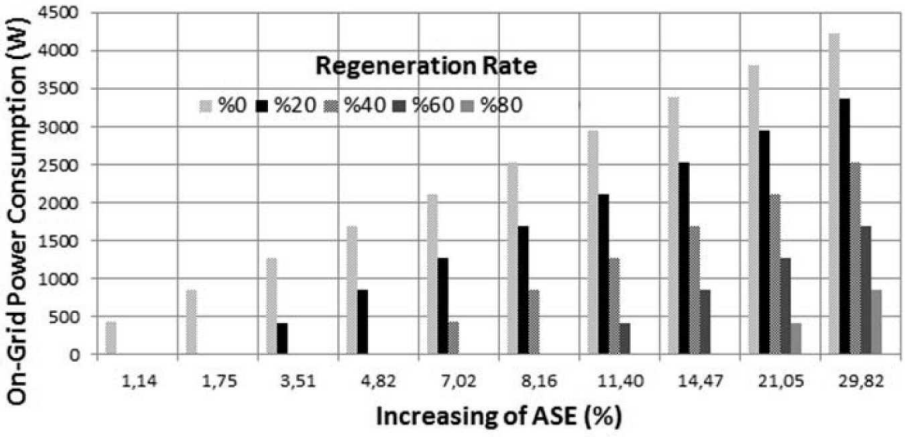


Figure 3.6. Amount of on-grid energy consumption for extra ASE.

dotted lines. For example, if RES has a 60% regeneration rate, we need to choose the P_i^{tx} $2.5W$ or below value for zero carbon emission rate. Finally, in Figure 3.6, we show the extra on-grid energy consumption results if we operate BSs over the zero carbon emission bound. For example, if we need an additional 8% ASE and the regeneration rate of the BSs is 40%, we need $800W$ on-grid power.

3.5. Discussion

This chapter represents a BS deployment problem of a RAN with RES. We combine three issues for this RAN; deployment of micro BSs in a region which is already deployed with macro BSs, using RES with these BSs efficiently, and adjusting the transmission power of BSs to improve the QoS. Even though these issues are already investigated in other studies, we combine them into the same problem and offer a unified solution. Our results indicate that solving these problems with a joined methodology does not only reduce carbon emission rates but also decrease the operational cost of an MNO.

In the next chapter, we study a RAN with micro and macro BSs that are deployed before and focus on reducing the TCO in this RAN.

4. REDUCING THE TOTAL COST OWNERSHIP OF A THIRD GENERATION RADIO ACCESS NETWORK

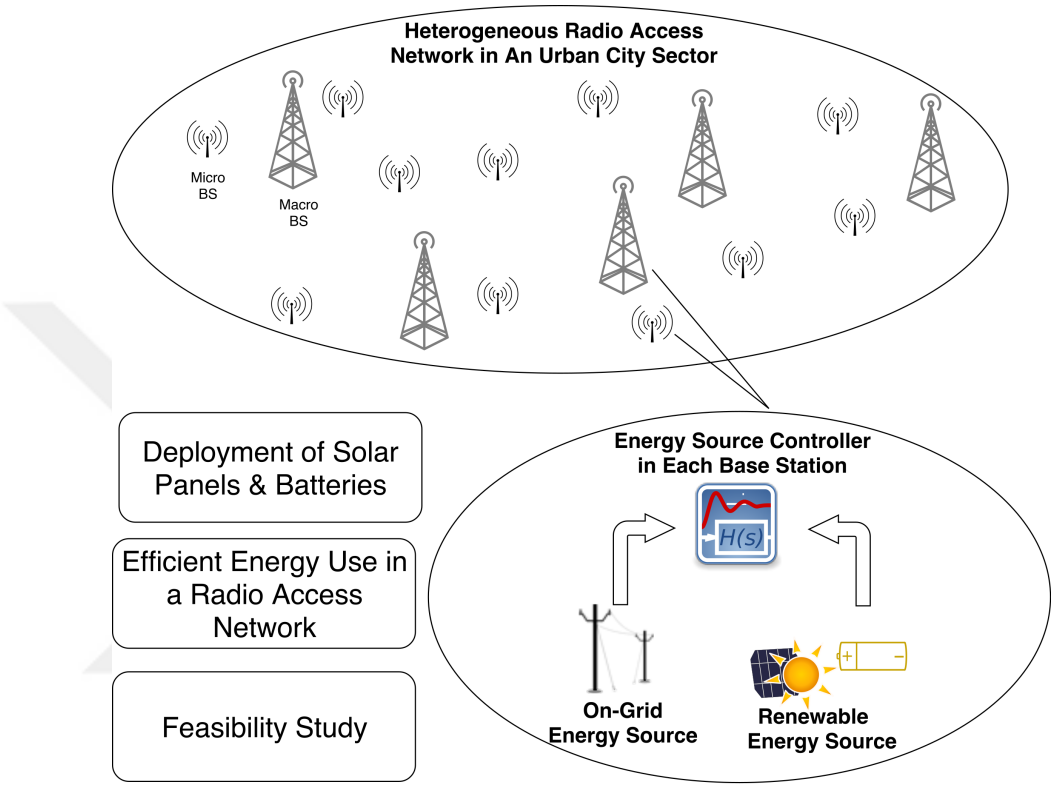


Figure 4.1. HEBRAN system model.

4.1. Introduction

This chapter focuses on reducing the TCO of a packet-switched RAN in which all BSs have both renewable and on-grid energy sources. While the RES reduces the electrical grid energy consumption of the BSs in this network, the electrical grid provides the energy demand in the case of the lack of insufficient renewable energy. This type of network is named as hybrid energy based radio access network (HEBRAN) [68]. Figure 4.1 shows the HEBRAN model used in this chapter. This model emphasizes that deploying a solar panel in each BS provides better results. Besides, the findings from this study, which is published in Wireless Networks journal [69], confirm that considering the remaining energy in the batteries of a HEBRAN system is crucial to reduce the TCO. The main contributions of this chapter are as follows:

(i) MNOs typically use RESs in the rural area on isolated macro BSs. Findings confirm that it may also be beneficial to use these energy sources in an urban area.

(ii) We provide a feasibility study that shows the economic efficiency of this hybrid energy sourced RAN in an urban area.

(iii) We formulate an offline problem which aims to find the cost-effective size for the solar panels and batteries, and provide a solution with a MILP solver. Moreover, we propose a heuristic algorithm for the same problem which outperforms this MILP solver for larger and realistic size instances.

(iv) We provide an online algorithm for using renewable energy more efficiently. Thus, we surpass the classical methods which consider only the traffic variation for reducing the OpEx and carbon emission rates.

(v) The related studies focus only on deploying solar panels on one type of BS. On the other hand, we deploy solar panels on two different types of BSs. The results show that it is cost-effective to deploy RESs on a heterogeneous network.

(vi) We test our methods for different traffic and solar radiation rates. In addition, we use real solar data and test our methods for a year period to see the effect of seasonal changes in four different geographical areas in the world with significantly different solar radiation patterns.

The remainder of this chapter is organized as follows. We describe this new type of RAN and its cost optimization problem in the second and third sections, respectively. In the fourth section, we propose novel solutions to overcome this problem. The fifth section provides the results of these solutions, and the last section discusses the results.

4.2. System Description

In this section, we describe the essential parts of a HEBRAN system, which are traffic, channel, and energy consumption models.

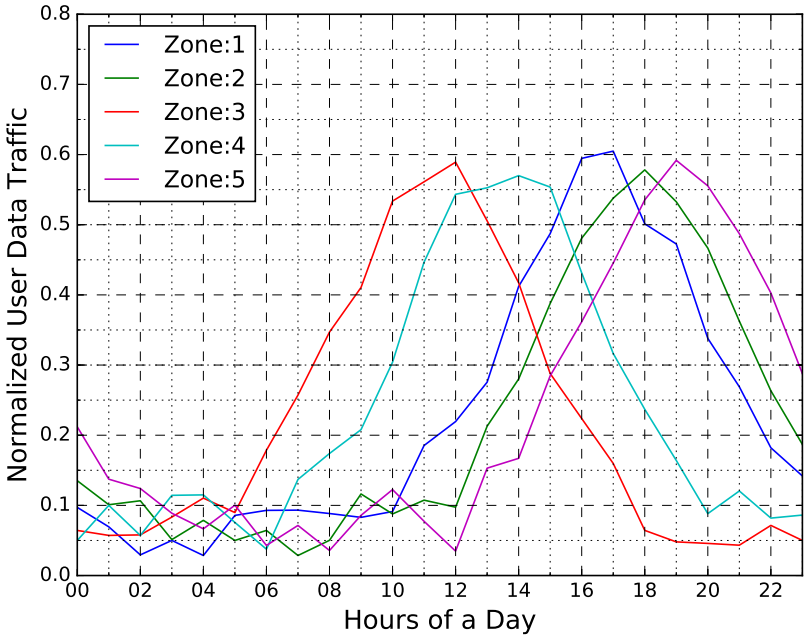


Figure 4.2. Five different data traffic patterns in a day period.

4.2.1. Traffic Model

First, we formulate the downlink data traffic. The reason is that this type of traffic rapidly increases by the increasing usage of the internet and the invention of the new wireless network devices. On the other hand, mobile users need far less bitrate for uplink traffic [70]. For that reason, providing an energy-efficient solution for the downlink traffic is more crucial than a solution for the uplink traffic. In addition, the new technologies use packet switching technologies for voice traffic [71]. We should also notice that even though we only consider the downlink traffic in this study, our methods are also applicable to the uplink traffic.

One of the most important studies about the dynamics of the data traffic in urban sectors is written by Peng et al. [70], in which they analyze two-month long real network data of a real MNO. Their analysis shows that the data traffic significantly changes both temporally and spatially in four different urban regions. In addition, they present two critical findings that inspire our solution in this study. The first one is that the temporal change of data traffic is more potent in a day period, but it is not significant between the consecutive days. The second is that the data traffic loads are diverse

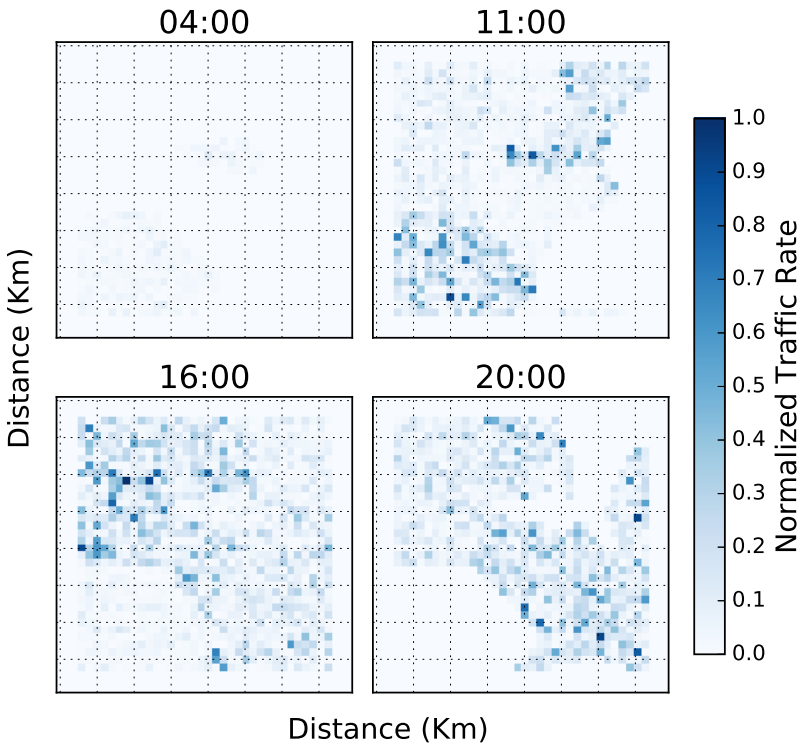


Figure 4.3. The traffic rate of our covered sector in a day period.

between very close locations, especially in their peak hours. For that reasons, although we do not use real data traffic in this study, we model it by considering these authors' findings and make it diverse both temporally and spatially, which are explained in the following paragraphs.

The temporal traffic profile we use in this chapter evolves from several papers. First, Marsan et al. [72] propose a formula that creates a one day period sinusoidal shape traffic for a RAN. Then, Hossain et al. [73] modify this formula by adding a random fluctuation in a day period. Finally, Zhang et al. [22] add a multiplier into this formula to create diversity between different locations. We modify this last formula by adding a fluctuation between the days of a year and try to make it diverse between the weekdays and weekends by considering the findings of Peng et al. [70]. Our formula is given in Equation 4.1 in which κ is the value of the peak hour traffic which depends on whether it is a weekday or weekend, φ is a random value between the $3\pi/4$ and $7\pi/4$ which determines the peak hour of the traffic profile, ν determines the abruptness of the traffic profile and $n(t)$ is a random value which provides a fluctuation in this traffic

profile. Therefore, we can model the variation of data traffic between each hour and each day by this formula.

$$f_z(t) = \frac{\kappa}{2^\nu}[1 + \sin(\pi t/12 + \varphi)]^\nu + n(t) \tag{4.1}$$

$$\lambda(j,t) = f_{H_j^z(.)}(t), H_j^z(.) = \{z | z < 5, z \in N)\} \tag{4.2}$$

$$U_{jt}^{BS} = \lambda(j,t)/\mu(j,t) \quad [in\ bps] \tag{4.3}$$

We use a three-step method to create traffic diversity between the locations of the urban sector, according to the findings in [70]. In the first step, we create five different traffic profiles using Equation 4.1 in which each traffic profile have different peak hours (Figure 4.2). In the second step, we create a map with different districts of the urban sector such as business or residential districts. In the third step, we assign the traffic profiles, which we create in the first step to these districts, by using a pre-calculated function $H_j^z(.)$, which maps the j^{th} location to the z^{th} traffic profile, shown in Equation 4.2. Therefore we create a spatial diversity between the five different districts which have different peak hours. We use this calculated value $\lambda(j,t)$ as a mean arrival rate of the user in a district of an urban sector. Finally, we create the traffic loads of the users by Equation 4.3. In this equation, user inter-arrival times have a Poisson distribution, and the requested data size is an exponentially distributed random variable with mean $1/\mu(j,t)$ [74]. Figure 4.3 and Figure 4.4 show the change in traffic rates in a day period and a week period for these different districts, respectively. Lastly, we minimize the traffic rates on the edge of the covered sector (white zones) to eliminate the border effect.

4.2.2. Channel Model

We consider an urban sector where a set of BSs (I) are already deployed to serve a set of locations (J) that demand service from these BSs. This section explains how these BSs satisfy the data traffic required by these locations (U_{jt}^{BS}, Section 4.2.1). First, we

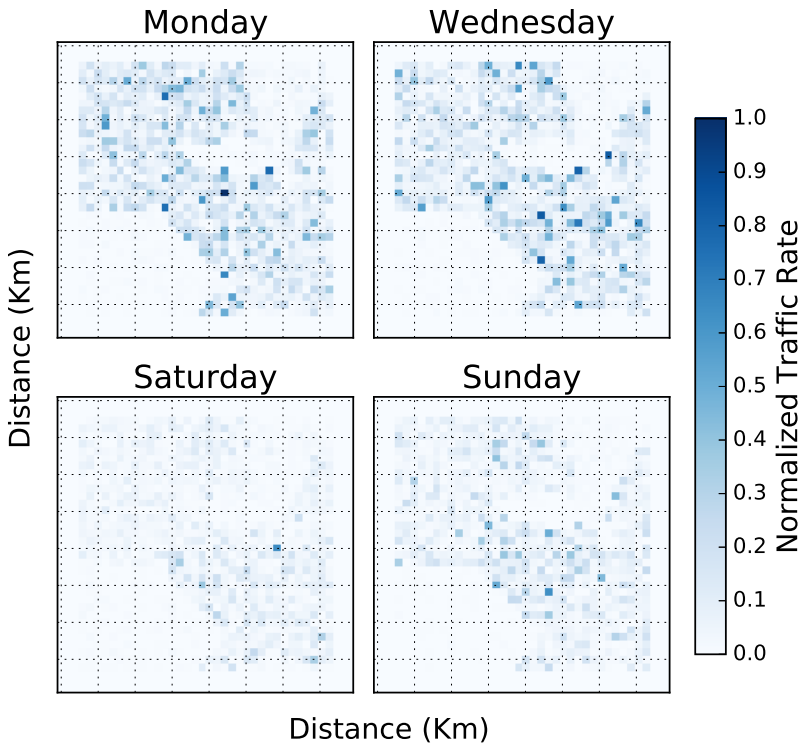


Figure 4.4. The traffic rate of our covered sector in a week period.

have to calculate the path loss (L_{ij}) between each BS ($i \in I$) and each location ($j \in J$) in this sector. For that purpose, we use the macro and micro NLOS path loss models from the ITU-R report [75] according to the type of the BS ($i \in I$). After calculating the path loss, we calculate the received signal - noise ratio (SNR, Γ_{ij}) at the location side by Equation 4.4.In this equation, L_{ij} is the path loss, P_i^{tx} is the transmission power of the BS $i \in I$, and σ^2 is the Gaussian noise. Dealing with the interferences between the BSs is out of scope in this study, and we assume it is well managed by the frequency planning. Finally, we use the Shannon capacity formula [76] to calculate the service rate (spectral efficiency) of a BS for a specific location (Equation 4.5). In this equation, BW_i represents the bandwidth allocated to the BS $i \in I$, and S_{ij}^{BS} represents the service rate of this BS to the location $j \in J$.

$$\Gamma_{ij} = \frac{L_{ij} P_i^{tx}}{\sigma^2} \tag{4.4}$$

$$S_{ij}^{BS} = BW_i \log_2(1 + \Gamma_{ij})(bit/sec) \tag{4.5}$$

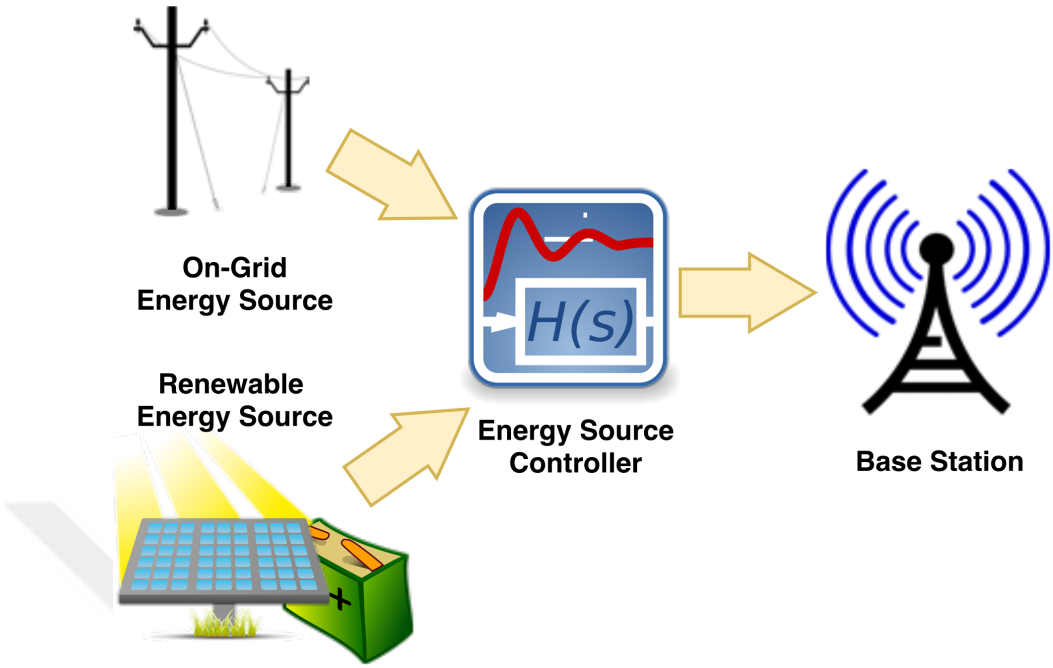


Figure 4.5. HEBRAN energy model.

4.2.3. Base Station Energy Consumption Model

Auer et al. analyze the energy consumption model of several types of BSs in their paper, including macro and micro BSs [77]. According to their findings, the energy consumption of an active BS in a time interval can be calculated with Equation 4.6.

$$E_{it}^{BS} = E_i^{BSS} + \sum_{j \in \mathcal{J}} \frac{U_{jt}^{BS}}{S_{ij}^{BS}} z_{ijt} * E_i^{BSD}, \forall t \in \mathcal{T} \tag{4.6}$$

In this equation, E_i^{BSS} is the static energy consumption in a BS, and it remains the same even if this BS does not serve any user. It includes power amplifier, feeder, power supply, signal processing, and air conditioning energy consumptions [22]. On the other hand, E_i^{BSD} is the dynamic energy consumption coefficient related to the system load of a BS. We provide these energy consumption values for both macro and micro BSs in Section 4.5. In addition to the active state of a BS, we can switch off a BS completely in our system, which means that we shut down all its components. Thus, in this state (deep sleep state), the energy consumption of a BS becomes zero [78].

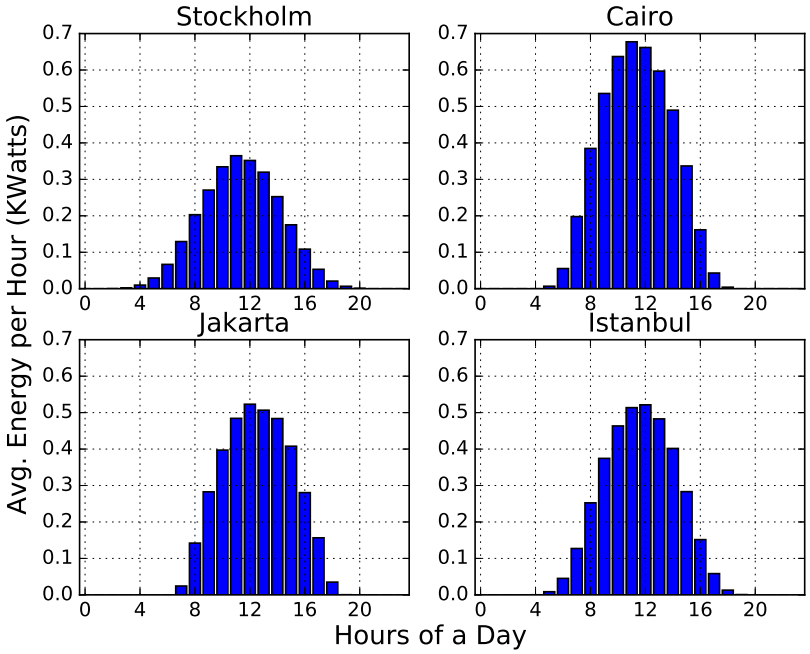


Figure 4.6. Distribution of harvested solar radiation in a day period.

4.2.4. Renewable Energy System Model

Figure 4.5 shows the electrical grid energy supported renewable energy system for a BS. In this system, the solar panel harvests the renewable energy from sunlight, the battery stores this energy and the energy source controller chooses the energy source that is used to supply the BS. According to Hassan et al. [79], itself based on [80], the harvested green energy may be used directly by the system or may be stored in a battery for future use. Storing the green energy in a battery does prevent not only the wasting of the excess green energy but also maintains the more efficient usage of the green energy. Although this system is not conventional for a BS nowadays, the Bloomberg Finance group announced in one of their latest reports that using battery storage alongside solar panels is a promising method for a rooftop system in 2020 [81]. Moreover, a recent report about solar panel technology in Germany also supported this new system. They suggest that the prices of solar panels drop 19% each year, and they mention that the prices continue to drop year by year [8]. With this in mind, we directly focus on the BSs with their own solar panels and batteries. We explain the model of a solar panel and a battery in our system in the following sections.

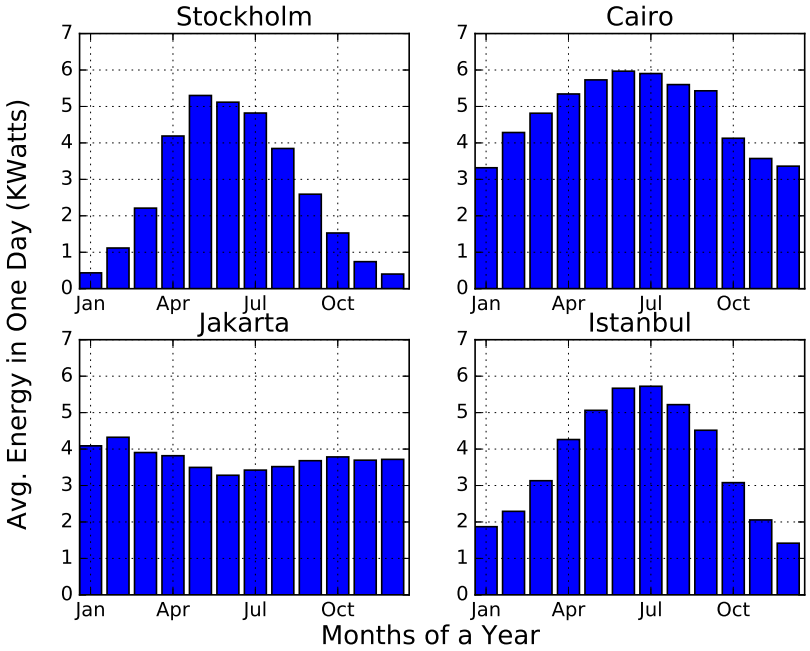


Figure 4.7. Distribution of harvested solar radiation in a year period.

4.2.4.1. Solar Panel Model. Choosing an appropriate solar panel size[2] for a BS in a HEBRAN is crucial for both increasing the renewable energy generating capacity and reducing the CapEx of this network. The relation between the size of a solar panel and the amount of the generated renewable energy by this panel is linear, according to National Renewable Energy Laboratory [82]. While considering this relation, we use the empirical data from the pvWatts application to calculate the amount of the generated energy of a solar panel for each time interval [82]. Their 30 years of historical weather data provide us to calculate the detailed solar energy generation rate of a panel (G_t^{BS}) for different cities. They provide each hour of the day data; thus, we can simulate the change of solar energy in several time scales. Figure 4.6 and Figure 4.7 show the variation of generated energy of a $4kWh$ size of a solar panel for different cities.

$$Panel\ Cost\ (\$) = \sum_{i \in \mathcal{I}} c^S * \alpha_i^{BS} \tag{4.7}$$

$$Array\ Area\ (m^2) = \frac{Size(kWh)}{Efficiency(\%)} * \frac{m^2}{1kWh} \tag{4.8}$$

[2]We have to clarify that in this chapter, we use the "solar panel size"clause to define the energy generating capacity of this panel.

The other important thing is that the size of a solar panel directly affects the installation cost (CapEx) of a HEBRAN. Equation 4.7 shows how to calculate this installation cost, in which c^S is the unit cost of a solar panel α_i^{BS} is the solar panel size of BS i. We can use this linear cost model if the energy harvesting capacity of these panels is lower than $10kWh$ [82]. However, the solar panel size is not limited by only its installation cost. According to our scenario, we have to install these solar panels near to the BSs, which are usually on a rooftop of a building in an urban sector. Therefore, we have to limit the size of a solar panel by looking at the array area of this panel. Equation 4.8 shows the relation between the array area and the size of a solar panel [82, 83]. We limit the maximum size of a solar panel as $6kWh$ as a result of this relation.

4.2.4.2. Battery Model. First of all, we have to give some explanation about the battery technology we use in this study. We choose the lithium-ion based batteries in the light of a recent report published by the International Renewable Energy Agency (IRENA) [9]. This report emphasizes that lithium-ion batteries have several advantages when we compare them with the other battery types. Especially their deep discharge cycle capability that helps the BSs to consume a high amount of energy in a short time and their power density, which makes them preferable to be used in a small area, encourage us to choose lithium-ion batteries. The same report also advises the lithium-ion cells because of their decreasing price trends. Lastly, the Navigant Research emphasizes that the distributed energy storage system (DESS) market - our system is a kind of DESS - prefers lithium-ion batteries as their first choice for a battery [84].

One of the purposes of this work is the appropriate battery size selection for an energy-efficient solution. However, the battery size and renewable energy consumption rate have a complicated relationship, which increases the complexity of this size selection problem. Han et al. [56] propose Equation 4.9 to define this non-linear relation, itself based on [85]. In this equation, b_{it}^{BS} is the stored/remaining battery energy of the BS $i \in I$ in time interval $t \in T$. The maximum value of b_{it}^{BS} is the battery storage capacity value, $u^B \beta_i^{BS}$, in which u^B is the unit storage capacity, and β_i^{BS} is the size

of the battery, which is a decision parameter in our objective function. G_t^{BS} is the generated renewable energy of a unit size solar panel in the time interval t, α_i^{BS} is the size of the solar panel and E_{it}^{BS} is the energy consumption of a BS in the time interval t. Finally, the most important part, $b_{i(t-1)}^{BS}$ is the remaining battery energy from the previous time interval, which means that the s_{it}^{BS} decisions and G_t^{BS} values in the previous time intervals, directly affect the current b_{it}^{BS} decision. In summary, our problem becomes a non-linear problem due to this relation.

$$b_{it}^{BS} = \min\Big\{ \max\left\{b_{i(t-1)}^{BS} + \alpha_i^{BS} G_t^{BS} - E_{it}^{BS} s_{it}^{BS}, 0\right\}, u^B \beta_i^{BS}\Big\}, \quad \forall i \in \mathcal{I}, \forall t \in \mathcal{T} \quad (4.9)$$

The price of a lithium-ion battery changes linearly with the capacity of this battery [86]. Equation 4.10 shows this relation, in which c^B is the unit battery price, and β_i^{BS} is the size of the battery at BS i. The other cost components of a battery system are omitted in this study because they do not change with the size of a battery, but can be added easily as a constant without changing the performance of the proposed solution. Also, we assume the batteries in our system are charged/discharged linearly in their lifetime for simplicity.

$$\textit{Battery Cost (\$)} = \sum_{i \in \mathcal{I}} c^B * \beta_i^{BS} \quad (4.10)$$

4.3. Cost Optimization Problem of a HEBRAN

In the previous section, we describe a system in which the renewable energy systems used together with the BSs in an urban sector, and we explain the critical parts of this system. This section describes the optimization problem, which begins with the details of the objective function and the constraints in the problem. It finishes with a description of the complexity of this formulated problem.

4.3.1. Problem Formulation

The optimization problem of a HEBRAN can be given as:

Minimize:

$$\sum_{i\in\mathcal{I}} c^S \alpha_i^{BS} + \sum_{i\in\mathcal{I}} c^B \beta_i^{BS} + \sum_{i\in\mathcal{I}}\sum_{t\in\mathcal{T}} c^E E_{it}^{BS}(1 - s_{it}^{BS}) w_{it} \tag{4.11}$$

Subject to:

$$\sum_{i\in\mathcal{I}} S_{ij}^{BS} z_{ijt} \geq U_{jt}^{BS}, \qquad \forall j \in \mathcal{J}, \forall t \in \mathcal{T} \tag{4.12}$$

$$\sum_{j\in\mathcal{J}} \frac{U_{jt}^{BS}}{S_{ij}^{BS}} z_{ijt} \leq \rho, \qquad \forall i \in \mathcal{I}, \forall t \in \mathcal{T} \tag{4.13}$$

$$\sum_{i\in\mathcal{I}} z_{ijt} \leq 1, \qquad \forall j \in \mathcal{J}, \forall t \in \mathcal{T} \tag{4.14}$$

$$w_{it} \left|J\right| - \sum_{j\in\mathcal{J}} z_{ijt} \geq 0, \qquad \forall i \in \mathcal{I}, \forall t \in \mathcal{T} \tag{4.15}$$

$$s_{it}^{BS} \leq \min\left\{\frac{b_i^{BS}(t)}{E_{it}^{BS}} w_{it}, 1\right\}, \qquad \forall i \in \mathcal{I}, \forall t \in \mathcal{T} \tag{4.16}$$

$$s_{it}^{BS} \geq \min\left\{\frac{b_i^{BS}(t)}{E_{it}^{BS}} w_{it}, 1\right\}, \qquad \forall i \in \mathcal{I}, \forall t \in \mathcal{T} \tag{4.17}$$

We aim to minimize the TCO of this system, the sum of the CapEx and the OpEx. Migrating to a renewable energy system has two main CapEx types, which are shown as the first two components in Equation 4.11. The first one is the installation cost of the solar panels, and the second one is the installation cost of the batteries. Since these components are briefly explained in Section 4.2.4, we skip the details of the calculation of these components in this section. The third component in Equation

4.11 formulates the on-grid energy consumption, in which c^E is the electrical grid cost per kilowatt in a time interval, E_{it}^{BS} is the energy consumption of a BS in time interval t, s_{it}^{BS} is the ratio of the renewable energy consumption, and w_{it} is the binary decision variable states that the BS i is in switched on (active) mode. This equation shows that we can reduce OpEx by increasing either the renewable energy consumption ratio (s_{it}^{BS}) or decreasing the number of active BSs (w_{it}) in this network. Moreover, we have to notice that OpEx is calculated as the summation of every time interval during the life-cycle of this renewable system. The maintenance cost of this renewable system, which is another component of the OpEx, is not included in Equation 4.11. The reason is that this maintenance cost is a constant value and does not change by any decision variable in Equation 4.11.

We explained how to calculate the traffic rates of the locations in an urban sector in Section 4.2.1. To satisfy this data traffic (QoS), each location in this sector should be serviced by a BS at every time interval. Inequality 4.12 formulates this assigning operation, in which U_{jt}^{BS} is the traffic rate of the location j in the time interval t, S_{ij}^{BS} is the maximum service rate of the BS i to the location j, and z_{ijt} is a binary decision variable which equals to one when the BS i is assigned to the location j in the time interval t. We have to notice that instead of adding another constraint for the coverage of the region, we choose the minimum U_{jt}^{BS} larger than zero for each location and the time interval. Since at least one BS should be assigned to a location with a traffic rate larger than zero, Inequality 4.12 also provides the full coverage of the region.

In addition to satisfying the traffic rates of the locations and providing the coverage of the sector, the delay of service in the BSs should be lower than reasonable value for QoS. Inequality 4.13 provides this restriction by limiting the total service load on a BS, in which ρ is the maximum system load that is allowed on a BS in this network.

Inequality 4.12 allows that more than one BS may serve to the same user in a location in the same time interval. Although a wireless communication technology that has a Coordinated Multi-Point (CoMP) property may use more than one BS to

serve the same user [87], the technology that we study may not support this property. Therefore, we add Inequality 4.14 to guarantee that a user is served by only one BS in the same time interval. For the CoMP cases, this inequality can be removed.

The decision parameter z_{ijt} also determines one of the objective function parameters: the BS switch on/off decision (w_{it}). If a BS serves at least one location in a time interval, that BS should not switch off in this time interval. Inequality 4.15 defines this relation.

As mentioned before, the BSs in a HEBRAN can be supplied from a RES, and the on-grid energy source simultaneously. The ratio of the energy consumption between these two sources is determined by the renewable energy ratio variable (s_{it}^{BS}), which is formulated in Inequality 4.16 and Inequality 4.17. This value can be the maximum one, which means that a BS consumes only renewable energy in this time interval. However, assuming that the renewable energy of a BS $b_i^{BS}(t)$ is not enough to supply this BS (E_{it}^{BS}) in the duration of the time interval t, the renewable energy consumption and on-grid energy consumption will be equal to the $b_i^{BS}(t)$ and $E_{it}^{BS} - b_i^{BS}(t)$, respectively. In this case, the ratio of renewable energy consumption equals to $\frac{b_i^{BS}(t)}{E_{it}^{BS}}$. We assume that a BS always prefers to consume renewable energy over the on-grid energy which is provided by Inequality 4.17. Since the on-grid energy price does not change between the time intervals in our scenario, this assumption does not have a negative effect on minimizing the OpEx.

4.3.2. The Complexity Analysis

Proposition 4.1. *Minimizing the TCO of a HEBRAN model is an NP-hard problem.*

Proof. (Sketch) Let us consider a special case of the problem in which the unit solar panel (c^S) and the unit battery (c^B) are overpriced that deploying these new equipment does not have any benefit to reducing the TCO. Then the objective function can be simplified as Equation 4.18, while the constraints 4.12 - 4.15 remain the same for this

specific scenario.

$$\min \left\{ \sum_{i \in \mathcal{I}} \sum_{t \in \mathcal{T}} c^E E_{it}^{BS} w_{it} \right\} \tag{4.18}$$

This problem is the best-known BS switching problem for any instance of a time interval, and it can be reduced from a vertex cover problem [74, 88]. Therefore the problem in this chapter is also an NP-hard problem. □

4.4. Proposed Algorithms for the Optimal Design and Operation of a HEBRAN

In this section, we propose novel algorithms to solve the NP-hard problem explained in the previous section. First, we explain the framework that we use for these algorithms, then give their details. As an alternative for our proposed algorithms, we create a reduced model of the HEBRAN optimization problem to solve it in a MILP Solver, Gurobi [89]. We give the details of this solution in the result section.

As mentioned in the previous section, the solar panels and the batteries are the main investment cost of a mobile operator. The size of these new components should be selected carefully to maximize the economic benefits of the mobile operator. This problem is an offline problem and should be solved before the installation of the panels and the batteries on the BSs. On the other hand, the third component in the objective function (Equation 4.11) is related to the on-grid energy consumption of the BSs. We may reduce this component by using the BS switch on/off algorithms. However, these algorithms depend on the data traffic rates, and harvesting solar energy by the solar panels, which changes temporally and we can only forecast their values. Therefore this problem is an online decision problem and should be solved for each day with new predicted data.

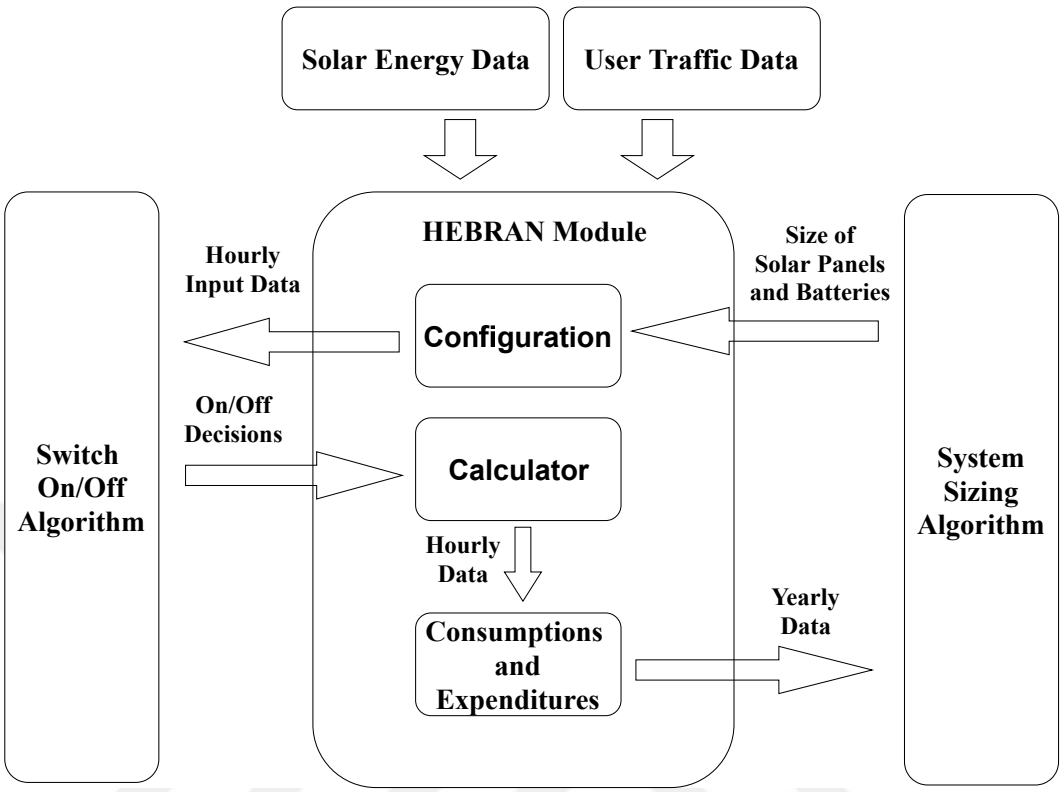


Figure 4.8. HEBRAN solution framework.

Despite the online problem, the decisions of the offline problem (choosing the size of solar panels and the batteries) directly change the renewable energy ratio of the BSs which affects the results of this online decision problem. This relation emphasizes that we have to create a framework in which the problem is decomposed into the two separate parts. In the first part, we have to focus on an offline algorithm which aims to choose the size of the solar panels and the batteries for the different traffic rates and harvesting renewable energy rates. In the second part, we have to focus on an online algorithm that will run during the operation of the system by using the size of renewable energy components found in the first part. Then, we reoperate the first part by using the data established in the second part. Figure 4.8 illustrates this proposed framework.

4.4.1. HEBRAN Framework

The harvested renewable energy varies in different months (Figure 4.7), and investigating the effect of this variation is one of the purposes of this study. Hence, a

HEBRAN operator module is at the core of this framework and is responsible for operating this network for one year. For this purpose, this module begins with receiving the problem data that are generated with the methods mentioned in Section 4.2. In the next step, the module runs the system for one year with a switch on/off algorithm. This algorithm makes decisions on which BSs switching off in each time interval. The algorithms used in this module are explained briefly in Section 4.4.3. The module receives the decisions from this algorithm and logs each time interval to calculate the energy consumptions and expenditures that are used by the system sizing algorithm (Section 4.4.2).

```
1:  initial: T̂CO_0 = ∞, itrt = 0, step = 0, fail = 0, Ŝ_0 = Î, B̂_0 = Î
2:  while step <= 3 do
3:      T̂CO_{itrt+1} ← Run the System for One Year
4:      if T̂CO_{itrt+1} > T̂CO_{itrt} then
5:          fail = fail + 1
6:          if fail >= 2 then
7:              fail = 0 AND step = step + 1
8:          end if
9:      else
10:         fail = 0
11:     end if
12:     new_sizing = False
13:     while new_sizing = False do
14:         if step=0 OR step=2 then
15:             Ŝ_{itrt+1} ← Run ISSP ALGORITHM
16:             if Ŝ_{itrt+1} = Ŝ_{itrt} then
17:                 step = step + 1
18:             else
19:                 new_sizing=True
20:             end if
21:         end if
22:         if step=1 OR step=3 then
23:             B̂_{itrt+1} ← Run ISB ALGORITHM
24:             if B̂_{itrt+1} = B̂_{itrt} then
25:                 step = step + 1
26:             else
27:                 new_sizing=True
28:             end if
29:         end if
30:     end while
31:     itrt = itrt + 1
32: end while
33: return arg min_{TCO_{itrt}} (Ŝ_{itrt}, B̂_{itrt})
```

Figure 4.9. Sizing Algorithms: Main algorithm.

4.4.2. Sizing of Solar Panels and Batteries

As we explained in the previous section, deciding the size of the solar panels and the batteries that reduce the TCO of a HEBRAN is one of our framework's primary goals. For this purpose, we implemented an offline sizing algorithm (Figure 4.9). This algorithm starts with the minimum size of solar panels and batteries. Then we create a four-step decision loop that, in the first and third steps, we run the increasing size of solar panels algorithm (ISSP, Figure 4.10); otherwise, we run the increasing size of batteries algorithm (ISB, Figure 4.11). In this loop, we always start with running the system for one year with the online algorithms (Section 4.4.3) and calculating the TCO. Then we compare this value with the TCO in the previous iteration. If the TCO increases twice in a row, we switch the type of the increasing algorithm. In addition, we also switch the type of the increasing algorithm if one of the algorithms fails to make a change in the size of panels or batteries which means that it is not feasible to make any more incrementation. Finally, in each iteration, we record the sizing configuration ($\hat{S}_{itrt}$, $\hat{B}_{itrt}$), and after the breaking of the loop, we return the sizing configuration of the iteration that has the minimum TCO.

In the ISSP algorithm, first, we sort the BSs according to their energy consumption reducement potential ($\hat{pot}$) if we choose these BSs to increase their panel size for the next iteration ($\hat{S}_{itrt+1}$). The criteria for this potential depends on the total energy consumption ($\hat{texp}$) and grid energy consumption ($\hat{gexp}$) in these BSs in one year period. Then, we limit the number of BSs that can be selected to increase their solar panel size which reduces in each iteration. After this limitation, we check the feasibility of the size incrementation by comparing the reduction in the electricity price (OpEx) and the increase in the price of solar panels (CapEx). In the last while loop, we also eliminate the BSs which are close to each other, and we choose only the BSs which have better potential to decrease the TCO.This elimination prevents unnecessary solar panel incrementation at the BSs in a small area. On the other hand, in the next iterations in which we run the system with the new size configuration ($\hat{S}_{itrt+1}$), we can choose these eliminated BSs if these BSs sustain their potential to decrease the TCO.

The ISB algorithm is very similar to the ISSP algorithm. However, the potential criteria in this algorithm depends on the unstored[3] renewable energy ($\hat{unstrd}_{itrt}$) in the batteries of BSs in the previous iteration.

given: $itrt$, $\hat{texp}_{itrt}$, $\hat{gexp}_{itrt}$, $\hat{S}_{itrt}$
for all $i \in I$ **do**
  $\hat{pot}^i = \frac{1}{\hat{S}^i_{itrt}} * \hat{texp}^i_{itrt}$
  $\hat{pot}^i = \min(\hat{pot}^i, \hat{gexp}^i_{itrt})$
end for
$\hat{pot} \leftarrow sort(\max(\hat{pot}))$
$max_count = |I|/2 - (itrt * 4)$
$CLIST = \emptyset$
for $i := 1$ **to** max_count **do**
  if $\hat{pot}^i * c^E * |\mathrm{T}| * 15 > c^S$ **then**
    $CLIST = CLIST \bigcup \{i\}$
  else
    break
  end if
end for
$mindist = 600$
$LIST = \emptyset$
while $CLIST \neq \emptyset$ **do**
  $LIST = LIST \bigcup CLIST^0$
  for all $i \in CLIST$ **do**
    if $dist(LIST^{-1}, CLIST^i) < mindist$ **then**
      $CLIST = CLIST \setminus CLIST_i$
    end if
  end for
end while
for all $i \in I$ **do**
  if $i \in LIST$ **then**
    $\hat{S}^i_{itrt+1} = \hat{S}^i_{itrt} + 1$
  else
    $\hat{S}^i_{itrt+1} = \hat{S}^i_{itrt}$
  end if
end for
return $\hat{S}_{itrt+1}$

Figure 4.10. Sizing Algorithms: ISSP algorithm.

4.4.3. Base Station Switch On/Off Algorithms

The evidences show that BSs consume a very high amount of energy even if they do not provide a service to any location [77]. This energy consumption arises from

[3]The unstored energy is the harvested energy by a solar panel but could not be stored in a battery due to a fully charged state of this battery.

given: $itrt$, $\hat{unstrd}_{itrt}$, $\hat{gexp}_{itrt}$, $\hat{B}_{itrt}$
for all $i \in I$ **do**
  $\hat{pot}^i = \min(\hat{unstrd}^i_{itrt}, gexp^i_{itrt})$
end for
$\hat{pot} \leftarrow sort(\max(\hat{pot}))$
$max_count = |I|/2 - (itrt * 4)$
$LIST = \emptyset$
for $i := 1$ **to** max_count **do**
  if $\hat{pot}^i * c^E * |\mathrm{T}| * 15 > c^B$ **then**
    $LIST = LIST \bigcup \{i\}$
  else
    break
  end if
end for
for all $i \in I$ **do**
  if $i \in LIST$ **then**
    $\hat{B}^i_{itrt+1} = \hat{B}^i_{itrt} + 1$
  else
    $\hat{B}^i_{itrt+1} = \hat{B}^i_{itrt}$
  end if
end for
return $\hat{B}_{itrt+1}$

Figure 4.11. Sizing Algorithms: ISB algorithm.

non-traffic related operations such as cooling the BS or running the BBU subsystem. Therefore, either a load-balancing method or a cell-breathing technique may not reduce the energy consumption of a BS significantly. For that reason, the online algorithms in this chapter aim to completely switch off as many as possible BSs in the network.

A major problem of a switch on/off algorithm appears on the prediction of the arriving traffic. The real traffic data from the study of Peng et al. [90] show that the traffic patterns of the consecutive days are similar to each other (Figure 4.3). Despite this, Saturday and Sunday have different patterns from the previous day, but their patterns are similar to the previous weekend patterns (Figure 4.4). We adopt these findings to forecast the arriving traffic data for each day. As an alternative forecasting method, more extended historical data may also be collected to predict the arriving traffic data. Peng et al. provide a formula for this purpose in their paper [90]. Finding the best forecasting method is out of the scope of this study, but it can be easily incorporated into our solution.

The online algorithms in this chapter are running in the core network. They start from an initial state, assuming that each BS in the network switches on to provide a service to any location, and the locations are assigned to the BS that provides the best SNR value without violating the maximum utilization value of this BS. This assumption is acceptable for a typical RAN which does not use any energy-efficiency method [5]. We should notice that these algorithms run for each time interval separately, and for the sake of keeping the notation simple, we suppress the time interval index t in these algorithms.

given: U_j^{BS}, S_{ij}^{BS}, z_{ij}, b_i^{BS}, $\forall i \in \mathcal{I}$, $\forall j \in \mathcal{J}$
calculate $SL_{ij} = U_j^{BS}/S_{ij}^{BS}$, $\forall i \in \mathcal{I}$, $\forall j \in \mathcal{J}$
$I^a = \mathcal{I}$
$I^s = sort(\arg\min_{i \in \mathcal{I}}(b_i^{BS}))$
while $I^s \neq \emptyset$ **do**
  $z_{ij}^P = z_{ij}$, $\forall i \in \mathcal{I}$, $\forall j \in \mathcal{J}$
  $BL_i = \sum_{j \in \mathcal{J}} SL_{ij} * z_{ij}$, $\forall i \in \mathcal{I}$
  $I^a = I^a \setminus I_1^s$
  $J^{I_1^s} = \emptyset$
  for all $j \in J$ **do**
    if $z_{I_1^s j} = 1$ **then**
      $J^{I_1^s} = J^{I_1^s} \bigcup \{j\}$
      $z_{I_1^s j} = 0$
    end if
  end for
  for all $j \in J^{I_1^s}$ **do**
    $I^j = sort(\arg\min_{i \in \mathcal{I}}(SL_{ij}))$
    for all $i \in I^j$ **do**
      $BL_i^N = BL_i + SL_{ij}$
      if $BL_i^N \leq \rho$ **then**
        $BL_i = BL_i^N$
        $z_{ij} = 1$
        break
      end if
    end for
  end for
  if $z_{ij} = \emptyset$, $\exists j \in J^{I_1^s}$, $\forall i \in \mathcal{I}^a$ **then**
    $z_{ij} = z_{ij}^P$, $\forall i \in \mathcal{I}$, $\forall j \in \mathcal{J}$
    $I^a = I^a \bigcup I_1^s$
  end if
  $I^s = I^s \setminus I_1^s$
end while

Figure 4.12. BS switch on/off algorithms: Battery-aware algorithm.

In the first algorithm (Figure 4.12), we aim to switch off the BSs which have

the lower renewable energy stored in their battery (b_i^{BS}). There are two main energy-efficient benefits in this decision. First, these BSs can increase their stored renewable energy in their battery in the current time interval; thus, the ratio of electrical grid energy usage in these BSs reduces in the following time intervals. Second, the other BSs, which have more renewable energy in their batteries, can spend their renewable energy in the current time interval. Therefore, the probability of the fully charged batteries, which means that we could not store the renewable energy in these batteries, can reduce by activating the BSs that have less reserve capacity in their battery.

The algorithm starts by calculating the additional system load on a BS if a location is assigned to it (SL_{ij}). Then, it initializes the active BS set (I^a), which includes all the BSs of the network. Next, the algorithm orders the BSs (sorted set I^S) by considering the renewable energy stored in their batteries. The order is from the lowest one to the highest one. Finally, the algorithm starts to operate a three-step iteration on this sorted set.

In the first step of the iteration, the algorithm takes a snapshot of the current z_{ij}^P assignment, calculate the current system load (BL_i) in each BS, switches off the first BS in the sorted set (I_1^s) and creates an orphaned location set $J^{I_1^s}$ which includes the locations that are previously assigned to this switched off BS. In the second step, the algorithm tries to assign these locations to the other BSs in the network without violating the capacity constraints (Equation 4.13). This assignment effort is iterated on each active BS (I^a) until a BS is found to assign this location. The order starts with the BS, which gets the lowest traffic load from this location.

In the third step, the algorithm checks the result of the second step, and if any uncovered location cannot be assigned to one of the active BSs, it returns the configuration of the network at the beginning of this iteration. This algorithm stops when the sorted set I^S becomes empty. In the end, the algorithm provides a set of BSs with the highest amount of renewable energy in their battery. In the following time interval, these BSs stay in the active mode and can consume renewable energy from

their batteries, which have a higher amount of energy than the batteries at switched off BSs.

1: **given:** U_j^{BS}, S_{ij}^{BS}, z_{ij}, b_i^{BS}, $\forall i \in \mathcal{I}$, $\forall j \in \mathcal{J}$
2: **calculate** $SL_{ij} = U_j^{BS}/S_{ij}^{BS}$, $\forall i \in \mathcal{I}$, $\forall j \in \mathcal{J}$
3: $I^a = \mathcal{I}$
4: $BL_i = \sum_{j \in \mathcal{J}} SL_{ij} * z_{ij}$, $\forall i \in \mathcal{I}$
5: $I^s = sort(\arg\min_{i \in \mathcal{I}}(BL_i + \left[\frac{b_i^{BS}}{\beta_i^{BS}}\right]^2))$
6: **while** $I^s \neq \emptyset$ **do**
7: $z_{ij}^P = z_{ij}$, $\forall i \in \mathcal{I}$, $\forall j \in \mathcal{J}$
8: $I^a = I^a \setminus I_1^s$
9: $J^{I_1^s} = \emptyset$
10: **for all** $j \in J$ **do**
11: **if** $z_{I_1^s j} = 1$ **then**
12: $J^{I_1^s} = J^{I_1^s} \bigcup \{j\}$
13: $z_{I_1^s j} = 0$
14: **end if**
15: **end for**
16: **for all** $j \in J^{I_1^s}$ **do**
17: $I^j = sort(\arg\min_{i \in \mathcal{I}}(SL_{ij}))$
18: **for all** $i \in I^j$ **do**
19: $BL_i^N = BL_i + SL_{ij}$
20: **if** $L_i^N \leq \rho$ **then**
21: $BL_i = BL_i^N$
22: $z_{ij} = 1$
23: *break*
24: **end if**
25: **end for**
26: **end for**
27: **if** $z_{ij} = \emptyset$, $\exists j \in J^{I_1^s}$, $\forall i \in \mathcal{I}^a$ **then**
28: $z_{ij} = z_{ij}^P$, $\forall i \in \mathcal{I}$, $\forall j \in \mathcal{J}$
29: $I^a = I^a \bigcup I_1^s$
30: **end if**
31: $I^s = I^s \setminus I_1^s$
32: $BL_i = \sum_{j \in \mathcal{J}} SL_{ij} * z_{ij}$, $\forall i \in \mathcal{I}$
33: **end while**

Figure 4.13. BS switch on/off algorithms: Hybrid algorithm.

The second algorithm (Figure 4.13), called hybrid, also considers traffic rates in addition to the battery status. To implement this new adaptation, we have to make two changes in the first algorithm. First, the new algorithm orders the BSs according to a new parameter. The fifth line shows this parameter, which is the summation of the square of the remaining renewable energy ratio in the battery of a BS i ($\left[\frac{b_i^{BS}}{\beta_i^{BS}}\right]^2$) and the system load of this BS (BL_i). Second, since the system loads of the BSs

change after each switch off decision, the algorithm orders the BSs in each iteration. Figure 4.14 shows the results of this algorithm for some selected time intervals.

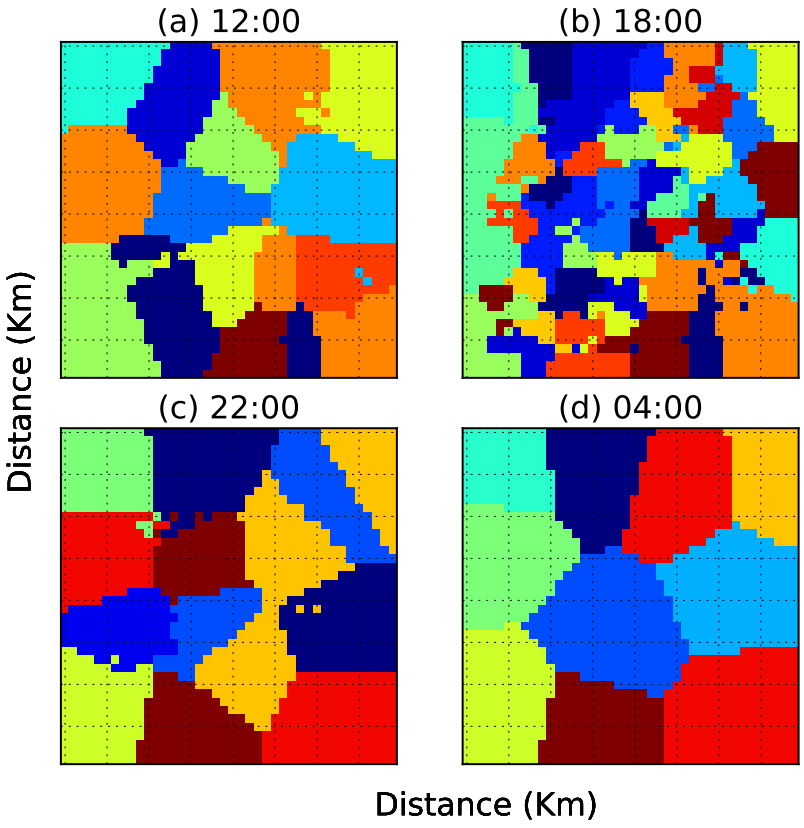


Figure 4.14. Assignment decisions of hybrid algorithm for different time intervals.

4.5. Computational Experiments

The performance of algorithms is investigated in a $9km^2$ geographical area that is covered by several macro and micro BSs. The number of BSs in an area depends on the traffic rate in this area, and we repeat the tests for four different traffic rates (Figure 4.15). In addition, Figure 4.6 and Figure 4.7 show the harvested energy distribution of four different cities we use in the tests to analyze the effect of solar radiation on our algorithms. Lastly, we create ten different instances for each traffic and solar radiation rate combination to control the variance of results. Thus, 160 different combinations were run on this platform (Table 4.1). The system used in this analysis is detailed in Section 4.2.

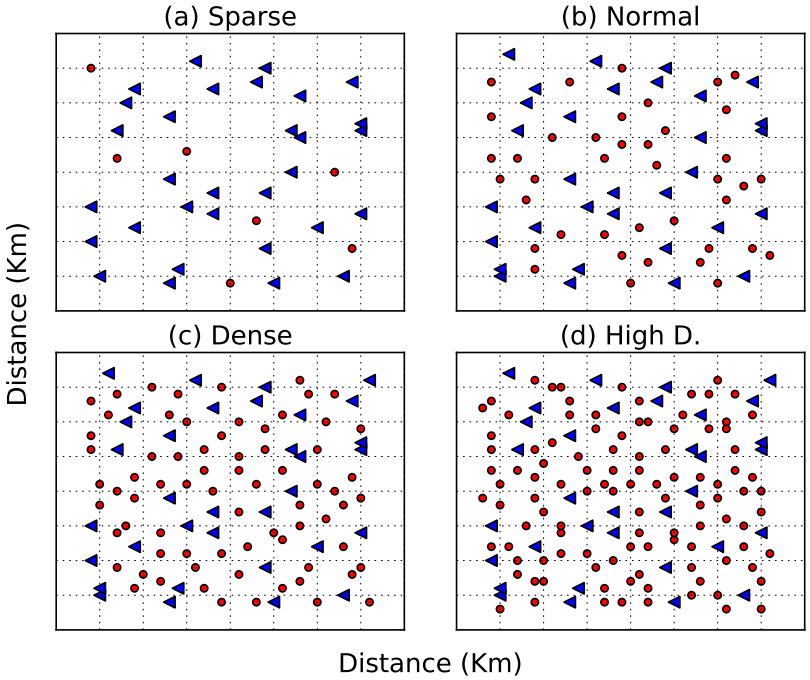


Figure 4.15. The distribution of BSs in different traffic rates. Triangles: macro BSs, circles: Micro BSs.

Table 4.1. HEBRAN test configurations.

Traffic Rate	# BS	Solar Radiation	(kW-day)
Sparse	38	Stockholm	986
Normal	72	Istanbul	1349
Dense	106	Jakarta	1359
High Dense	141	Cairo	1748

Table 4.2. HEBRAN experiment parameters.

Parameter	Unit	Macro BS	Micro BS
E_i^{BSS}	Wh	780	112
E_i^{BSD}	Wh	564	32.76
c^S	\$	1000	1000
c^B	\$	500	500
c^E	\$	0.16	0.16

Table 4.2 shows the test parameters for the energy consumptions and the prices of the system. Auer et al. [77] calculate the value $780Wh$ and $564Wh$ for the static energy consumption of a macro BS and a micro BS, respectively. In addition, they find that the energy consumption of a BS changes linearly with the system load, and this table also shows these slope coefficients. The system pricing is forecasted by expecting to operate the system between 2020 and 2035. Therefore, the expenditure costs are calculated for 2020, in which the price of a solar panel is projected to drop to 1$ per Watt-hour [91], and the price of a lithium-ion battery is expected to drop by 0.2$ per Watt-hour [9, 86]. Besides, the price of grid electricity is the average price between 2020 and 2035, in which we also consider the increase in the price of 4% per annum, according to [92]. Lastly, the channel model for macro and micro BSs are chosen as Urban-Macro (UMa) and Urban-Micro (UMi) NLOS cell scenarios from the ITU-R Report [75]. The parameters used to calculate the path loss are listed in Table 4.3.

Table 4.3. HEBRAN channel model parameters.

Explanation	Parameter	Value
The Carrier Frequency	f_c	1.9 GHz
The Channel Bandwidth	BW_i	20 MHz
Street Width	W	20 m
Avg. Build Height	h	20 m
BS Height	h_{bs}	20 m
User Equipment Height	h_{UT}	1.5 m
Tx Power of Macro BSs	P_i^{tx}	20 W
Tx Power of Micro BSs	P_i^{tx}	6.7 W

One of the main goals of our design is to find an online algorithm to reduce the electrical grid energy consumption cost. For this purpose, we proposed two algorithms in the previous section. We compare these two algorithms with a well-known switch on/off algorithm proposed by Niu et al. [66]. The main idea of this algorithm is to switch off as many BSs as possible based on their traffic loads. Figure 4.16 shows the performance of the algorithms in different test configurations[4] . A number of issues can

[4]We should notice that the size of the solar panels and the batteries in Figure 4.16 and Figure 4.17 are determined by using the sizing heuristic algorithm. Also, the results are the average of ten instances in each test configuration.

be identified by this figure. First, the TCO of the system sharply drops with increasing solar radiation. This is a noticeable result; the more solar radiation provides the more renewable energy generation and yields lower on-grid energy consumption. Second, the normalized TCO of the system, which is the cost of the system to serve each megabit in one kilometer-square per day, remarkably decreases with the rising traffic rates. This finding provides important support for using RESs in urban sectors, in contrast to the common tendency of using RESs in rural sectors. Lastly, the hybrid algorithm performs better than the grid system in any traffic rate and solar radiation combinations. This result shows that investing in a HEBRAN is cost-efficient for different cities around the world, which have different traffic rates and solar radiation.

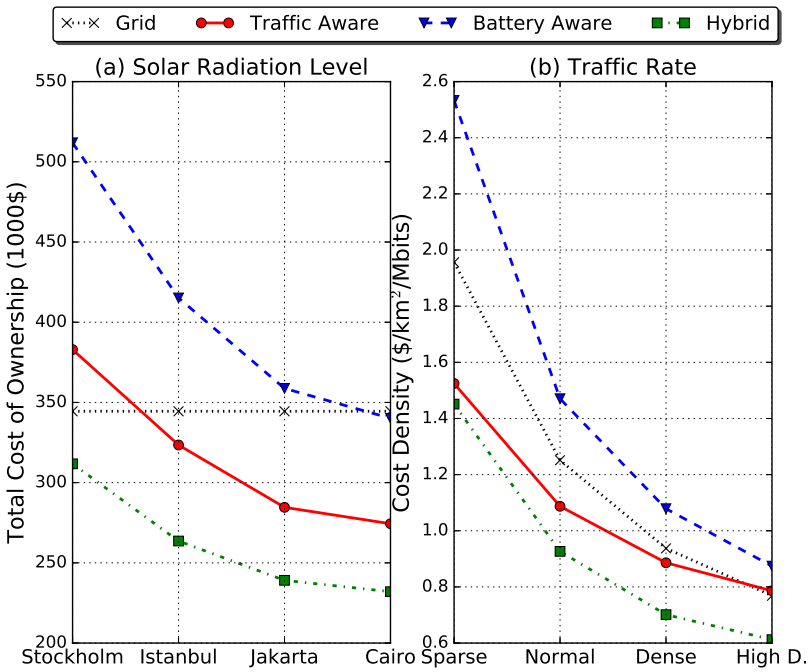


Figure 4.16. Solar radiation and traffic rates impact on online algorithms.

If we now focus on the comparison of the algorithms, for each solar radiation and traffic rate, the hybrid algorithm is far better than the other two online algorithms. Figure 4.17, which shows the nominal expenditure of our two algorithms according to the Niu et al. algorithm (traffic-aware algorithm), demonstrates that the hybrid algorithm outperforms the Niu et al. algorithm in all test cases in the range 10% to 30%. While this superior performance does not significantly change with the increasing solar radiation, it gradually increases according to the rising traffic rates. This result

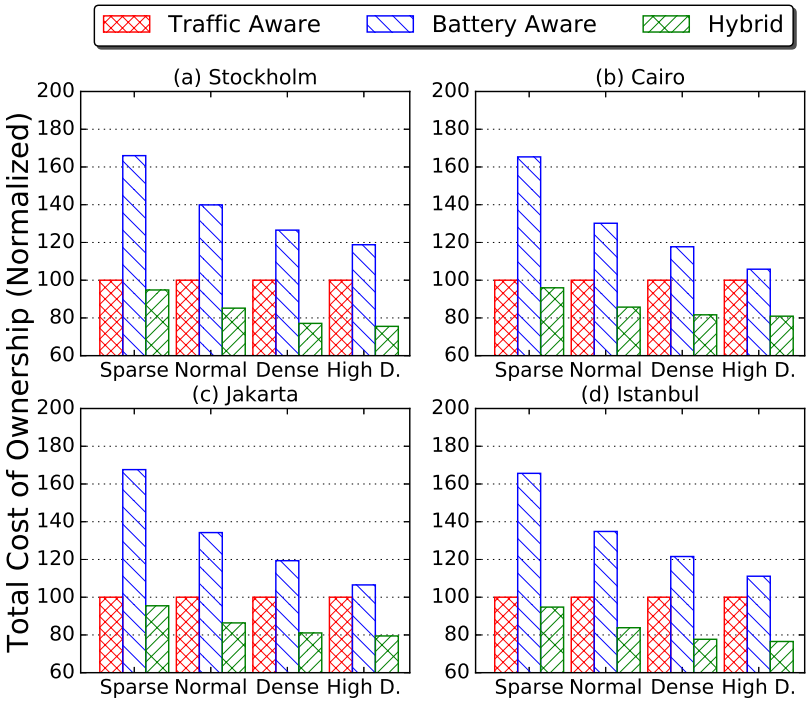


Figure 4.17. Comparison of online algorithms in different configurations.

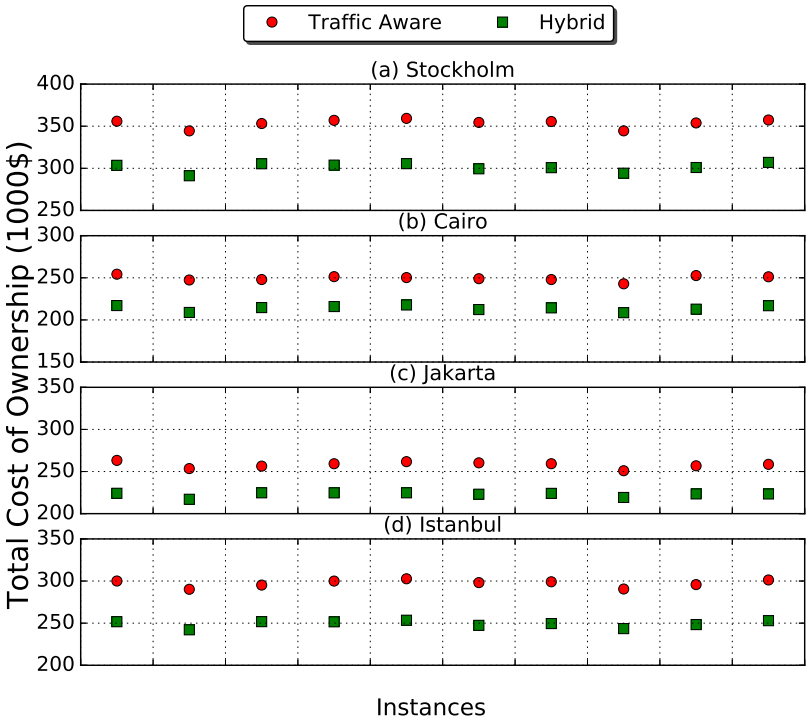


Figure 4.18. Instance based comparison of traffic aware and hybrid algorithms. (Normal Traffic Rates)

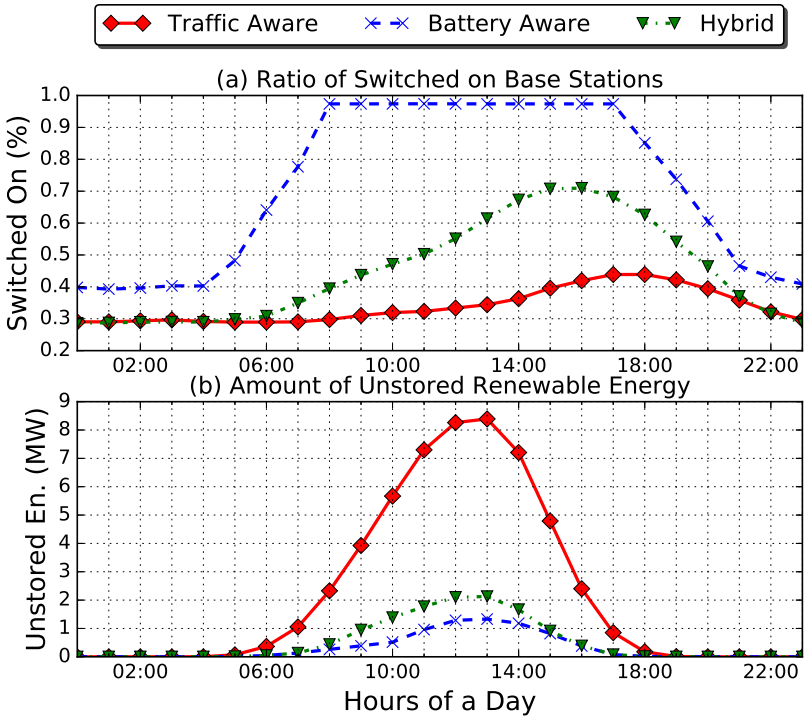


Figure 4.19. Comparison of online algorithms in a day period (Istanbul - sparse traffic).

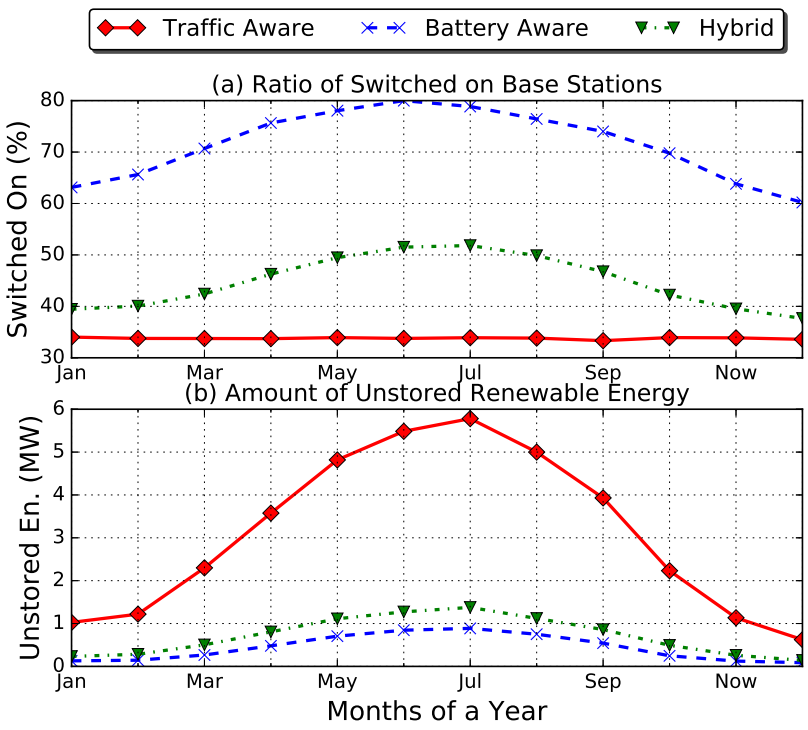


Figure 4.20. Comparison of online algorithms in a year period (Istanbul - sparse traffic).

yields that our novel algorithm further boosts the idea of using RESs in crowded urban regions. Lastly, Figure 4.18 shows that the hybrid algorithm surpasses the Niu et al. algorithm in all instances.

Turning now to the performance of the battery-aware algorithm, Figure 4.17 provides two essential findings. First, despite the improving performance in higher traffic rates, it could not reach the performance of the standard and hybrid algorithms. That poor performance can be seen in Figure 4.19, which shows that this algorithm has a higher ratio of switched-on BSs during a day period, which addresses that the BSs operated with this algorithm could not adapt to the traffic loads efficiently. Second, the battery-aware algorithm provides better performance in the cities that receive more steady solar radiation in different months. The main reason for this result can be demonstrated in Figure 4.20. Figure 4.20a shows that the variation of the number of switched on BSs between different months is significantly high (more than 20%) for the battery-aware algorithm, which means that the battery-aware algorithm is more fragile for the change of solar radiation. Figure 4.20b shows that in the summer months, the battery-aware algorithm reduces the unstored energy significantly, which is the main benefit of this algorithm, as we mentioned earlier. In overall, the battery-aware algorithm yields some cost benefits due to the efficient battery usage, but it has a lack of adaptation to the changes in solar radiation and traffic rates. To sum up, our hybrid algorithm provides a balance between the adaption to the traffic fluctuations and battery utilization; thus, it gives better results to reduce the TCO.

To investigate our sizing heuristic algorithm's performance, we compare it with the results of a MILP Solver, Gurobi. [89]. As mentioned in Section 4.2.4.2, the time-coupling property of the original model prevents us from solving it in a MILP Solver. Therefore, we have to use a reduced model in the MILP Solver in which the BSs should have used their remained renewable energy in a day period. In addition, we have to reduce the number of the time intervals to the 96 (4 days, by using the average solar radiation rates and the traffic rates in a season) to find a solution in a reasonable time in Gurobi. Finally, we run the solver for 14 hours to compare it with our heuristic,

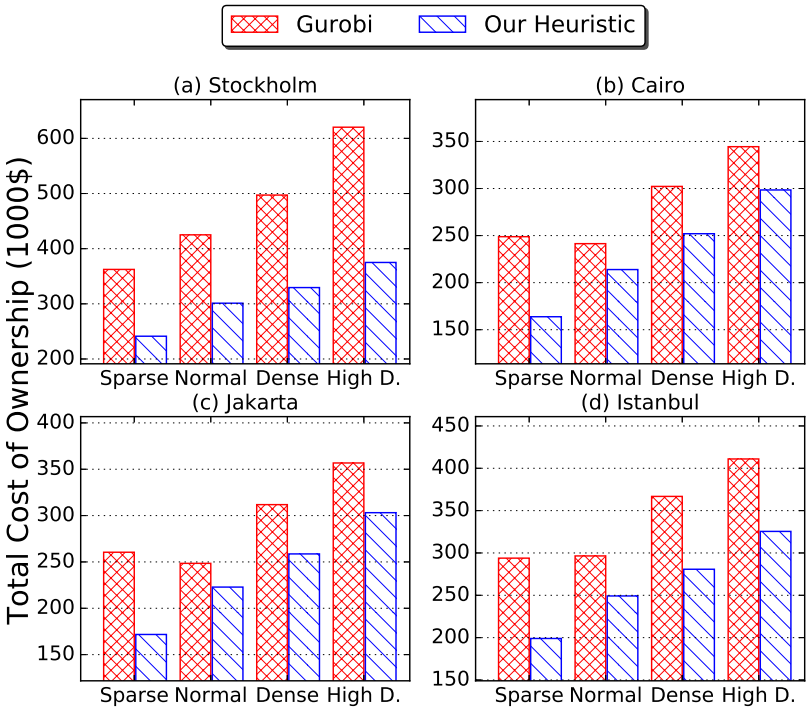


Figure 4.21. Comparison of the TCO with Gurobi solution.

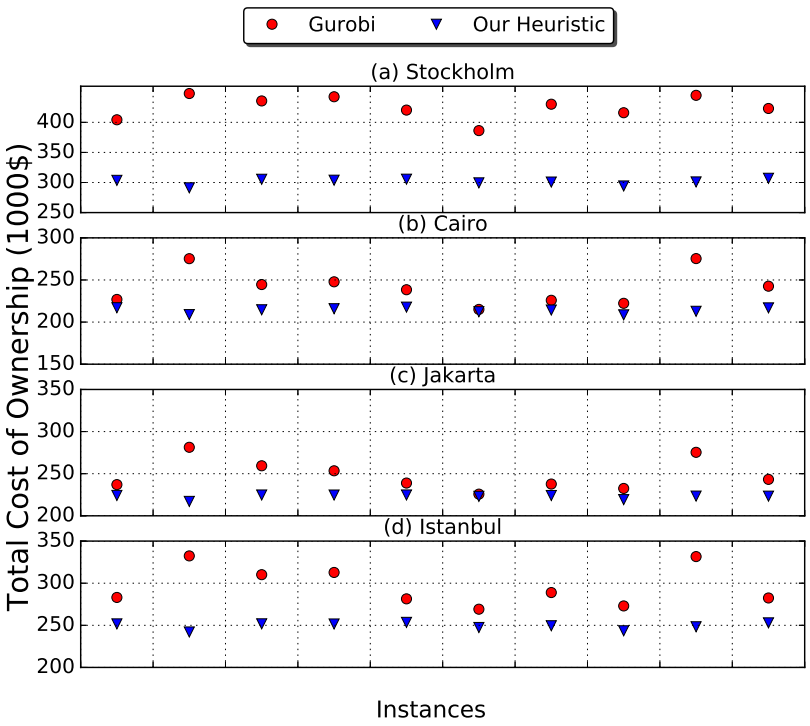


Figure 4.22. Instance based comparison of the TCO with Gurobi solution (normal traffic).

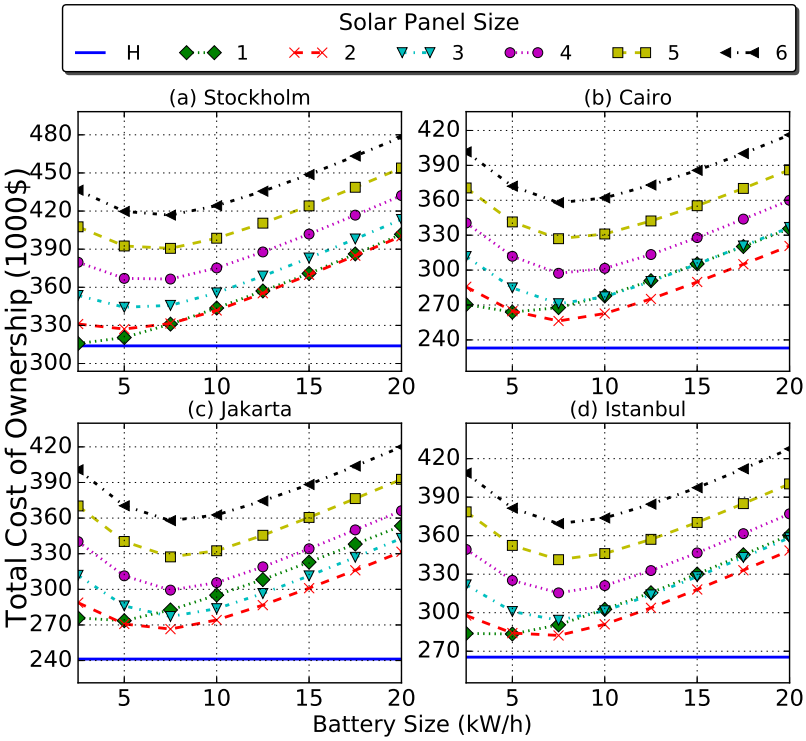


Figure 4.23. Comparison of the TCO in different solar radiations.

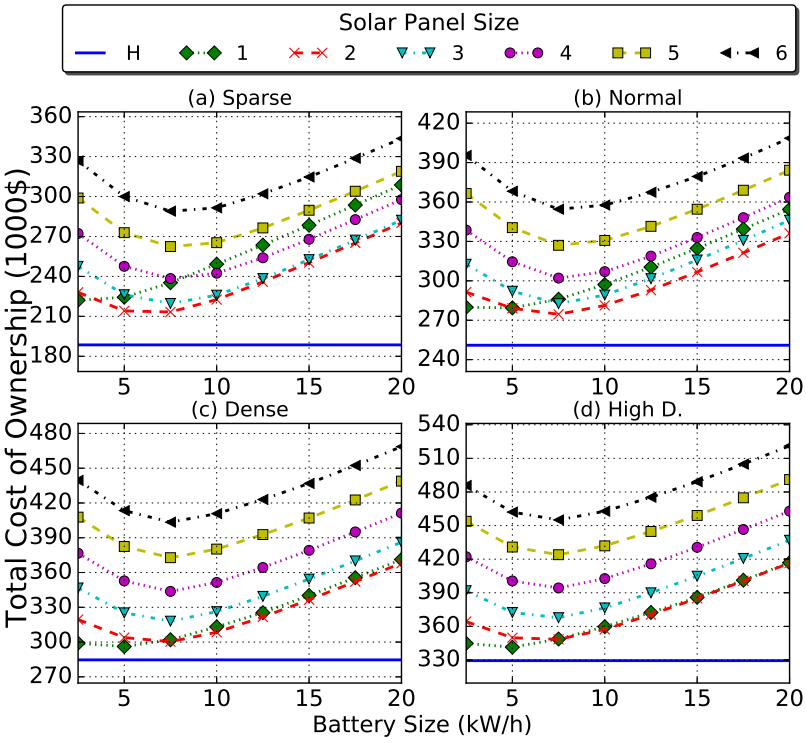


Figure 4.24. Comparison of the TCO in different traffic rates.

which finds the solution in less than 30 minutes on the same computer[5] . Figure 4.21 shows that we can come up with better solutions for all traffic rates and solar radiation we studied[6] . Moreover, Figure 4.22 shows that the heuristic surpasses GUROBI in all instances for normal traffic rate[7] for the given running time (14 hours).

Our sizing heuristic also outperforms the systems with the identical size solar panels and batteries in any solar radiation rate (Figure 4.23) and the traffic rate (Figure 4.24). Those results can encourage the MNOs to employ our heuristic with the historical solar radiation and traffic data to decide on the size of solar panels and the size of batteries to reduce their TCO. On the other hand, these two figures provide us valuable information about the correlation between the size of solar panels and cities/traffic rates. For example, in Stockholm, where the solar radiation rate is very low and its variation is very high (Figure 4.7), the smaller solar panels provide more profit to an MNO (Figure 4.23). However, we could not find a strong correlation between the increasing solar radiation and the solar panel sizes by comparing the results of the other cities. Another result is that the smaller solar panels are more cost-efficient in the test cases that have higher traffic rates. The main reason for this outcome is the higher amount of BSs in these sectors, thereby increasing CapEx. This result can be seen more easily in Figure 4.24 which shows the TCO according to the mean values of four cities. In the subfigures 4.24c and 4.24d for higher traffic rates, the offsets between the consecutive solar panel sizes are larger than subfigures 4.24a and 4.24b, which means that the reducing amount of OpEx could not compensate the increasing amount of CapEx in the higher traffic rates.

4.6. Discussion

Increasing electrical energy costs force the mobile network industry to focus on energy-efficient solutions. Besides, reducing the carbon emission rates is an emerging

[5]Please note that all test cases have been executed on a supercomputer (Nvidia DGX-1 Station [93]) with a Dual 20-Core Intel Xeon E5-2698 v4 2.2 GHz.

[6]As mentioned before, the hybrid algorithm outperforms the other two algorithms in any test case. However, we present only the sizing results that use the hybrid algorithm as an online algorithm.

[7]Our heuristic surpasses the MILP solution in all instances for any traffic rate.

issue for RANs. This chapter describes a new type of RAN in which the BSs in this network has a connection to the electrical grid and have their own solar panel and battery. We formulate an optimization problem that aims to reduce the TCO in this network and propose a framework for the solution. In our solution, we describe several algorithms that target to find both the ideal solar panel and battery sizes in the BSs and the ideal schedules for these BSs to reduce the electrical grid cost of the MNO.

The results show that our sizing algorithm is more efficient than the MILP solver in all cases we studied given extended run times for the solver. This algorithm also outperforms the systems in which the size of solar panels and batteries are identical. Our hybrid switch on/off algorithm manages the renewable energy in the batteries of the BSs in an efficient way and get benefits from the data traffic variation in a RAN to reduce the on-grid electricity. Interestingly, the results show that HEBRAN provides better results with the increasing traffic rates. In conclusion, our framework and proposed algorithms reduce the TCO and provide an environmental network; thus, they support the usage of the RESs by an MNO, especially in the urban sector of a city.

5. REDUCING OPERATIONAL EXPENDITURE OF A HYBRID CLOUD RADIO ACCESS NETWORK

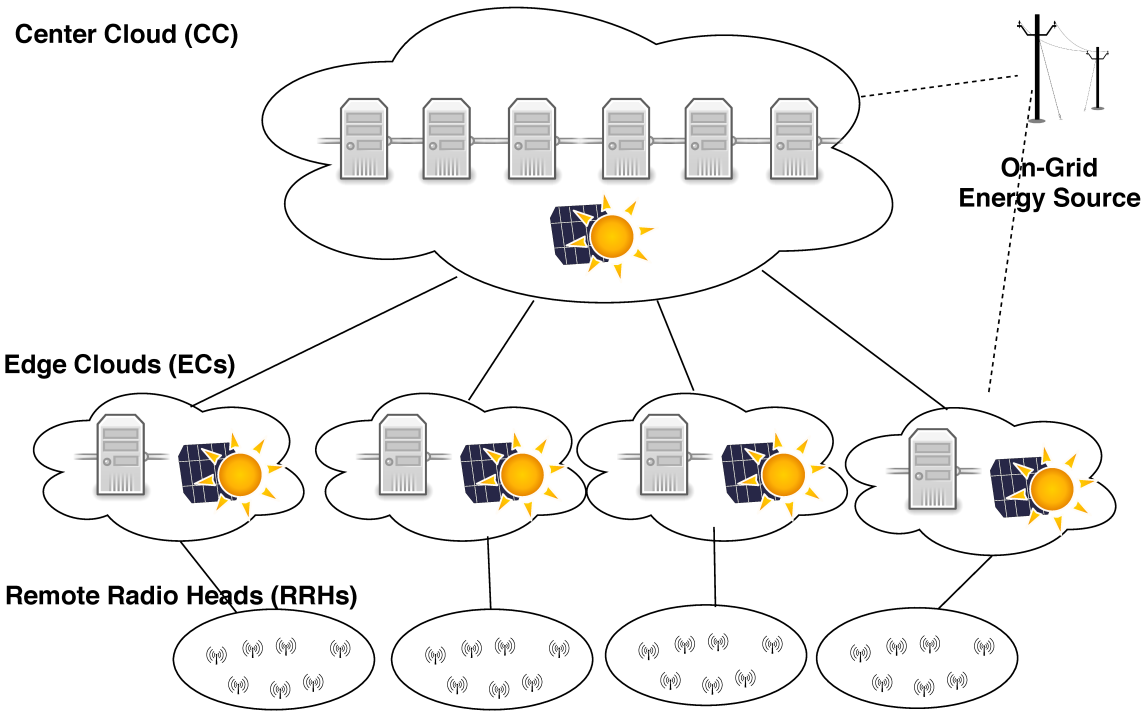


Figure 5.1. Green hybrid C-RAN system model.

5.1. Introduction

Several network models are proposed for function splitting methods in a C-RAN. The common idea of these models is to process some BBU functions near to the mobile user/equipment. Therefore, this architecture supports reducing the end-to-end delay and the required fronthaul bandwidth between the analog unit and the centralized BBU pool. In this chapter, we introduce a hybrid C-RAN model, in which some of the functions processed in an edge cloud (EC) as an alternative to the center cloud (CC). In addition, we will use RES in these clouds for additional energy-saving and cost optimization for an MNO. To the best of our knowledge, this study, which is also accepted by Mobile Networks and Applications [94], is the first to formulate an optimization problem that aims to reduce the OpEx in this C-RAN by formal function splitting decisions. The main contributions of this chapter are as follows:

(i) While there are separate studies that focus on function splitting and using RESs in wireless networks, our study is the first one that uses RESs in a hybrid C-RAN architecture.

(ii) We formulate an online problem that aims to reduce OpEx of this new architecture. We present that in this network, we have to make decisions to split functions by considering to use RESs efficiently.

(iii) While MILP solvers produce reasonable solutions for this problem in a small RAN, they are not suitable for large RANs. Thus, we introduce a heuristic approach for larger RANs.

(iv) We test our methods for different traffic loads and solar radiation rates. Besides, we use real solar data and test our methods for different seasons to see the effect of seasonal changes in four different geographical areas in the world. We demonstrate the performance of our method in different locations with significantly different solar radiation patterns.

(v) We provide a feasibility study to show the profitability of the green systems in a hybrid C-RAN architecture.

The remainder of this chapter is organized as follows. We describe this new type of C-RAN and its cost optimization problem in the second and third sections, respectively. In the fourth section, we explain a heuristic approach for large RANs. In the fifth section, we provide the results, and in the last section, we discuss the results.

5.2. Green Hybrid Cloud Radio Access Network Model

Figure 5.1 shows the network architecture. In a classical RAN, BBU functions physically exist in one place. In this architecture, we break the chain of these functions in two certain split points and perform them in three layers, which are CC, ECs, and RRHs. We may divide these functions into two main groups, cell-related functions (CRFs) and user-related functions (URFs) [36]. In this architecture, the chain of cell-related BBU functions may be broken between the RRH and EC. Then, they are operated either in an RRH or in an EC. This decision depends on the preferences of

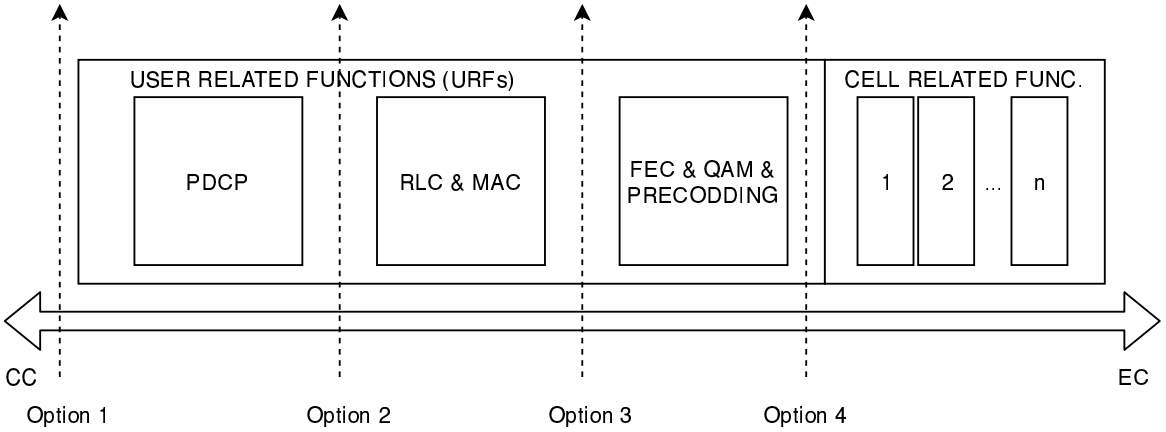


Figure 5.2. Splitting options of green hybrid C-RAN system.

the MNO. According to Small Cell Forum, splitting after CRFs reduces the required midhaul bandwidth significantly [12, 95]. Therefore, to reduce the required midhaul bandwidth, the CC does not process CRFs in our network architecture. Besides, splitting after CRFs have multiplexing benefits because the interface and processing rates for URFs depend on the user traffic loads [11, 35].

URFs may operate in the ECs or the CC, and this chapter concentrates on these decisions. We have four different splitting options in the CC (Figure 5.2) :

(i) CC does not process any URF. This option literally yields a distributed RAN which does not have any C-RAN benefit but very efficient for a user traffic demand which have extremely strict delay requirement.

(ii) CC processes only Packet Data Convergence Protocol (PDCP). The functions in this protocol are not very strict about delay requirements. Besides, centralizing the PDCP functions promotes mobility across the ECs [12].

(iii) CC processes Radio Link Control (RLC) and Medium Access Control (MAC) in addition to the PDCP. Thus, it processes all URFs in the MAC layer and above. This option is more strict in terms of delay, but have several centralization advantages such as allowing traffic aggregation [96].

(iv) CC processes Forward Error Correction (FEC), Quadrature Amplitude Modulation (QAM), and precoding processes, which means that it processes all URFs, including the physical layer functions. This split is the most energy-efficient op-

tion in this paper, but the delay requirement should be very non-stringent.

In addition to these splitting points, there are also other splitting point options that may be chosen according to MNO's requirements [12]. Briefly, the more URFs are processed in the CC, and the more energy-saving will be provided by MNOs. However, we increase the required bandwidth and end-to-end latency with the extension in centralization [38].

The traffic model in this chapter is explained in Section 4.2.1 in detail. The main traffic modeling difference between the two chapters is due to the mapping of the traffic profiles which have different peak hours to mimic different districts of a city. These profiles were mapped to the geographical regions in the previous chapter, on the other hand, they are mapped to a particular EC in this chapter.

The renewable energy system model is also elaborated in Section 4.2.4. In the model in this chapter, we also introduce an additional option for MNOs. As seen in Figure 5.3, an MNO may also sell the excessive renewable energy to the grid with a penalty price. The energy source controller determines the energy source that is used to supply the cloud station. This component is critical for reducing the OpEx which is explained in the next section. The energy consumption in a station has two elements; the first one is the static energy consumption, which does not change by the amount of processing activity in this station, such as cooling the system. The other one is the dynamic energy consumption that depends on the number of active digital units (DUs)[8] in this station. Equations 5.1 and 5.2 calculate the total energy consumption in a CC and ECs, respectively. In these equations, E^{CCS} and E^{CCD} state the static and dynamic energy consumptions, and a_{dt} is a binary decision variable state which

[8]A DU is a processing unit in a cloud that processes the functions of a classic BBU.

equals to one if DU d is active in time interval t.

$$E_t^{CC} = \left[E^{CCS} + \sum_{d \in \mathcal{D}^{CC}} a_{dt} E^{CCD} \right] \tag{5.1}$$

$$E_{rt}^{EC} = \left[E^{ECS} + \sum_{d \in \mathcal{D}_r} a_{dt} E^{ECD} \right] \tag{5.2}$$

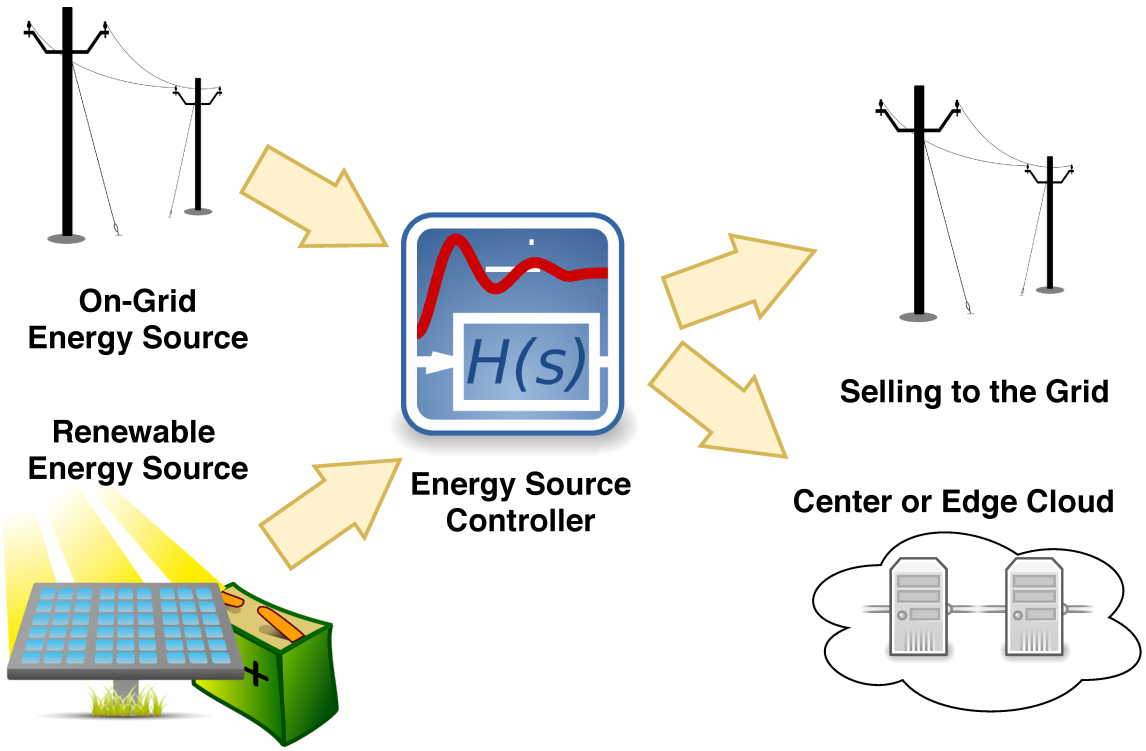


Figure 5.3. Green hybrid C-RAN energy model.

5.3. Green-Aware Function Splitting Optimization Problem

The objective function points that we have to consider three significant actions to reduce the cost of an MNO (Equation 5.3). The first one is reducing the total energy consumptions in the CC (E_t^{CC}) and ECs (E_{rt}^{EC}). We can achieve that by lowering the number of active DUs in these stations (clouds). The second one is increasing the usage of renewable energy in these stations (s_t^{CC} and s_{rt}^{EC}). This action principally depends

on the size of solar panels and the batteries in these stations and planning the use of renewable energy in these batteries in an efficient way. Alternatively, MNO may sell this valuable energy to the grid network at a reduced price [28].

Minimize:

$$\sum_{t\in\mathcal{T}}\left[E_t^{CC} - s_t^{CC} - \Psi * p_t^{CC} + \sum_{r\in\mathcal{R}}(E_{rt}^{EC} - s_{rt}^{EC} - \Psi * p_{rt}^{EC})\right] * c_t^E \tag{5.3}$$

Subject to:

$$\sum_{f\in\mathcal{F}}\sum_{j\in\mathcal{J}} U_{jt}^{EC} m_{jdft} < \Lambda^{CC}, \qquad \forall d \in \mathcal{D}^{CC}, \forall t \in \mathcal{T} \tag{5.4}$$

$$\sum_{f\in\mathcal{F}}\sum_{c\in\mathcal{C}_r}\sum_{j\in\mathcal{J}_c} U_{jt}^{EC} m_{jdft} < \Lambda^{EC}, \qquad \forall d \in \mathcal{D}_r, \forall r \in \mathcal{R}, \forall t \in \mathcal{T} \tag{5.5}$$

$$M * a_{dt} - \sum_{f\in\mathcal{F}}\sum_{j\in\mathcal{J}} m_{jdft} \geq 0, \qquad \forall d \in \mathcal{D}^{CC}, \forall t \in \mathcal{T} \tag{5.6}$$

$$M * a_{dt} - \sum_{f\in\mathcal{F}}\sum_{c\in\mathcal{C}_r}\sum_{j\in\mathcal{J}_c} m_{jdft} \geq 0, \qquad \forall d \in \mathcal{D}_r, \forall r \in \mathcal{R}, \forall t \in \mathcal{T} \tag{5.7}$$

$$\sum_{f\in\mathcal{F}}\sum_{d\in\mathcal{D}^{CC}\cup\mathcal{D}_r} m_{jdft} = |\mathcal{F}|, \qquad \forall j \in \mathcal{J}_c, c \in \mathcal{C}_r, \forall r \in \mathcal{R}, \forall t \in \mathcal{T} \tag{5.8}$$

$$\sum_{f\in\mathcal{F}}\sum_{d\in\mathcal{D}^{CC}} m_{jdft} < \delta_{jt}, \qquad \forall j \in \mathcal{J}, \forall t \in \mathcal{T} \tag{5.9}$$

$$b_t^{CC} = b_{(t-1)}^{CC} - s_t^{CC} - p_t^{CC} + \alpha^{CC} G_t^{CC}, \qquad \forall t \in \mathcal{T} \tag{5.10}$$

$$b_{rt}^{EC} = b_{r(t-1)}^{EC} - s_{rt}^{EC} - p_{rt}^{EC} + \alpha_r^{EC} G_{rt}^{EC}, \qquad \forall r \in \mathcal{R}, \forall t \in \mathcal{T} \tag{5.11}$$

$$b_t^{CC} \leq \beta^{CC}, \qquad \forall t \in \mathcal{T} \tag{5.12}$$

$$b_{rt}^{EC} \leq \beta_r^{EC}, \qquad \forall r \in \mathcal{R}, \forall t \in \mathcal{T} \tag{5.13}$$

$$s_t^{CC} \leq E_t^{CC}, \qquad \forall t \in \mathcal{T} \tag{5.14}$$

$$s_{rt}^{EC} \leq E_{rt}^{EC}, \qquad \forall r \in \mathcal{R}, \forall t \in \mathcal{T} \tag{5.15}$$

The third one is that we have to consider the changing electricity prices in a day period (c_t^E) to reduce the overall cost of the MNO[9] . The maintenance cost of this green system, which is another component of the OpEx, is not included in Equation 5.3. The reason is that this maintenance cost is a constant value in this system and does not change by any decision variable in this equation. Besides, we provide a feasibility analysis in the results section which considers the maintenance cost of the renewable system.

DUs have limited capacities (Λ^{CC} and Λ^{EC}) to execute URFs (m_{jdft}). Inequalities 5.4 and 5.5 show this limitation in CC and ECs, respectively. According to Mharsi et al., the processing requirement of user functions depend on the traffic loads [39]. Therefore, we also add the traffic load of each user (U_{jt}^{EC}) in these inequalities.

As we mentioned before, we try to minimize the number of active DUs (a_{dt}) to reduce the total energy consumption. However, we have to activate a DU, if it is used for processing a user function (m_{jdft}). Inequalities 5.6 and 5.7 provide this relation for CC and ECs, respectively. Inequality 5.8 guarantees another critical constraint which provides that DUs in both cloud side process all demanded URFs ($|\mathcal{F}|$) of each user. End-to-End delay is essential for QoS and Inequality 5.9 bounds the delay for each user with a threshold δ_{jt} [10] .

The amount of the green energy we can use in a station depends on the remaining energy in the battery from the previous time interval ($b_{r(t-1)}^{EC}$), consumed green energy ($s_{r(t)}^{EC}$), the sold energy to the grid ($p_{r(t)}^{EC}$) and generated renewable energy ($\alpha_r^{EC} G_{rt}^{EC}$). Inequalities 5.10 and 5.11 provide this relation by calculating the remaining energy in the batteries of CC and ECs, respectively. The limited capacity of the batteries (β_r^{EC}) is another important restriction of using green energy in the network and Inequalities 5.12 and 5.13 show this limitation for CC and ECs. Lastly, it is clear that the consumed

[9]We have to notice that this is an online problem, the bandwidth between the ECs and CC is already leased before the splitting decisions. Therefore, minimizing the bandwidth is not considered in this problem.

[10]The computing costs are assumed the same for each URF. Therefore, deciding the number of URFs in one cloud side provides us a certain splitting point in the chain of the URF.

green energy (s_{rt}^{EC}) should not be higher than the required energy in a station (E_{rt}^{EC}). Inequalities 5.14 and 5.15 provide this limitation for CC and ECs, respectively.

This problem involves the bin packing problem [38]; thus, it is an NP-Hard problem, and we use a MILP Solver for up to certain size problems and provide a novel heuristic approach to find a solution for larger RANs. This heuristic is explained in the next section.

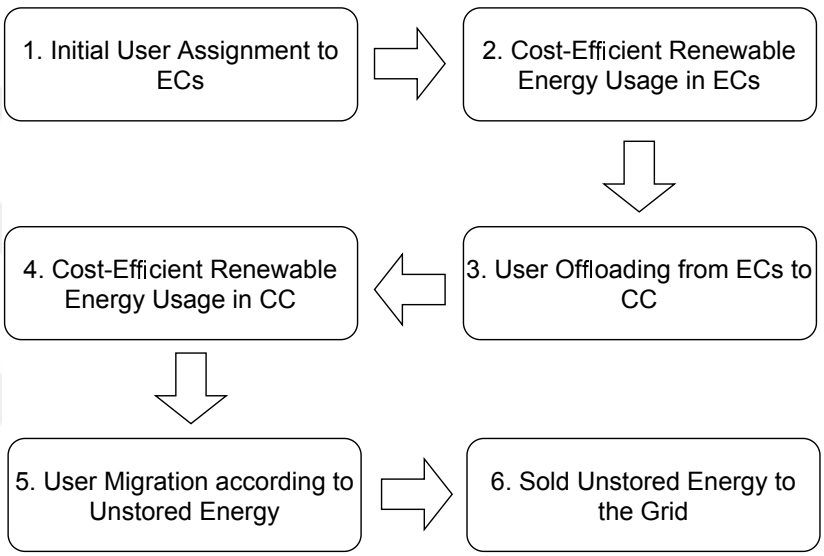


Figure 5.4. Heuristic: Main algorithm.

5.4. A Heuristic Approach for Green Energy-Aware Function Splitting Optimization Problem

Figure 5.4 shows the main steps of the heuristic. The first step is that the initial assignment of the user functions to the ECs shown in Figure 5.5. This algorithm runs for each EC separately; thus we omit the cloud indices for the presentation simplicity. The notation $L\hat{U}D$ represents loads of the DUs. At the beginning of the algorithm, DUs do not serve any user function; thus loads of DUs are initialized with zero. Then, we assign each user function to a DU in an ascending order ($m_{jdf} = 1$). If a DU load gets full, we increase the index (d) and assign this user function to the next DU. After we finish the assignment of user functions to the DUs, we check the activity of the DUs in this cloud. If a DU serves any user function, we switch on this DU $a_d = 1$. The

complexity of this algorithm is $O(\frac{|J|}{|R|}|F| + \frac{|D|}{|R|}\frac{|J|}{|R|}|F|)$. We have to run this algorithm for each time interval and each EC. Thus, the total complexity of the first step equals to $O(\frac{|J|}{|R|}|T||D||F|)$.

```
1: Given: U^EC, r
2: Output: m̂, â, LÛD
3: d = 0, LÛD = Ô
4: for all j ∈ J_r do
5:    for all f ∈ F do
6:       if LÛD + U_j^EC ≤ Λ^EC then
7:          d = d + 1
8:       end if
9:       LÛD_d = LÛD_d + U_j^EC
10:      m_jdf = 1
11:   end for
12: end for
13: for all d ∈ D_r do
14:   for all j ∈ J_r do
15:      for all f ∈ F do
16:         if m_jdf = 1 then
17:            a_d = 1
18:         end if
19:      end for
20:   end for
21: end for
```

Figure 5.5. Heuristic: Initial user assignment to ECs.

In the second step, we make the decisions of using renewable energy for each ECs (Figure 5.6). Notice once again that we omit the cloud indices for presentation simplicity. The notation $T\hat{E}C$ represents the total energy consumption, which is the summation of the grid and renewable energy consumptions in each time interval. The notation $R\hat{E}S$ represents the amount of the reserved energy for each time interval. This vector variable is the fundamental concept of this algorithm which provides us to use the renewable energy in the most profitable time interval without violating the physical constraints of the solar panel and the battery in the renewable energy system of an EC.

The algorithm starts with sorting the time intervals by considering the electricity prices in these time intervals. Then, by starting with the highest priced time interval, we check whether the $R\hat{E}S$ equals to the initial value or not. A previous assignment to

the $R\hat{E}S$ means that for a later time interval of a day, we need to reserve the renewable energy of this time interval; thus, we restrict the usage of renewable energy in this situation. Otherwise, available energy $availableEn$ equals to the generated renewable energy in this time interval. In the next step, we sum the available energy and the remaining energy in the battery to find the permitted renewable energy ($nextB$) that we can use in this time interval. Besides, between lines 16-20, we restrict the usage of renewable energy by the total energy consumption for avoiding unnecessary renewable energy consumption.

```
1:  Given: T̂EC, b̂, PrevDayEn
2:  Output: ŝ, b̂
3:  d = 0, L̂UD = 0̂, R̂ES = MAGIC_NUMBER
4:  T^s = sort(arg max_{t∈T}(c_t^E))
5:  for all t ∈ T^s do
6:      if R̂ES_t = MAGIC_NUMBER then
7:          availableEn = G_t
8:      else
9:          availableEn = − max(R̂ES_t, 0)
10:     end if
11:     if t=0 then
12:         nextB = PrevDayEn + availableEn
13:     else
14:         nextB = b_{t−1} + availableEn
15:     end if
16:     if nextB ≥ T̂EC_t then
17:         s_t = T̂EC_t
18:     else
19:         s_t = nextB
20:     end if
21:     for t^l := t to | T | do
22:         Update(b_{t^l})
23:     end for
24:     if t ≠ 0 then
25:         demandedEn = max(s_t − G_t, 0)
26:         for t^p := t − 1 to 0 do
27:             if R̂ES_{t^p} = MAGIC_NUMBER then
28:                 R̂ES_{t^p} = demandedEn − G_{t^p}
29:                 demandedEn = demandedEn − G_{t^p}
30:             else
31:                 R̂ES_{t^p} = R̂ES_{t^p} + demandedEn
32:             end if
33:             if R̂ES_{t^p} ≤ 0 then
34:                 BREAK
35:             end if
36:         end for
37:     end if
38: end for
```

Figure 5.6. Heuristic: Cost-efficient RES usage in a cloud.

After deciding the amount of renewable energy use in this time interval (s_t), we update the remaining energy in the batteries for the later time intervals in the lines between 21-23. Lastly, we update the reserved energy of the previous time intervals of the day in the lines between 24-36. The notation *demandedEn* represents the demanded renewable energy in the previous time intervals. We subtract the generated energy (G_t) on each time interval if we have not used it previously. When the *demandedEn* become non-positive, we stop the loop. In conclusion, with this algorithm, we can freely choose any time interval to use the renewable energy. The remaining energy $\hat{b}$ prevents the use of non-generated renewable energy in the following time intervals and, $\hat{RES}$ precludes the use of reserved energy in the previous time intervals. In overall, the time complexity of the second step equals to $O(|R||T|^2)$.

```
1:  Given: m̂, â, L̂UD
2:  Output: m̂, â, L̂UD
3:  m̂^P = m̂
4:  â^P = â
5:  L̂UD^P = L̂UD
6:  NDU^P = ∑(m_jf)
7:  for d :=| D_r | to 0 do
8:      if a_d ≠ 0 then
9:          if GridConsumptionInEC then
10:             for all j ∈ J_r do
11:                 for all f ∈ F do
12:                     if m_jdf = 1 then
13:                         if DelayCheckOk then
14:                             UserOffloading(j, d, f)
15:                         else
16:                             BREAK
17:                         end if
18:                     end if
19:                 end for
20:             end for
21:         end if
22:     end if
23:     if NDU^P ≤ ∑(m_jf) then
24:         m̂ = m̂^P
25:         â = â^P
26:         L̂UD = L̂UD^P
27:     end if
28: end for
```

Figure 5.7. Heuristic: User offloading decision from ECs to CC.

In the third step, we offload the users from ECs to CC to reduce the grid energy

consumption in ECs and to get benefits of the generated renewable energy in CC. Figure 5.7 shows how to choose the appropriate user function to offload to the CC. We run this algorithm for each EC and the time interval separately. Thus, we omit the cloud and time interval notations in the algorithm for simpler presentation. The idea of this algorithm relies on reducing the number of active DUs in EC. In the first step of the heuristic (Figure 5.5), we assign the user functions to the DUs of EC in an ascending order. Therefore, the highest indexed DUs tend to have lower traffic load ($L\hat{U}D$). Thus, in this algorithm (Figure 5.7), we choose the user functions from the DUs in reverse order. In the loop section, we start to check whether the DU is active or not and if the EC consumes grid energy. If the EC consumes only green energy, we do not have to continue to migrate the user functions to the CC. Then for all user functions, we check that if this user function is assigned to the related DU. Lastly, we check the delay constraint. If we violate the delay constraint, we should not operate this migration.

1: Given: $\hat{m}, \hat{a}, L\hat{U}D, j, d, f$
2: Output: $\hat{m}, \hat{a}, L\hat{U}D$
3: $m_{jdf} = 0$
4: **if** $\sum_{j \in \mathcal{J}} \sum_{f \in \mathcal{F}} m_{jdf} = 0$ **then**
5: $a_d = 0$
6: **end if**
7: **for** $d^{CC} := 0$ **to** $\mid D^{CC} \mid$ **do**
8: **if** $L\hat{U}D_{d^{CC}} + U_j^{EC} \leq \Lambda^{CC}$ **then**
9: $L\hat{U}D_{d^{CC}} = L\hat{U}D_{d^{CC}} + U_j^{EC}$
10: $m_{jd^{CC}f} = 1$
11: $a_{d^{CC}} = 1$
12: BREAK
13: **end if**
14: **end for**

Figure 5.8. Heuristic: User offloading operation from ECs to CC.

If the user function passes from all checks, we run the user offloading operation algorithm (Figure 5.8). First, we disconnect the user function from the DU in the EC. Then, we check if any user function is assigned to this DU. If this DU does not serve any user function, we switch it off to preserve the energy consumption. In the third step, we start to check each DU in CC in ascending order. If the DU capacity is enough to serve this new user function, we provide the assignment operations. Otherwise, we

continue the checking operation by the next DU in CC. After finishing all migrations in an EC, we check whether we reduce the number of active DUs in Line 22. If we fail to reduce it, we reverse all migrations to prevent impractical traffic loads in CC. The computational complexity of this step equals to $O(\frac{|J|}{|R|}|T||D||F||D^{CC}|)$.

```
1: Given: UnstoredEn, m̂, â, LÛD
2: Output: m̂, â
3: for all t ∈ T do
4:    if UnstoredEn_t^CC > 0 then
5:       for all r ∈ R do
6:          if UnstoredEn_rt = 0 then
7:             for all j ∈ J and f ∈ F do
8:                UserOffloading(j, d, f)
9:                if UnstoredEn_t^CC = 0 then
10:                  BREAK
11:               end if
12:            end for
13:         end if
14:      end for
15:   else
16:      for all r ∈ R do
17:         if UnstoredEn_rt > 0 then
18:            for all j ∈ J and f ∈ F do
19:               UserOffloading(j, d, f)
20:               if UnstoredEn_rt = 0 then
21:                  BREAK
22:               end if
23:            end for
24:         end if
25:      end for
26:   end if
27: end for
```

Figure 5.9. Heuristic: User migration decision between the ECs and CC.

In the fourth step of the heuristic, we provide a cost-efficient renewable energy usage in CC. This algorithm is the same algorithm we use for the ECs (Figure 5.6) and it has the same time complexity. In the fifth step (Figure 5.9), we make migration of the user functions in two-way directions (ECs to CC and CC to ECs) according to unstored renewable energy in the batteries of the clouds. If only one side has unstored energy, we migrate the user functions from the other side to this side. The complexity of this step equals to $O(\frac{|J|}{|R|}|T||D||F||D^{CC}|)$. Finally, in the last step of the heuristic, we calculate the sold energy to the grid. This step has a trivial algorithm that directly sells the unstored renewable energy in the batteries of each EC and the CC in each

Table 5.1. Green hybrid C-RAN experiment parameters.

Parameter	Unit	CC Side	EC Side
E^S	Wh	1500	500
E^D	Wh	750	250
Λ	URF	50	15
α	kWh	20	5
β	kWh	20	5
c_t^E	TRY	[0.29, 0.46, 0.70]	[0.29, 0.46, 0.70]
Ψ	-	0.5	0.5

time interval. Its complexity equals to $O(|T||R|)$.

If we now calculate the total complexity of the heuristic, we will find the value $O(\frac{|J|}{|R|}|T||D||F||D^{CC}| + |R||T|^2)$. That result points out that the solution time of the heuristic changes linearly with the increasing number of users, ECs, DUs, and user functions of the network. Also, solution time increases quadratically by the number of time intervals. Thus, this heuristic provides fast solutions for large solution spaces. The computational experiments in the next section, which we compare this heuristic with two MILP models, support this complexity analysis.

5.5. Case Study and Results

We test the system for different solar radiation distributions. We use the empirical data from the pvWatts application to calculate the amount of the generated energy of a solar panel for each time interval [82]. Their 30 years of historical weather data provide us to calculate the detailed solar energy generation rate data of a panel in a cloud station (G_{rt}) for four different cities. They provide each hour of the day data; thus, we can simulate the change of solar energy in several time scales. Figure 4.6 and 4.7 show the change of generated energy of a $4kW$ size of a solar panel for different cities in a day and a year period, respectively. The delay constraints for each user (δ_{jt}) are chosen randomly, uniformly distributed on [0, $\mid \mathcal{F} \mid$]. Table 5.1 shows the other test parameters. The pricing data changes frequently, and there is a significant difference between each city. The pricing data in our experiments comes from Republic of Turkey

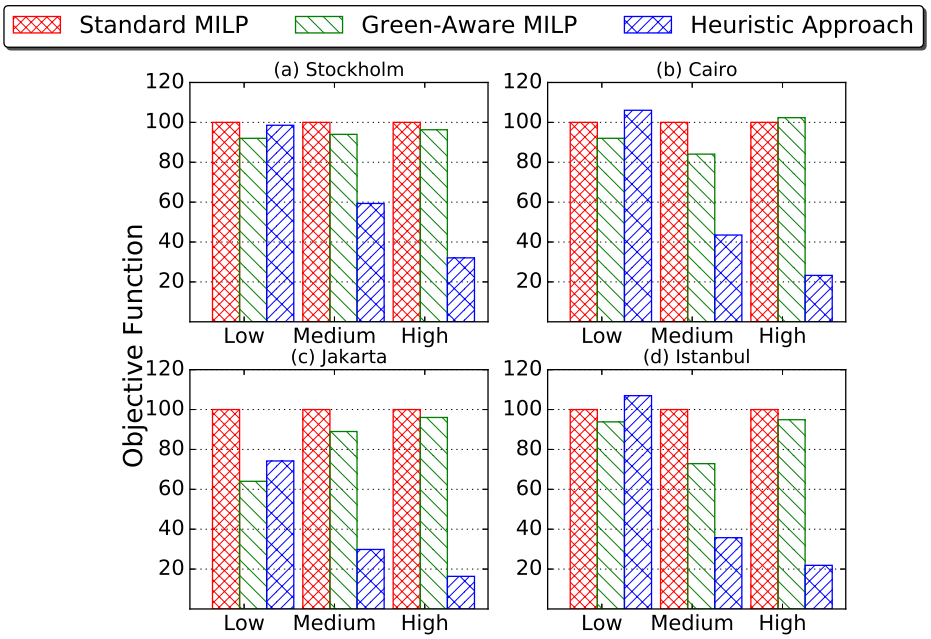


Figure 5.10. Comparing the performance of the methods.

Energy Market Regulatory Authorities (EPDK) [97]. We use different prices according to the time of the day.

In our experimental setup, we study with 20 ECs and 1 CC. Each EC serves 8 RRHs, and each RRH serves 5, 10, or 15 demand points, which are called *Low*, *Medium*, and *High* traffic in the following results. Therefore, we can test the proposed heuristic and MILP solutions with different size RANs. These demand points may represent the user groups that demand the data traffic from an RRH.

Besides the heuristic we explain in the previous section, we use a MILP Solver, Gurobi [89] to solve the green energy-aware function splitting optimization problem. Computation experiments were run on an Nvidia DGX-1 Station [93] with a Dual 20-Core Intel Xeon E5-2698 v4 2.2 GHz. The termination time is chosen as 4 hours. We compare the MILP solution and the heuristic with a standard method in which the energy source controller uses the RES whenever it is available and does not determine the splitting decisions by considering renewable energy.

First, we have to explain the performance of the solver for that size of a problem.

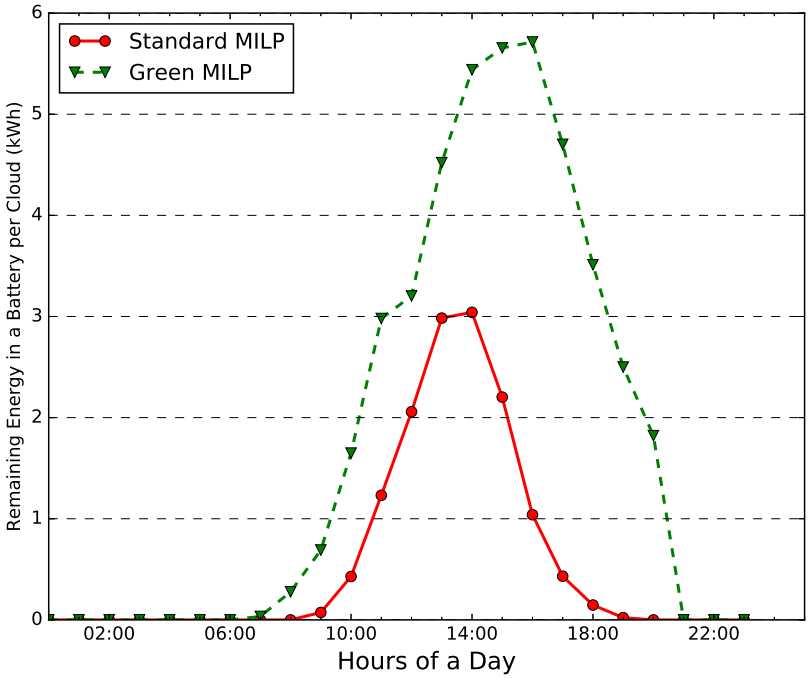


Figure 5.11. Average remaining energy in the batteries of ECs and CC (Jakarta medium traffic).

Gurobi finds the optimum solution only in a low traffic rate and for only the standard MILP model. Green energy-aware MILP has around 5% gap compared to the lower bound in low traffic rate. In medium and higher traffic rates, the gaps with respect to the lower bound were higher than 30% for each model. The reason is that the solution space expands exponentially, and 4 hours time limit is not sufficient to reach the optimum solution. Although we increased the solution time limit to 24 hours, we could not reduce the gap significantly. Besides, we deal with an online problem; we have to find a solution in an hour for a real scenario. Hence, we propose a heuristic to find a faster solution.

Figure 5.10 shows the comparison of each method. If we compare two MILP solutions, it is obvious that green energy-aware splitting decisions provide better results for most of the traffic rates and solar radiation distributions we studied. There are two reasons for that outcome as demonstrated in Figure 5.11. This figure shows the variation of the average remaining energy in the batteries of the clouds (ECs and CC) in a day period for Jakarta and medium traffic rate configuration. The first advantage of green-aware MILP is that it promotes using the remaining energy in more profitable

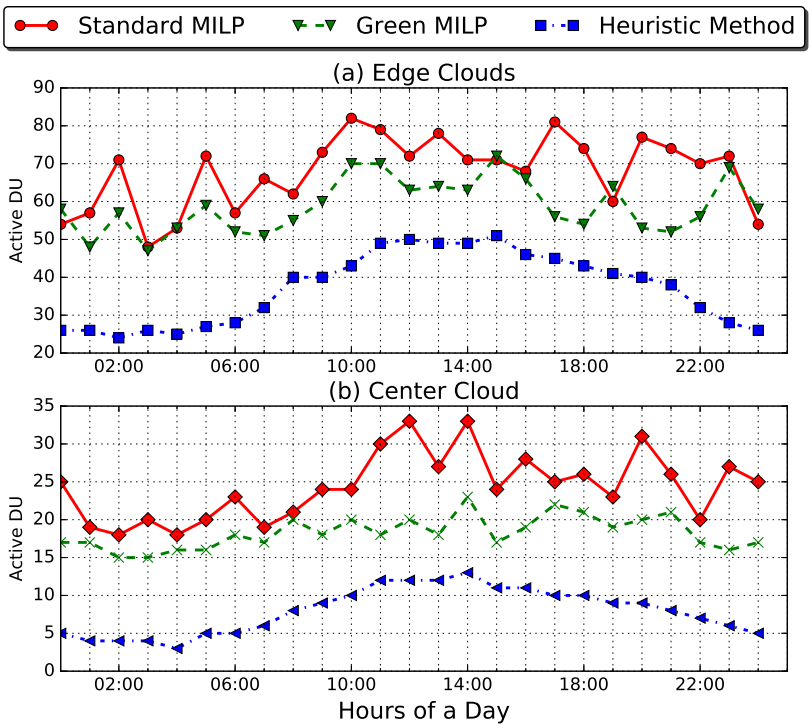


Figure 5.12. Number of active DUs in each cloud in a day period (Istanbul medium traffic).

hours. Second, it provides a better load balance between the CC and ECs, deciding the splitting decisions by promoting the station which has more renewable energy. Thus, it prevents the MNO to sell its renewable energy in a low profitable value. Overall, an MNO may reduce its OpEx by using a green MILP solution.

If we now compare our proposed heuristic and the MILP solutions, Figure 5.10 clearly states that our heuristic approach provides outstanding results for medium and high traffic rates. Figure 5.12, which shows the number of active DUs for medium traffic rate in Istanbul points out that outcome. We may recognize that the number of active DUs in the heuristic solution is lower than both MILP solutions for CC and ECs. As we know from the objective function (Equation 5.3), the number of active DUs directly increases the energy consumption in the clouds and raise the overall OpEx of an MNO. Thus, our heuristic outperforms the MILP solutions by providing better performance to switching off the DUs.

We also analyze the results in a year period. Figure 5.13 shows the consumption

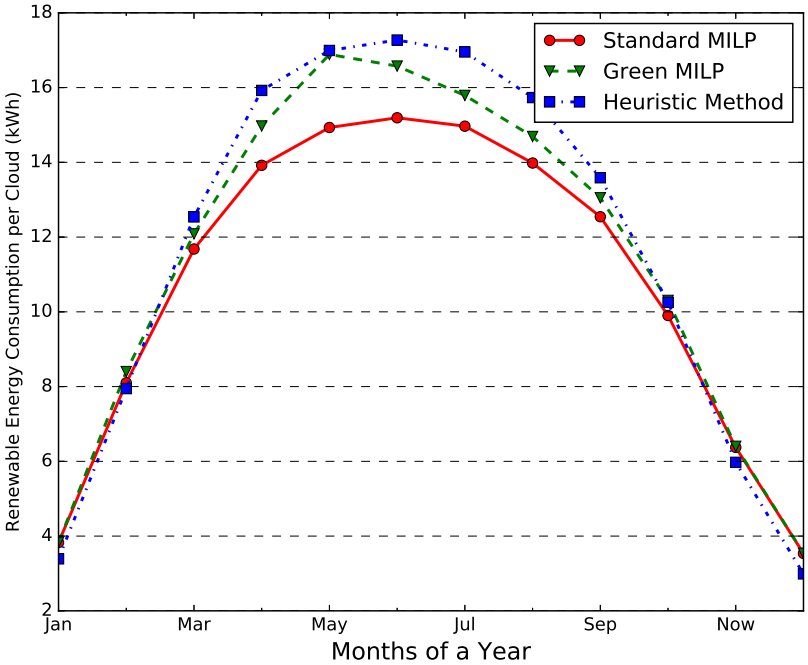


Figure 5.13. Distribution of renewable energy consumption in a year period (Stockholm low traffic).

of renewable energy in a year period. Even though both solutions have the same size of solar panels and batteries, the heuristic approach provides a higher level of renewable energy consumption, especially in summer seasons in Stockholm. This result validates that the heuristic approach is better for promoting renewable energy consumption even in lower-traffic rates. Figure 5.14 demonstrates the distribution of sold energy in a year period for different cities. Stockholm and Istanbul have a significant variation between different seasons. The sold energy is higher in the summer season in these cities. Therefore, instead of selling this exceeded energy at a low price, an MNO may increase its profit by using this energy for its cooling systems in ECs and CC.

We also investigate the economic feasibility of a renewable system for a Hybrid C-RAN. For this purpose, we have to calculate the CapEx of a renewable energy system, which is the summation of the solar panel and battery deployment costs. According to an investigation of Energysage, the price of a solar panel is 2$ per Watt in 2019 [98]. In another study, Goldie-Scott expects the battery prices to be around 0.15$ per Watt in 2019 [99]. In addition to the CapEx, a renewable system have a maintenance cost, which is around 300 $ per year, according to Fixr [100].

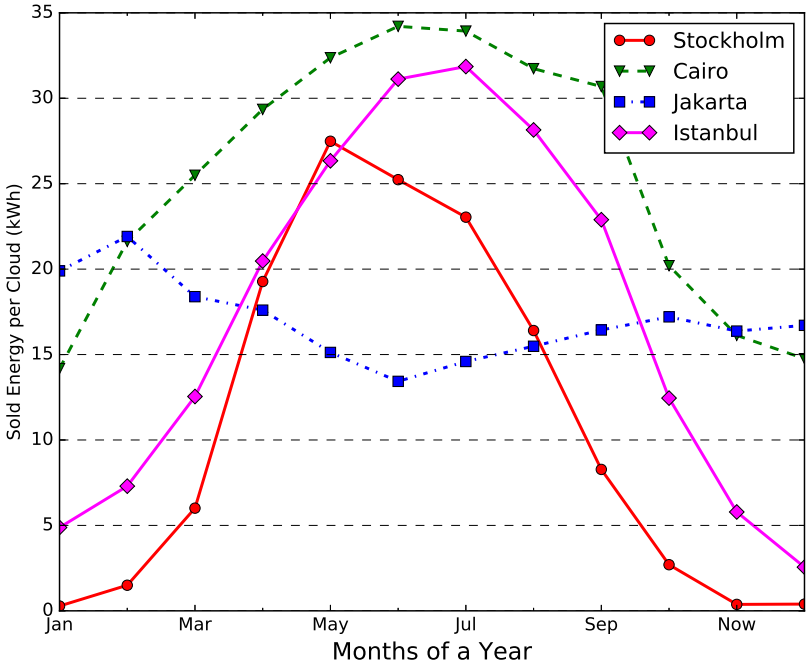


Figure 5.14. Distribution of the sold energy in a year period.

By using these prices, we calculate the CapEx and OpEx of our renewable system. Also, we model a new pure grid system for the MILP solver. The network model in this system is the same as our hybrid C-RAN, but this new system does not have any renewable components. Thus, this system does not have any CapEx but has higher operating expenses as a result of higher grid energy consumption. We compare the change of TCO of these two systems for each year. Figure 5.15 shows the results for different solar radiation and traffic rates. The return of capital (RoC) does not change with the traffic rates in three cities. The main reason for this finding is that an MNO has the same CapEx for all traffic rates. Also, the OpEx gap between the two systems does not change with the traffic rates. Besides, the city of Stockholm, which has inadequate solar radiation average in a year period, offers meager performance with a renewable system. The RoC of an MNO that invests in renewable components in this city is thirty years on average. However, in sunnier cities, the RoC is reasonable.

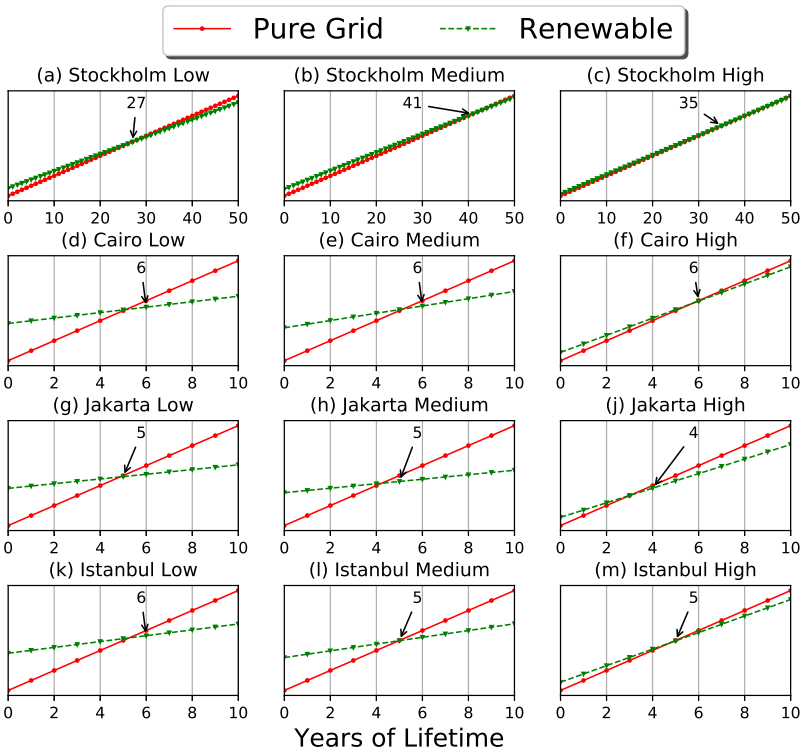


Figure 5.15. The Cost of a pure grid and a renewable system in lifetime period.

5.6. Discussion

A pure C-RAN needs an enormous bandwidth capacity between an RRH and a BBU. Thus, splitting the BBU functions is proposed in recent studies. The study in this chapter advanced these studies by adding RESs in CC and ECs. We explain the network architecture, the traffic, and the energy model of this novel system. We formulate an OpEx minimization problem which decides the splitting options by considering to increase the renewable energy consumption, reducing the number of active DUs, and balancing the URFs between the stations and between the time intervals. The results show that our proposed model, which considers the renewable energy amount in the batteries, reduces more OpEx, and provides more profit to the MNOs. In addition, this problem is an online problem, and an MNO should solve it on a daily basis. Thus, we proposed a fast heuristic, and the results showed that it provides an exceptional solution for large RANs. Lastly, we compare our proposed green system with the pure grid system. The results will encourage the MNOs to use RESs in a hybrid C-RAN architecture.

6. GROVE: RADIO OVER ETHERNET IMPLEMENTATION IN RADIO ACCESS NETWORKS

6.1. Introduction

Deployment of C-RAN architecture causes additional CapEx costs, such as the connections between the CC and ECs [101]. RoE, which is proposed by the IEEE 1914 Next Generation Fronthaul Interface Working Group, is a promising approach to reduce these costs [102]. Their standard document details this approach, in which the radio traffic between an EC and the CC is encapsulated in Ethernet frames on a multihop mesh network topology [13]. This approach is more economical than the dedicated links approach by using the advantage of aggregating the traffic of different ECs in the same network lines.

In this chapter, we integrate the RoE approach with our previous chapter concept. Then, we jointly focus on three significant decisions in a C-RAN: splitting the BBU functions between a CC and several ECs, transferring the traffic between them with the RoE approach, and using RESs as an alternative energy source in these units. To the best of our knowledge, there are no studies to model this problem and find a joint solution to reduce OpEx. Besides, we submitted this study to the Journal of IEEE Transactions on Green Communications and Networking [103]. Our contributions can be summarized as follows:

(i) We model the Green Radio OVer Ethernet (GROVE) concept. This novel concept is a promising approach to make a C-RAN architecture cost-effective for an MNO.
(ii) We formulate an optimization problem that aims to reduce the OpEx of this new model. We present that in this model, we have to jointly make decisions for the function splitting, dynamic choice of the paths between the CC and ECs, and considering to use the RESs efficiently.
(iii) We linearize the quadratic constraints in the problem so that it can be solved

with a MILP Solver.

(iv) We experiment with different traffic loads to show the performance of the solution for diverse city populations. Besides, we use real solar data and examine our solution for different seasons to see the impact of seasonal changes in four different geographical areas in the world, which have significantly different solar radiation distributions.

(v) We demonstrate a feasibility study which provides the RoC of this RESs system for different size of solar panels and the renewable energy storage units.

The remainder of this chapter is organized as follows. We define the GROVE system model and its cost optimization problem in the second and third sections, respectively. In the fourth section, we present the results of the computational experiments, followed by the concluding remarks in the last section.

6.2. GROVE System Model

Figure 6.1 illustrates the overall architecture of the GROVE model. We consider a scenario that a set of ECs, $\mathcal{R}$, are connected to a CC through a packet-based network $G = (\mathcal{V}, \mathcal{E})$, where $\mathcal{V}$ is the superset of routers, the set of ECs, and the CC; and $\mathcal{E}$ is the set of links between these components. Each link $e \in \mathcal{E}$ has a limited capacity $\Omega_e \geq 0$ for the downlink transmissions from CC to ECs. Although we just consider the downlink transmissions, the network model can be straightforwardly extended to include uplink transmissions.

Each EC has a Radio Frequency (RF) equipment with an antenna. Besides, there is a set of RRHs, $\mathcal{C}$, that are connected to their corresponding EC with a point-to-point millimeter-wave or dedicated fiber links [104]. While these RRHs do not have any BBUs, this architecture provides throughput enhancement with lower costs. Since the RRHs are geographically close to their corresponding EC, the CapEx of the MNO to connect them remains at lower values.

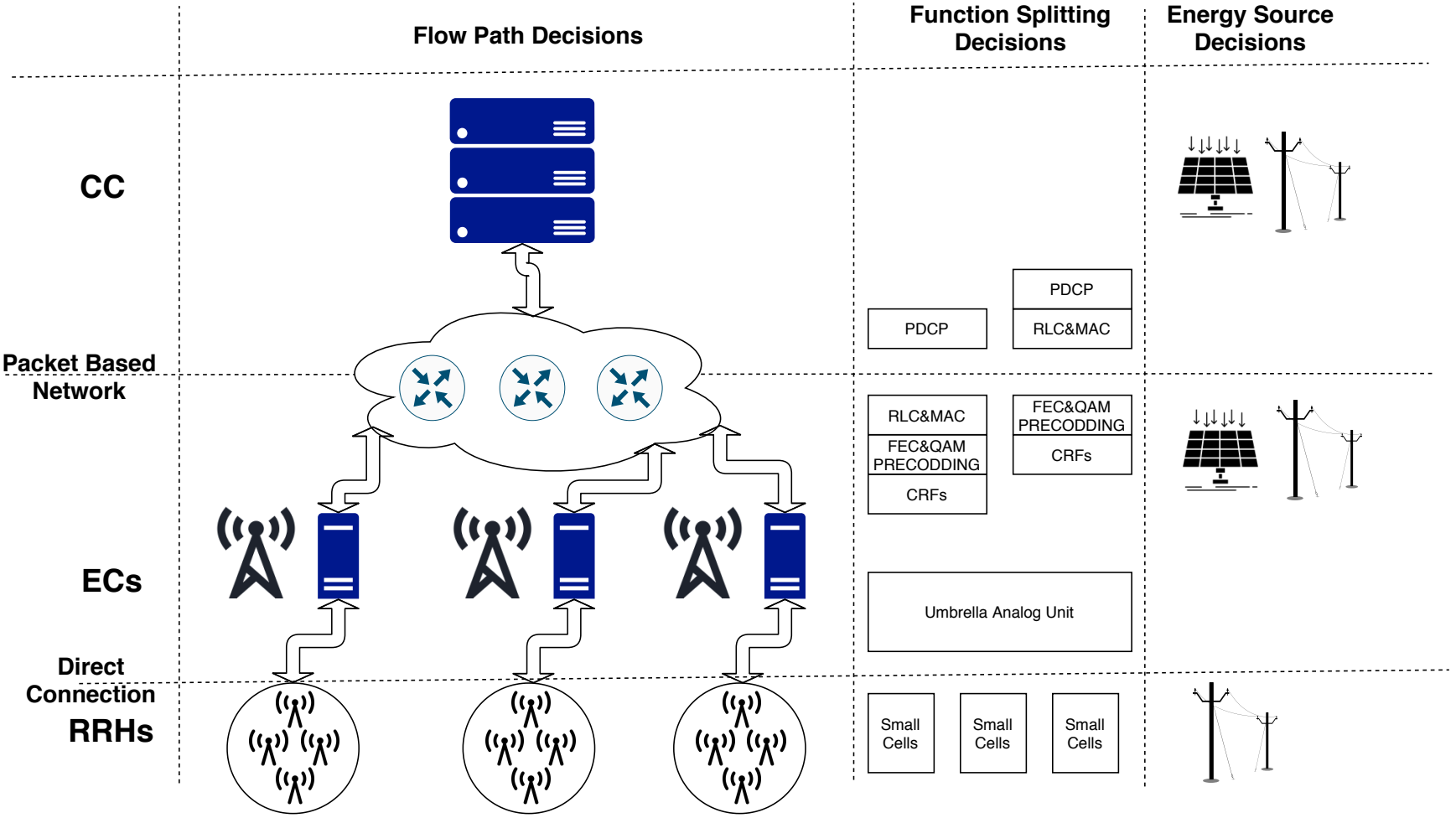


Figure 6.1. GROVE: Green Radio over Ethernet system architecture. Combining the three fundamental decisions of a next-generation wireless network.

BBU functions are provided by the DUs in the ECs and CC, collectively. The chain of these functions is broken in a certain split point. This point is dynamically decided for a set of time intervals in a day period for each user. These users have a different data traffic load on the DUs, U_{jt}^{EC}, and the maximum delay threshold, δ_{jt}, according to their required service.

CRFs and user-related functions (URFs) are the two main divisions of the BBU functions [38]. According to the Small Cell Forum, breaking the chain after CRFs reduces the required bandwidth significantly [12]. While the packet-based network between the CC and ECs should have a limited capacity to achieve a reasonable CapEx of the MNO, we prefer to process all CRFs in the ECs side. Moreover, the processing load and the bandwidth consumption of URFs vary with the user traffic demands; thus, splitting after CRFs also have multiplexing benefits. Figure 6.2 represents the function splitting options in GROVE system model. The details are explained in Section 5.2.

If we now move to the energy model, Figure 6.1 illustrates that the CC and the ECs have two different energy sources to facilitate their operations. While the first one, the solar panel, reduces the OpEx of the MNO with renewable energy, the second one, on-grid energy, becomes a reliable source in the case of the lack of insufficient green energy. The other components in the system, RRHs, have only an on-grid energy source. Since most of the 5G RRHs are expected to be indoor, the MNO can easily position them in an indoor area that is not directly exposed to solar radiation. But if needed, RESs can also be used for RRHs. The details of energy consumptions in the ECs (E_{rt}^{EC}) and the CC (E_{t}^{CC}) are explained in Section 5.2.

The connections between the CC and ECs also consume energy. However, most of this energy consumption does not change with the traffic load and remains as a static value. The only way to reduce this energy consumption is by completely switching off these connections [105]. Despite this, in our system model, the links are always active, and we do not need to optimize this energy consumption; thus, we do not include it to the objective function.

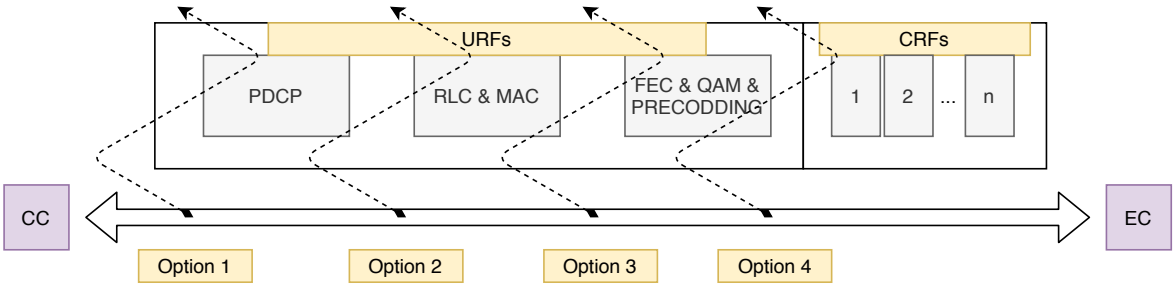


Figure 6.2. Function Splitting Options in GROVE System Model.

6.3. Minimizing the Operational Expenditures in GROVE Model

6.3.1. Problem Formulation

Over the GROVE system model explained in the previous section, our primary purpose is to reduce the OpEx of this system (Equation 6.1). We aim to reduce the overall on-grid electricity bills of the CC and the ECs. We have to deal with three fundamental problems to reduce these bills. First, we have to reduce the total energy consumptions in the CC (E_t^{CC}) and the ECs (E_{rt}^{EC}) by switching off as many as DUs in these units. Second, we have to favor the usage of renewable energy (s_t^{CC} and s_{rt}^{EC}) instead of on-grid energy consumption. This action principally depends on the size of solar panels and the batteries in these units and planning the use of renewable energy in these batteries in an efficient way. Otherwise, the MNO should sell this valuable energy to the grid network at a reduced price ($\Psi * p_t^{CC}$ and $\Psi * p_{rt}^{EC}$). Lastly, we have to consider the variation of the electricity prices in a day period (c_t^E) and try to use renewable energy as much as possible in the time intervals that the price of the electricity is higher than the average price. It should be noticed that the electricity cost of the RRHs and the maintenance cost of the GROVE system are not included in this OpEx calculation. The reason is that these costs do not change by any decision variable. Besides, we include the maintenance cost in the last section for the cost

feasibility comparison of a pure grid system and a RESs system.

Minimize:

$$\sum_{t\in\mathcal{T}}\left[E_t^{CC}-s_t^{CC}-\Psi*p_t^{CC}+\sum_{r\in\mathcal{R}}(E_{rt}^{EC}-s_{rt}^{EC}-\Psi*p_{rt}^{EC})\right]*c_t^E \tag{6.1}$$

Subject to:[11]

$$\sum_{f\in\mathcal{F}}\sum_{j\in\mathcal{J}}U_{jt}^{EC}m_{jdft}<\Lambda^{CC}, \qquad \forall d\in\mathcal{D}^{CC} \tag{6.2}$$

$$\sum_{f\in\mathcal{F}}\sum_{c\in\mathcal{C}_r}\sum_{j\in\mathcal{J}_c}U_{jt}^{EC}m_{jdft}<\Lambda^{EC}, \qquad \forall d\in\mathcal{D}_r^{EC},\forall r\in\mathcal{R} \tag{6.3}$$

$$M*a_{dt}-\sum_{f\in\mathcal{F}}\sum_{j\in\mathcal{J}}m_{jdft}\geq 0, \qquad \forall d\in\mathcal{D}^{CC} \tag{6.4}$$

$$M*a_{dt}-\sum_{f\in\mathcal{F}}\sum_{c\in\mathcal{C}_r}\sum_{j\in\mathcal{J}_c}m_{jdft}\geq 0, \qquad \forall d\in\mathcal{D}_r^{EC},\forall r\in\mathcal{R} \tag{6.5}$$

$$\sum_{f\in\mathcal{F}}\sum_{d\in\mathcal{D}^{CC}\cup\mathcal{D}_r^{EC}}m_{jdft}=|\mathcal{F}|, \qquad \forall j\in\mathcal{J}_c,c\in\mathcal{C}_r,\forall r\in\mathcal{R} \tag{6.6}$$

$$\sum_{f\in\mathcal{F}}\sum_{d\in\mathcal{D}^{CC}}m_{jdft}<\delta_{jt}, \qquad \forall j\in\mathcal{J} \tag{6.7}$$

$$b_t^{CC}=b_{(t-1)}^{CC}-s_t^{CC}-p_t+\alpha^{CC}G_t^{CC} \tag{6.8}$$

$$b_{rt}^{EC}=b_{r(t-1)}^{EC}-s_{rt}^{EC}-p_{rt}^{EC}+\alpha_r^{EC}G_{rt}^{EC}, \qquad \forall r\in\mathcal{R} \tag{6.9}$$

$$b^{CC}t\leq\beta^{CC} \tag{6.10}$$

$$b_{rt}^{EC}\leq\beta_r^{EC}, \qquad \forall r\in\mathcal{R} \tag{6.11}$$

$$s_t^{CC}\leq E_t^{CC} \tag{6.12}$$

$$s_{rt}^{EC}\leq E_{rt}^{EC}, \qquad \forall r\in\mathcal{R} \tag{6.13}$$

$$\sum_{y\in\mathcal{V}}l_{rt(x,y)}-\sum_{y\in\mathcal{V}}l_{rt(y,x)}=\begin{cases}1,\text{if } x\in\mathcal{V}^{EC},\\ -1,\text{if } x\in\mathcal{V}^{CC}, & \forall x\in\mathcal{V}\\ 0,\text{otherwise}, & \forall r\in\mathcal{R}\end{cases} \tag{6.14}$$

$$\sum_{r\in\mathcal{R}}l_{rt(x,y)}\sum_{c\in\mathcal{C}_r}\sum_{j\in\mathcal{J}_c}\sum_{d\in\mathcal{D}^{CC}}\sum_{f\in\mathcal{F}}U_{jt}^{EC}m_{jdft}\leq\Omega_{(x,y)}, \qquad \forall(x,y)\in\mathcal{E} \tag{6.15}$$

The first two constraints (Inequalities 6.2 and 6.3) model the DUs capacity limitations. Λ^{CC} and Λ^{EC} are the maximum numbers of URFs that can be executed in a DUs of a CC or an EC, respectively. As stated by Mharsi et al., a URF's processing demand correlates with the traffic load of the corresponding user; thus, the number of executed URFs in a DU (m_{jdft}) is multiplied with the traffic load in these constraints [39]. Meanwhile, deciding to execute a URFs in a DU leads up to activate that DU (a_{dt}).

Constraints 6.4 and 6.5 grant this causality for the CC and the ECs, respectively. Inequality 6.6 guarantees another critical constraint: processing of all URFs ($f \in \mathcal{F}$) of each user in DUs. Furthermore, the choosing of the cloud side for processing a URF depends on the delay threshold of the corresponding user (δ_{jt}), which is maintained by Inequality 6.7. In order to keep the problem complexity low, the computing costs are assumed the same for each URF. Therefore, deciding the number of URFs in one cloud side provides us a certain splitting point in the chain of the URF.

Inequalities 6.8 to 6.13 regulate renewable energy usage restrictions. The first two of them calculate the remaining energy in a battery (b^y_{rt}) according to the remaining energy in the previous time interval ($b^y_{r(t-1)}$), consumed green energy (s^y_{rt}), the sold energy to the grid (p^y_{rt}), and the generated renewable energy in this time interval ($\alpha^y_r G^y_{rt}$). The capacity of the batteries (β^y_r) limits the maximum stored renewable energy in these batteries, and Inequalities 6.10 and 6.11 show this limitation for the CC and the ECs. Lastly, it is clear that the consumed green energy (s^y_{rt}) can be as high as the total energy consumption in the CC and in the ECs (E^y_{rt}), which are granted by Inequalities 6.12 and 6.13.

Equation 6.14 ensures exactly one connection from each EC to the CC. $(x, y) \in \mathcal{E}$ represents an edge that connects the nodes $x \in \mathcal{V}$ and $y \in \mathcal{V}$. If the node is an EC node $x \in \mathcal{V}^{EC}$, there should be an edge that connects this node to another node in the network. On the other hand, if the node is a CC node $x \in \mathcal{V}^{CC}$, there should be an edge that connects another node in the network to this node. For the nodes

between the ECs and CC, the summation of the number of incoming and outcoming edges should be equal to zero, which means that the path could not be disconnected at a switch node. Although this equation does not restrict a cycle in the path, a cycle does not have any beneficial effect on the objective function and the constraints. Moreover, it increases the bandwidth usage, and by adding the bandwidth constraint (Inequality 6.15) to each edge, we eliminate a cycle in the network.

The edges in this model have a limited bandwidth capacity $\Omega_{(x,y)}$, which depends on two values: the number of URFs that execute in the DUs of the CC ($d \in D^{CC}$), and the traffic loads of each user (U_{jt}^{EC}). This relation is provided by Inequality 6.15. However, this inequality is a quadratic constraint as a result of the multiplication of the path existence decision variable $l_{rt(x,y)}$, and the URF usage decision variable m_{jdft}. Thus, we need to linearize this constraint to solve this mathematical model with a MILP solver, as shown in the next subsection.

6.3.2. Problem Linearization

Proposition 6.1. *Let $\omega_{rt(x,y)}$ is a continuous decision variable and can take on any value between $[0, \Omega_{(x,y)}]$. If m_{jdft}, $l_{rt(x,y)}$, and $\omega_{rt(x,y)}$ decision variables satisfy Inequalities 6.16 and 6.17, then the quadratic constraint Inequality 6.15 is also satisfied by the decision variables m_{jdft} and $l_{rt(x,y)}$.*

$$\sum_{c \in \mathcal{C}_r} \sum_{j \in \mathcal{J}_c} \sum_{d \in \mathcal{D}^{CC}} \sum_{f \in \mathcal{F}} U_{jt}^{EC} m_{jdft} \leq M * (1 - l_{rt(x,y)}) + \omega_{rt(x,y)}, \quad \forall r \in \mathcal{R}, \forall (x,y) \in \mathcal{E} \quad (6.16)$$

$$\sum_{r \in \mathcal{R}} \omega_{rt(x,y)} \leq \Omega_{(x,y)}, \quad \forall (x,y) \in \mathcal{E} \quad (6.17)$$

Proof. When $l_{rt(x,y)} = 0$, the first term of the right-hand side in Inequality 6.16 becomes very large due to the big M value. In that case, the decision variable $\omega_{rt(x,y)}$ can be chosen any value between $[0, \Omega_{(x,y)}]$ to achieve inequality. Besides, it should be noticed that a MILP solver is strongly motivated to select the lowest possible value for this

variable by the sake of Inequality 6.17.

For the case $l_{rt(x,y)} = 1$, the first term of right-hand side in Inequality 6.16 becomes zero. In that case, the decision value of $\omega_{rt(x,y)}$ should be large or equal to the total traffic of EC r on edge (x, y) [12] . Meanwhile, Inequality 6.17 restricts the summation of all $\omega_{rt(x,y)}$ from different ECs with the bandwidth capacity ($\Omega_{x,y}$) of the corresponding edge (x, y). Therefore, bandwidth capacity limitation of each edge (x, y) is ensured by these two inequalities. □

6.3.3. Complexity Analysis

Proposition 6.2. *Minimizing the OpEx of GROVE model is an NP-Hard problem.*

Proof. (Sketch) For the static routing case, we can remove Inequalities 6.14 and 6.15. Further, if we choose the size of solar panels and the batteries as zero, Inequalities 6.8 to 6.13 can be eliminated. Alabbasi et al. emphasize that this new reduced problem involves the bin packing problem [38] ; thus, it is an NP-Hard problem. □

6.4. Computational Experiments

We use a MILP solver to find solutions for the NP-Hard problem analyzed in the previous section. In this section, we detail the results and the findings from several cases.

6.4.1. Evaluation Settings

The network topology of our primary use case is shown in Figure 6.3. It contains 12 nodes (one CC, six ECs, and five switch nodes) and 29 edges ($(|\mathcal{V}|, |\mathcal{E}|) = (12, 29)$).First, user downlink data traffic flows from the CU to any of the two routers in

[12] It is essential to remind that by Constraint 6.14, there is only one path between an EC and the CC.

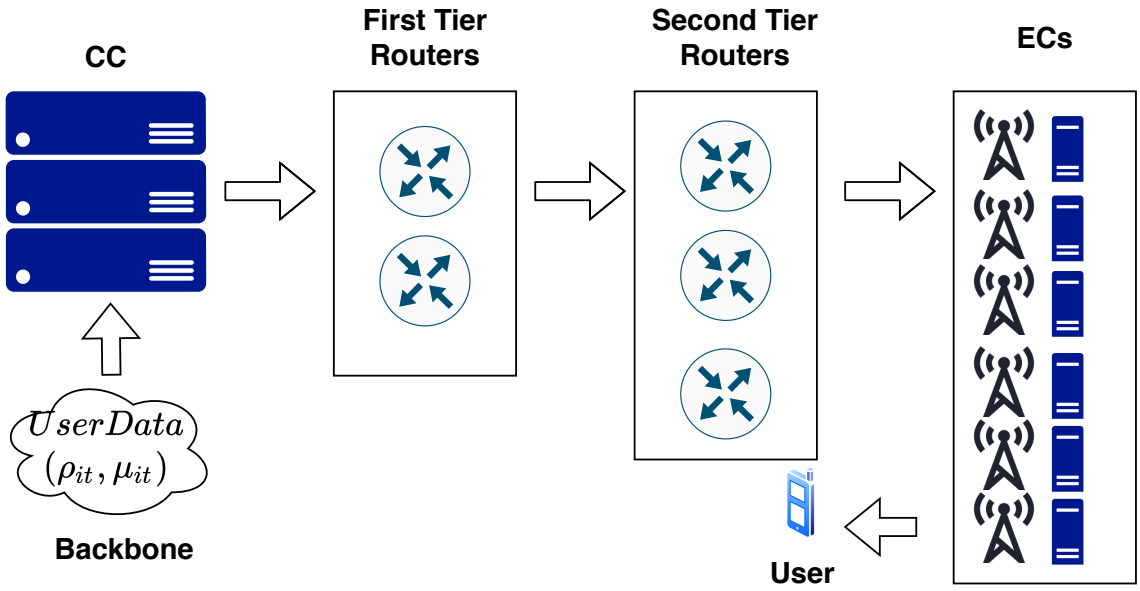


Figure 6.3. The Use case network topology.

the first tier. Then, the data flow to any of the three routers in the second tier, which are also connected by each other. In the next step, the data flows to the EC, which serves to the corresponding user. Finally, the data reaches the user either directly from the EC in an umbrella cell or from the RRH in a small cell.

The number of RRHs connected to a EC equals five ($\mid \mathcal{C}_r \mid = 5$), and there are ten users in each RRH small cell ($\mid \mathcal{J}_c \mid = 10$). The delay threshold of the required service from each user (δ_{jt}) is randomly generated in $[0, \mid \mathcal{F} \mid]$. These users have a daily sinusoidal shape traffic load created by Equation 4.1. The details of the user traffic creation are explained in Section 4.2.1. The difference in this chapter is related with the mapping of the traffic profiles. We map the different peak hours to each EC to mimic the distinctive zones in a city such as residential, industrial, or shopping areas. Thus, we simulate both temporal and spatial variations of a traffic load in the region of a city. Lastly, we multiply the calculated traffic load by $[0.5, 1, 1.5]$ to analyze the model for three traffic densities, which are called *Low*, *Medium*, and *High*.

Generated green energy from a solar panel (G^y_{rt}) is calculated by the pvWatts application [82]. We use the solar radiation data of four different cities (Stockholm, Istanbul, Cairo, Jakarta) that have a distinct distribution in a year period. Thus, we

Table 6.1. GROVE experiment parameters.

Parameter	Unit	CC Side	EC Side
E^S	Wh	1000	500
E^D	Wh	400	400
α	kWh	80	20
β	kWh	50	20
c_t^E	TRY	[0.29, 0.46, 0.70]	[0.29, 0.46, 0.70]
Ψ	-	0.5	0.5

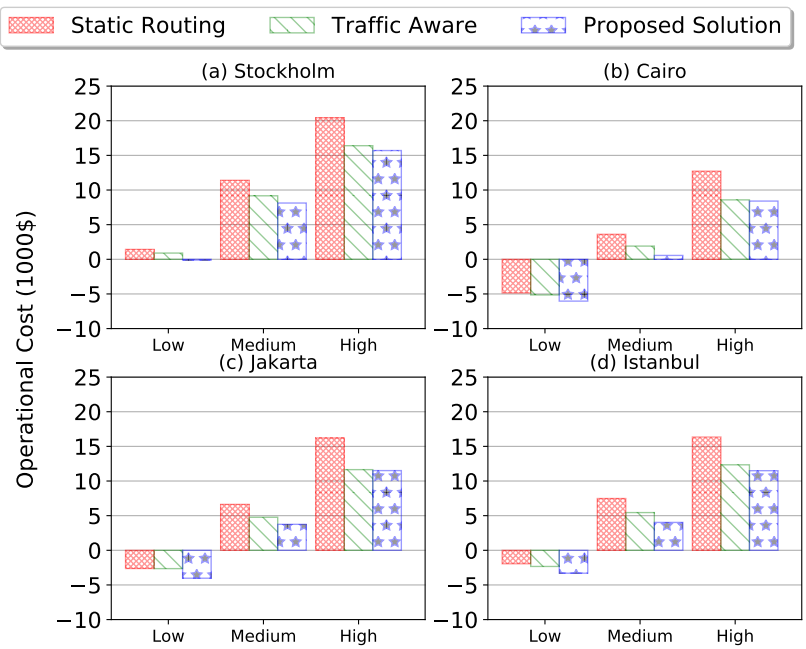


Figure 6.4. Operational costs in different traffic loads and solar radiations.

can investigate the effect of seasonal change in our model. Besides, energy prediction models may also be implemented easily in our system model [106]. The rest of the parameters used in our simulations are given in Table 6.1. The electricity price values are from EPDK's variable electricity tariff regulation that has different price policies according to the time of the day [97]. The exchange rate is chosen as $1\ USD = 7\ TRY$.

6.4.2. Performance of Operational Expenditure Minimization

We compare the results of our proposed solution with the results of two models: a model that jointly consider the function splitting and renewable energy but does

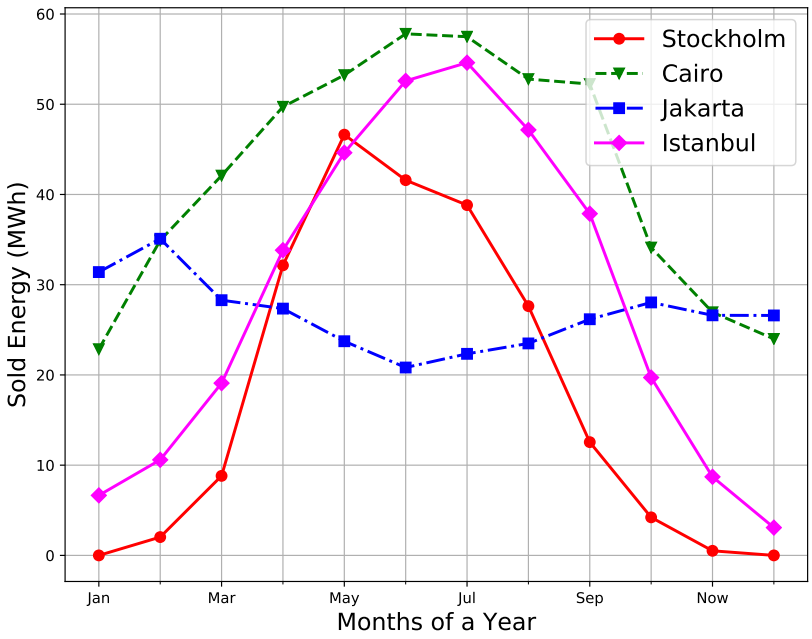


Figure 6.5. Remaining energy in ECs and CC in a year period.

not take into account the routing decisions, called ”Static Routing”, and a model that take into account the function splitting and the routing decisions together but ignore the renewable energy usage decisions, called ”Traffic-Aware.” We used Gurobi [89] as a MILP solver, and computational experiments were run on an Nvidia DGX-1 Station [93] with a Dual 20-Core Intel Xeon E5-2698 v4 2.2 GHz. The termination time was chosen as 4 hours.

Figure 6.4 shows the one year period OpEx results for different traffic loads and solar radiation distributions. The results confirm that our proposed solution has lower OpEx for any traffic load and solar radiation distribution. Thus, we can use this model for any city or urban region around the world. Meanwhile, Figure 6.4 also shows that with higher traffic loads, the OpEx increases due to the boosting of the number of active DUs[13] . Also, the cities that have higher solar radiation rates have lower OpEx owing to the increase in renewable energy availability. Moreover, these cities can earn higher profits by selling it to the grid, which is shown in Figure 6.5.

[13]The reason for some negative OpEx in the low traffic load is that the system’s profit gain of selling renewable energy is higher than the grid energy bills in this level of traffic load for this particular setup corresponding to a specific CapEx.

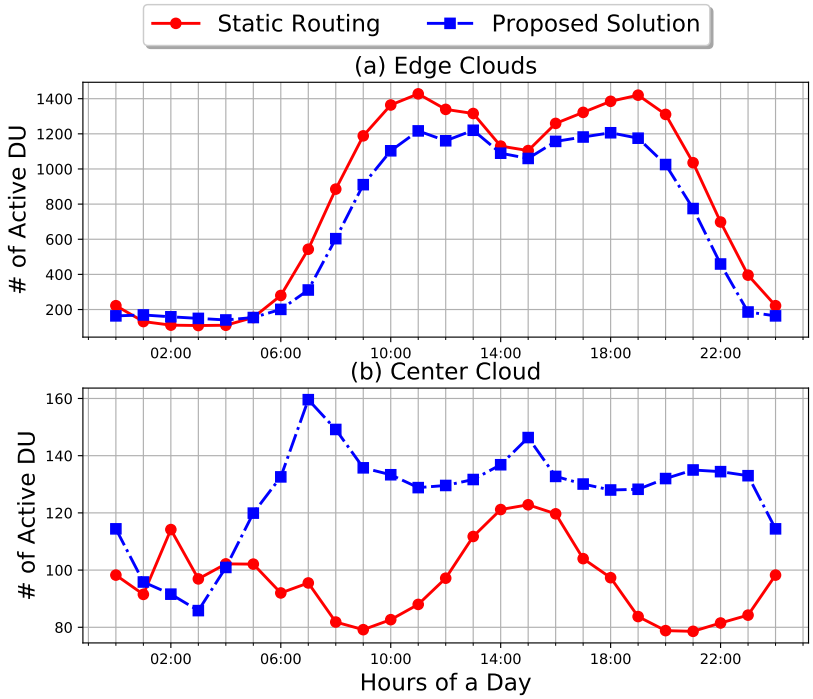


Figure 6.6. Number of active DUs in a day period in CC and ECs (average of 12 different scenarios).

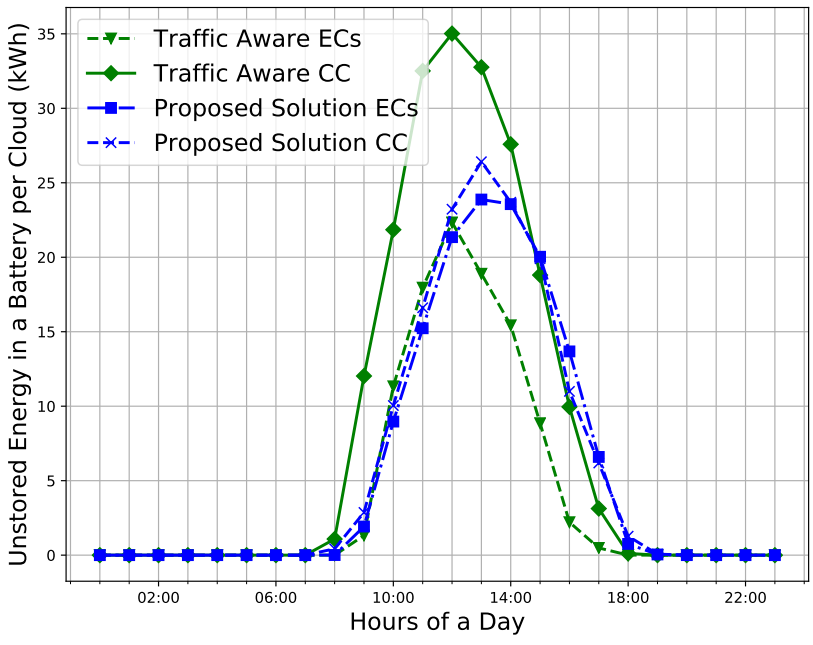


Figure 6.7. Unstored energy in ECs and CC in a day period.

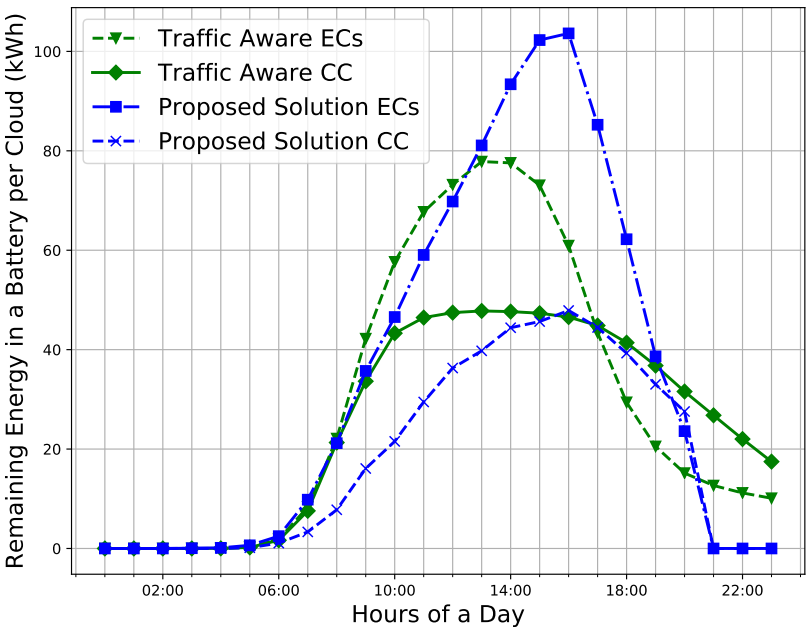


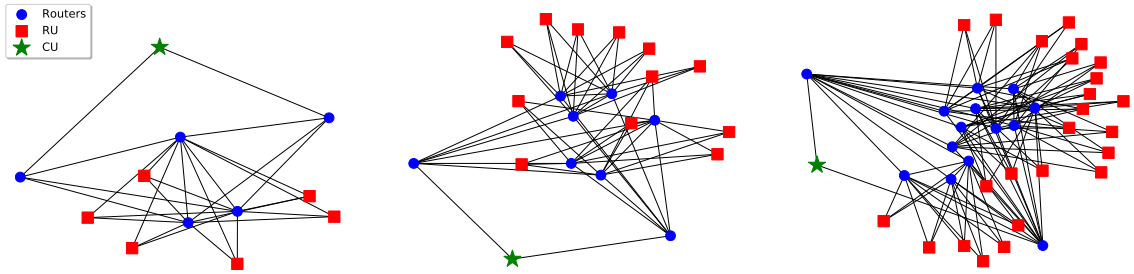
Figure 6.8. Remaining energy in the CC and ECs in a day period.

If we now turn to analyze why our proposed solution provides better results than the static routing, we have to focus on the number of active DUs in the ECs and CC. As we can see in Figure 6.6, our proposed solution decreases the number of active DUs in the ECs by choosing the flow paths efficiently. Thus we can reduce the overall energy consumption by centralizing the functions in the CC. In the meantime, our proposed solutions also beat the "Traffic-Aware" algorithm by activating the DUs of ECs which have renewable energy in their batteries. Thus we can use this valuable renewable energy-efficiently and prevent the unstored energy, which is shown in Figure 6.7. Moreover, our solution reserves the renewable energy of the ECs for more profitable hours (Figure 6.8). Therefore, we can reduce the OpEx further by considering the renewable energy in the batteries of the ECs and the CC.

6.4.3. Network Scalability Analysis

The standard network configuration we studied is explained in Section 6.4.1, and its results are represented in the previous subsection. Now, we will analyze the outcomes of larger topologies. Figure 6.9 shows three network topologies that have different sizes. Figure 6.9(a) is our standard topology, which has six ECs, and five

switch nodes connect them to the CC. In Figure 6.9(b), we doubled the number of ECs (12 ECs), and then we need eight switches to connect them to the center. Lastly, Figure 6.9(c) shows an architecture that has 24 ECs and 14 switches.



(a) 6 EC topology. (b) 12 EC topology. (c) 24 EC topology.

Figure 6.9. Analysis of network scalability: Topologies.

Due to the non-polynomial difficulty of the optimization problem, as the network size gets larger, the required memory (As indicated in Figure 6.10) and computational power are increasing very rapidly. Thus, the size of the third topology is a boundary for the GROVE Model by using the DGX-1 Station. Moreover, the increase in the network size reduces the performance of our proposed solution. The main reason for this outcome is related to the size of the solution space of the compared solutions. Our proposed solution has a more extensive solution space; thus, a MILP solver needs more processing time to approximate the lower bound. Besides, an MNO gets better results with our proposed solution for larger network sizes, according to the results shown in Figure 6.10.

6.4.4. Economic Feasibility Analysis

Reducing the OpEx of an MNO does not entirely satisfy the economic feasibility of the proposed network model. We also need to investigate the CapEx of this novel RESs system, which is the summation of the solar panel and battery deployment costs. In Equation 6.18, which represents this calculation, S and B stand for the size of solar panels and the batteries, respectively. The unit prices of these components are presented with c^S, and c^B. Energysage informs that the price of a solar panel is $c^S = 2\$$ per Watt in 2019 [98], and Goldie-Scott notifies the battery prices to be

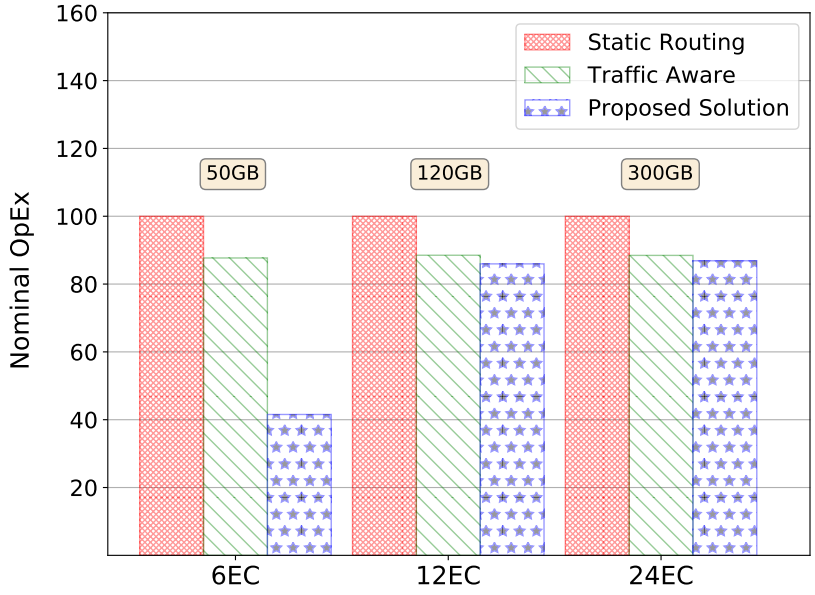


Figure 6.10. Analysis of network scalability: OpEx and memory consumptions.

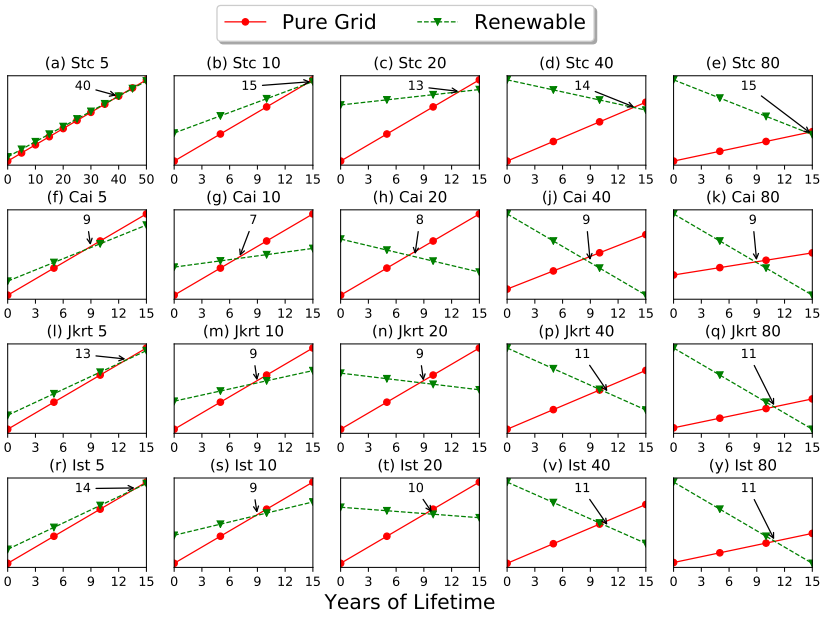


Figure 6.11. Analysis of RoC in low traffic (a)-(e): Stockholm, (f)-(k): Cairo, (l)-(q): Jakarta, (r)-(y): Istanbul. From left to right size of solar panels in ECs changes from 5 to 80.

around $c^B = 0.15\$$ per Watt in 2019 [99]. Calculating the other deployment costs (such as leasing cost) is out of scope in this chapter, but they can easily be added in this equation.

$$CapEx = \sum_{r \in \mathcal{R}} \left[\alpha_r^{EC} * c^S + \beta_r^{EC} * c^B \right] + \alpha^{CC} * c^S + \beta^{CC} * c^B \tag{6.18}$$

$$RoC = \left\lceil \frac{CapEx + OpEx^{RES} + MC}{OpEx^{GRID}} \right\rceil \tag{6.19}$$

Next, we model a new pure grid system for the MILP solver. The network model in this system is the same as our proposed C-RAN, but this new system does not have any renewable components. Thus, this system does not have any CapEx but has higher operating expenses as a result of higher grid energy consumption. Then, we calculate the RoC of an MNO that prefers a RESs system in their network. Equation 6.19 shows this calculation, in which $OpEx^{GRID}$, $OpEx^{RES}$ are the electricity costs of a pure grid and a RES system in a year, respectively. They are calculated by Equation 6.1 with considering the constraints in their corresponding network. Also, a RESs system has another operational cost, which is the maintenance cost (MC) of their renewable systems in a year period. This value does not change by the capacity of the renewable system components, and Fixr determines this value as $MC = 300\$$ per year for a single renewable system [100].

Figure 6.11 presents the change of TCO of the pure grid and the RESs networks in low traffic rates. The subfigures from up to down represent the diversity between the cities, and from left to right illustrate the impact of increasing the size of the RESs system. The solar panel and battery size values in Table 6.1 are multiplicated with the vector $[0.25, 5, 1, 2, 4]$, and the problem is solved again for each city to perform this variation. For example, the sizes of the RES components in $(d), (j), (p), (v)$ are the double size of the standard values.

The arrow markers show the RoC point of an MNO. This value is around eight years for any city except Stockholm, which has limited solar irradiation average in a year period. Besides, the proper system sizes that provide the minimum RoC value should be chosen when $OpEx^{RES} + MC$ value is near to zero; what is more, this significant finding can be applied for any city. One of the reasons is that selling the unused renewable energy to the grid is not profitable for an MNO. On the other hand, an insufficient amount of harvesting energy prevents the MNO to get the maximum profit from the GROVE model.

Lastly, the results of the other traffic rates are similar to their corresponding instances in Figure 6.11. There are two significant facts that yield this similarity. First, the OpEx gap between the two systems does not change with the traffic rates. Second, MNO has the same CapEx for all traffic rates.

6.5. Discussion

We propose a novel network model named GROVE as a cost-efficient solution for using RESs in a C-RAN architecture. Then, we formulate an OpEx minimization problem which jointly takes into account the function splitting, RoE, and renewable energy usage in this model. We linearize the quadratic constraints in the formulation to solve this problem with a MILP Solver. The results show that our model improves the performance of the disjoint approaches, and it is more feasible for different solar radiation distributions and various traffic densities. The proposed solution outperforms the static routing by multiplexing gain. Also, it performs better than the traffic-aware method by optimizing the usage of profitable renewable energy in the batteries of the CC and ECs.

The network scalability analysis shows that a MILP solver can maintain a network model with 40 nodes with reasonable RAM consumption. Besides, our proposed solution performs better results even with larger networks, and we may increase the termination time to reduce the gap between the lower bound of the MILP solver to

improve this performance. Lastly, our economic feasibility analysis addresses the RES sizing problem in the proposed network, and the findings are highly valuable to support MNOs to choose the proper size of solar panels and the batteries for their potential green C-RAN network.

7. CONCLUSION

Using RESs as an alternative energy source in mobile communication networks has several benefits from reducing the carbon emission rates and energy consumptions to improving the cost-efficiency and economic feasibility in these networks. However, RESs have two critical drawbacks. First, renewable energy should be stored in a storage system such as lithium-ion batteries to use it efficiently. Nevertheless, these systems have limited storing capacity and increasing their capacity impact directly the CapEx. Thus, we need to tend to the solutions which promote the practical usage of the valuable storage systems. Second, RESs are sporadic and unstable sources, and they provide highly unpredicted energy across time and space. Therefore, these sources usually need to be supported by a reliable source like on-grid electricity. In this thesis, we propose energy and cost optimization solutions in several research areas of RANs by considering these drawbacks of RESs.

First, we start with a micro BS deployment problem in a packet-switched network. We introduce the algorithms which reduce the operational costs with efficient network planning by using RESs and adaptively change the transmission power of BSs to improve the ASE in the overall network. The results are promising for considering deploying additional solar-powered micro BSs on a RAN, which is already operational using on-grid macro BSs. Second, we focus on reducing the total capital and operational expenses of an MNO in a packet-switched network by using RESs. Hence, we offer a novel network model called HEBRAN and then propose MILP and heuristic solutions for the MNOs to decide on the proper size of solar panels and the batteries in this network and how to operate them in a cost-efficient way. The results show that our methods perform better than the previous studies in the manner of energy, cost, and carbon emission rate minimization. The more crucial findings come from the results, which show that the performance of our HEBRAN model is improved by the increasing traffic rates; thus, it supports the usage of the RESs in an urban area.

In our third study, we concentrated on the problems in 5G mobile communication networks, particularly on cost-efficient function splitting decisions for C-RAN. We propose a model in which RESs supply the CC and ECs in this network, and we formulate a cost minimization problem by considering the user QoS and C-RAN specific constraints. We provide methods that specifically decide the function splittings according to the remaining energy in the batteries of the system. The results show that our solutions are more profitable than the disjoint methods for several distinctive solar radiation and user traffic distributions. In our fourth study, we enhance this study by adding the RoE approach to the problem. We propose a novel concept called GROVE, which improves the economic aspect of a hybrid C-RAN architecture for an MNO. We reduce the solution space in this problem and convert the problem in a suitable form to solve it with a MILP Solver. The findings offer the most cost-efficient sizing decisions for RES components and encourage the MNOs to implement RES systems in their projected C-RAN network.

In conclusion, our studies confirm that using RESs for RANs in an urban region is as efficient as using them in a rural area. Besides, we need to be aware of the unpredictable property of renewable energy and use this valuable energy by considering the most advantageous time of the day. Our methods show that preserving renewable energy does reduce not only the carbon emission rates and energy consumptions but also the costs of the MNOs. Furthermore, our cost feasibility analyses for different architectures guide the MNOs for cost-efficient RESs implementations in their projected networks. Therefore, this thesis improves the economic feasibility of RESs systems and promotes them in mobile communication networks.

This research has thrown up many questions in need of further investigation. While in the HEBRAN model, we decide on BS switching off techniques; in the GROVE model, we make decisions for splitting the BBU functions between ECs and CC. First, further work is needed to fully understand the performance improvement if we integrate these two approaches. Second, even though this study shows the economic efficiency of RESs in the GROVE model, still, a detailed cost feasibility study for the impact of

RoE integration in a C-RAN architecture is strongly recommended. Lastly, a service-oriented traffic classification should be carried out to improve the cost-efficiency of our proposed models.

REFERENCES

1. Pachauri, R. K. and A. Reisinger, *Contribution of Working Groups I, II and III to the Fourth Assessment Report of the Intergovernmental Panel on Climate Change*, Tech. rep., IPCC, 2007, `https://www.ipcc.ch/report/ar4/syr/`.

2. Quaschning, V., *Renewable Energy and Climate Change*, John Wiley & Sons, Ltd, Chichester, UK, feb 2010.

3. Gregory, J. M., P. Huybrechts and S. C. B. Raper, "Threatened loss of the Greenland ice-sheet", *Nature*, Vol. 428, No. 6983, pp. 616–616, apr 2004.

4. Capros, P., A. De Vita, N. Tasios, D. Papadopoulos, P. Siskos, M. Apostolaki, M. Zampara, K. Paroussos, N. Fragiadakis, N. Kouvaritakis and H. P. Witzke, *EU Energy, Transport and GHG Emissions: Trends to 2050 - Reference Scenario 2013*, Tech. rep., European Commission, 2013, `http://ec.europa.eu/transport/media/publications/doc/trends-to-2050-update-2013.pdf`.

5. Oh, E., B. Krishnamachari, X. Liu and Z. Niu, "Toward dynamic energy-efficient operation of cellular network infrastructure", *IEEE Communications Magazine*, Vol. 49, No. 6, pp. 56–61, jun 2011.

6. Pamuklu, T. and C. Ersoy, "Yeşil Hücresel Ağlarda Yenilenebilir Enerji Kaynaklarının Kullanımı", *Akademik Bilişim*, 2014.

7. Wang, L.-C. and S. Rangapillai, "A survey on green 5G cellular networks", *International Conference on Signal Processing and Communications (SPCOM)*, pp. 1–5, IEEE, jul 2012.

8. Wirth, H., *Recent Facts about Photovoltaics in Germany*, Tech. rep., Fraunhofer Institute for Solar Energy Systems, Freiburg, 2013, `https://www.freiburg.fraunhofer.de/`.

9. Kempener, R. and E. Borden, *Battery Storage for Renewables : Market Status and Technology Outlook*, Tech. Rep. January, IRENA, 2015, `https://www.irena.org/`.

10. Garcia-Saavedra, A., X. Costa-Perez, D. J. Leith and G. Iosifidis, "FluidRAN: Optimized vRAN/MEC Orchestration", *INFOCOM*, pp. 2366–2374, IEEE, apr 2018.

11. Dotsch, U., M. Doll, H.-P. Mayer, F. Schaich, J. Segel and P. Sehier, "Quantitative analysis of split base station processing and determination of advantageous architectures for LTE", *Bell Labs Technical Journal*, Vol. 18, No. 1, pp. 105–128, jun 2013.

12. Small Cell Forum, *Small cell virtualization fuctional splits and use cases*, Tech. rep., SCF, 2016, `https://scf.io/en/index.php`.

13. "IEEE Standard for Radio over Ethernet Encapsulations and Mappings", *IEEE Std 1914.3-2018*, pp. 1–77, 2018.

14. Gonzalez-Diaz, S., A. Garcia-Saavedra, A. De La Oliva, X. Costa-Perez, R. Gazda, A. Mourad, T. Deiss, J. Mangues-Bafalluy, P. Iovanna, S. Stracca and P. Leithead, "Integrating Fronthaul and Backhaul Networks: Transport Challenges and Feasibility Results", *IEEE Transactions on Mobile Computing*, Vol. PP, No. c, pp. 1–1, 2019.

15. Garcia-Saavedra, A., J. X. Salvat, X. Li and X. Costa-Perez, "WizHaul: On the Centralization Degree of Cloud RAN Next Generation Fronthaul", *IEEE Transactions on Mobile Computing*, Vol. 17, No. 10, pp. 2452–2466, oct 2018.

16. Richter, F., A. J. Fehske and G. P. Fettweis, "Energy Efficiency Aspects of Base Station Deployment Strategies for Cellular Networks", *IEEE 70th Vehicular Technology Conference Fall*, pp. 1–5, IEEE, sep 2009.

17. Badic, B., T. O'Farrrell, P. Loskot and J. He, "Energy Efficient Radio Access Architectures for Green Radio: Large versus Small Cell Size Deployment", *IEEE 70th Vehicular Technology Conference Fall*, pp. 1–5, IEEE, sep 2009.

18. Son, K., E. Oh and B. Krishnamachari, "Energy-aware hierarchical cell configuration: From deployment to operation", *INFOCOM*, pp. 289–294, IEEE, apr 2011.

19. Wu, J., Y. Zhang, M. Zukerman and E. K.-N. Yung, "Energy-Efficient Base-Stations Sleep-Mode Techniques in Green Cellular Networks: A Survey", *IEEE Communications Surveys & Tutorials*, Vol. 17, No. 2, pp. 803–826, 2015.

20. Yigitel, M. A., O. D. Incel and C. Ersoy, "Dynamic base station planning with power adaptation for green wireless cellular networks", *EURASIP Journal on Wireless Communications and Networking*, Vol. 2014, No. 1, p. 77, dec 2014.

21. Yildiz, A., T. Girici and H. Yanikomeroglu, "A Pricing Based Algorithm for Cell Switching Off in Green Cellular Networks", *77th Vehicular Technology Conference*, pp. 1–6, IEEE, jun 2013.

22. Hong Zhang, Jun Cai and Xiaolong Li, "Energy-efficient base station control with dynamic clustering in cellular network", *8th International Conference on Communications and Networking in China (CHINACOM)*, pp. 384–388, IEEE, aug 2013.

23. Carreno, M. and L. Nuaymi, "Renewable Energy Use in Cellular Networks", *IEEE 77th Vehicular Technology Conference (VTC Spring)*, pp. 1–6, IEEE, jun 2013.

24. Fan, Q. and N. Ansari, "Green energy aware user association in heterogeneous networks", *IEEE Wireless Communications and Networking Conference*, pp. 1–6, IEEE, apr 2016.

25. Chia, Y.-K., S. Sun and R. Zhang, "Energy Cooperation in Cellular Networks

with Renewable Powered Base Stations", *IEEE Transactions on Wireless Communications*, Vol. 13, No. 12, pp. 6996–7010, dec 2014.

26. Farooq, M. J., H. Ghazzai, A. Kadri, H. ElSawy and M.-S. Alouini, "A Hybrid Energy Sharing Framework for Green Cellular Networks", *IEEE Transactions on Communications*, Vol. 65, No. 2, pp. 918–934, feb 2017.

27. Sheng, M., D. Zhai, X. Wang, Y. Li, Y. Shi and J. Li, "Intelligent Energy and Traffic Coordination for Green Cellular Networks With Hybrid Energy Supply", *IEEE Transactions on Vehicular Technology*, Vol. 66, No. 2, pp. 1631–1646, feb 2017.

28. Ahmed, F., M. Naeem, W. Ejaz, M. Iqbal, A. Anpalagan and H. Kim, "Renewable Energy Assisted Traffic Aware Cellular Base Station Energy Cooperation", *Energies*, Vol. 11, No. 1, p. 99, jan 2018.

29. Lee, G., W. Saad, M. Bennis, A. Mehbodniya and F. Adachi, "Online Ski Rental for ON/OFF Scheduling of Energy Harvesting Base Stations", *IEEE Transactions on Wireless Communications*, Vol. 16, No. 5, pp. 2976–2990, may 2017.

30. Chiang, P.-H., R. B. Guruprasad and S. Dey, "Optimal Use of Harvested Solar, Hybrid Storage and Base Station Resources for Green Cellular Networks", *IEEE Transactions on Green Communications and Networking*, Vol. 2, No. 3, pp. 707–720, sep 2018.

31. Zhang, H., S. Huang, C. Jiang, K. Long, V. C. M. Leung and H. V. Poor, "Energy Efficient User Association and Power Allocation in Millimeter-Wave-Based Ultra Dense Networks With Energy Harvesting Base Stations", *IEEE Journal on Selected Areas in Communications*, Vol. 35, No. 9, pp. 1936–1947, sep 2017.

32. Zhang, H., J. Du, J. Cheng, K. Long and V. C. M. Leung, "Incomplete CSI Based Resource Optimization in SWIPT Enabled Heterogeneous Networks: A

Non-Cooperative Game Theoretic Approach", *IEEE Transactions on Wireless Communications*, Vol. 17, No. 3, pp. 1882–1892, mar 2018.

33. Reyhanian, N., V. Shah-Mansouri, B. Maham and C. Yuen, "Renewable energy distribution in cooperative cellular networks with energy harvesting", *IEEE 26th Annual International Symposium on Personal, Indoor, and Mobile Radio Communications (PIMRC)*, 142, pp. 1617–1621, IEEE, aug 2015.

34. Han, T. and N. Ansari, "On Optimizing Green Energy Utilization for Cellular Networks with Hybrid Energy Supplies", *IEEE Transactions on Wireless Communications*, Vol. 12, No. 8, pp. 3872–3882, aug 2013.

35. Checko, A., A. P. Avramova, M. S. Berger and H. L. Christiansen, "Evaluating C-RAN fronthaul functional splits in terms of network level energy and cost savings", *Journal of Communications and Networks*, Vol. 18, No. 2, pp. 162–172, apr 2016.

36. Wang, X., A. Alabbasi and C. Cavdar, "Interplay of energy and bandwidth consumption in CRAN with optimal function split", *IEEE International Conference on Communications (ICC)*, pp. 1–6, IEEE, may 2017.

37. Alabbasi, A. and C. Cavdar, "Delay-aware green hybrid CRAN", *15th International Symposium on Modeling and Optimization in Mobile, Ad Hoc, and Wireless Networks (WiOpt)*, Cc, pp. 1–7, IEEE, may 2017.

38. Alabbasi, A., X. Wang and C. Cavdar, "Optimal Processing Allocation to Minimize Energy and Bandwidth Consumption in Hybrid CRAN", *IEEE Transactions on Green Communications and Networking*, Vol. 2, No. 2, pp. 545–555, jun 2018.

39. Mharsi, N., M. Hadji, D. Niyato, W. Diego and R. Krishnaswamy, "Scalable and cost-efficient algorithms for baseband unit (BBU) function split placement", *IEEE Wireless Communications and Networking Conference (WCNC)*, pp. 1–6, IEEE, apr 2018.

40. Liu, J., S. Zhou, J. Gong, Z. Niu and S. Xu, "Graph-based framework for flexible baseband function splitting and placement in C-RAN", *IEEE International Conference on Communications (ICC)*, pp. 1958–1963, IEEE, jun 2015.

41. Shehata, M., A. Elbanna, F. Musumeci and M. Tornatore, "Multiplexing Gain and Processing Savings of 5G Radio-Access-Network Functional Splits", *IEEE Transactions on Green Communications and Networking*, Vol. 2, No. 4, pp. 982–991, dec 2018.

42. Harutyunyan, D. and R. Riggio, "Flex5G: Flexible Functional Split in 5G Networks", *IEEE Transactions on Network and Service Management*, Vol. 15, No. 3, pp. 961–975, sep 2018.

43. Harutyunyan, D., R. Riggio, S. Kuklinski and T. Ahmed, "CU placement over a reconfigurable wireless fronthaul in 5G networks with functional splits", *International Journal of Network Management*, Vol. 30, No. 1, pp. 1–22, jan 2020.

44. Garcia-Saavedra, A., G. Iosifidis, X. Costa-Perez and D. J. Leith, "Joint Optimization of Edge Computing Architectures and Radio Access Networks", *IEEE Journal on Selected Areas in Communications*, Vol. 36, No. 11, pp. 2433–2443, nov 2018.

45. Chang, C.-Y., N. Nikaein and T. Spyropoulos, "Impact of Packetization and Scheduling on C-RAN Fronthaul Performance", *IEEE Global Communications Conference (GLOBECOM)*, pp. 1–7, IEEE, dec 2016.

46. Chang, C.-Y., N. Nikaein, R. Knopp, T. Spyropoulos and S. S. Kumar, "FlexCRAN: A flexible functional split framework over ethernet fronthaul in Cloud-RAN", *IEEE International Conference on Communications (ICC)*, pp. 1–7, IEEE, may 2017.

47. Ojaghi, B., F. Adelantado, E. Kartsakli, A. Antonopoulos and C. Verikoukis,

"Sliced-RAN: Joint Slicing and Functional Split in Future 5G Radio Access Networks", *IEEE International Conference on Communications (ICC)*, IEEE, may 2019.

48. Diez, L., V. Gonzalez and R. Aguero, "Minimizing Delay in NFV 5G Networks by Means of Flexible Split Selection and Scheduling", *IEEE 90th Vehicular Technology Conference*, pp. 1–6, IEEE, sep 2019.

49. Alameer, A. and A. Sezgin, "Joint beamforming and network topology optimization of green cloud radio access networks", *9th International Symposium on Turbo Codes and Iterative Information Processing (ISTC)*, 1, pp. 375–379, IEEE, sep 2016.

50. Guo, S., D. Zeng, L. Gu and J. Luo, "When Green Energy Meets Cloud Radio Access Network: Joint Optimization Towards Brown Energy Minimization", *Mobile Networks and Applications*, Vol. 24, No. 3, pp. 962–970, jun 2019.

51. Temesgene, D. A., N. Piovesan, M. Miozzo and P. Dini, "Optimal Placement of Baseband Functions for Energy Harvesting Virtual Small Cells", *IEEE 88th Vehicular Technology Conference (VTC-Fall)*, pp. 1–6, IEEE, aug 2018.

52. Temesgene, D. A., M. Miozzo and P. Dini, "Dynamic Functional Split Selection in Energy Harvesting Virtual Small Cells Using Temporal Difference Learning", *IEEE 29th Annual International Symposium on Personal, Indoor and Mobile Radio Communications (PIMRC)*, pp. 1813–1819, IEEE, sep 2018.

53. Wang, L. and S. Zhou, "Flexible Functional Split in C-RAN with Renewable Energy Powered Remote Radio Units", *IEEE International Conference on Communications Workshops (ICC Workshops)*, pp. 1–6, IEEE, may 2018.

54. Ko, H. and S. Pack, "Energy-Efficient Mode Switching Mechanism With Flexible Functional Splitting in Energy Harvesting Cloud Radio Access Networks", *IEEE*

Access, Vol. 6, pp. 65078–65087, 2018.

55. Meng Zheng, P. Pawelczak, S. Stanczak and Haibin Yu, "Planning of Cellular Networks Enhanced by Energy Harvesting", *IEEE Communications Letters*, Vol. 17, No. 6, pp. 1092–1095, jun 2013.

56. Han, T. and N. Ansari, "Provisioning Green Energy for Base Stations in Heterogeneous Networks", *IEEE Transactions on Vehicular Technology*, Vol. 65, No. 7, pp. 5439–5448, jul 2016.

57. Han, T. and N. Ansari, "Provisioning green energy for small cell BSs", *IEEE Global Communications Conference*, Vol. 2, pp. 4935–4940, IEEE, dec 2014.

58. Wang, X., L. Wang, S. E. Elayoubi, A. Conte, B. Mukherjee and C. Cavdar, "Centralize or distribute? A techno-economic study to design a low-cost cloud radio access network", *IEEE International Conference on Communications (ICC)*, Vol. 9, pp. 1–7, IEEE, may 2017.

59. Pamuklu, T. and C. Ersoy, "Optimization of Renewable Green Base Station Deployment", *IEEE International Conference on Green Computing and Communications*, pp. 59–63, IEEE, aug 2013.

60. Rui Huang, Honggang Li, Deyi Gu, Yang-Seok Choi, S. M., *Proposal for the channel model in EMD of 802.16p*, Tech. rep., IEEE 802.16 M2M Task Group, 2011.

61. Tao Han and N. Ansari, "ICE: Intelligent Cell BrEathing to Optimize the Utilization of Green Energy", *IEEE Communications Letters*, Vol. 16, No. 6, pp. 866–869, jun 2012.

62. Hoydis, J., M. Kobayashi and M. Debbah, "Green Small-Cell Networks", *IEEE Vehicular Technology Magazine*, Vol. 6, No. 1, pp. 37–43, mar 2011.

63. Johansson, K., A. Furuskar, P. Karlsson and J. Zander, "Relation between base station characteristics and cost structure in cellular systems", *IEEE 15th International Symposium on Personal, Indoor and Mobile Radio Communications*, pp. 2627–2631, IEEE, 2004.

64. Gonzalez-Brevis, P., J. Gondzio, Y. Fan, H. V. Poor, J. Thompson, I. Krikidis and P.-J. Chung, "Base Station Location Optimization for Minimal Energy Consumption in Wireless Networks", *IEEE 73rd Vehicular Technology Conference (VTC Spring)*, pp. 1–5, IEEE, may 2011.

65. Kershenbaum, A., *Telecommunications Networks Design Algorithms*, McGraw Hill, 1993.

66. Niu, Z., Y. Wu, J. Gong and Z. Yang, "Cell zooming for cost-efficient green cellular networks", *IEEE Communications Magazine*, Vol. 48, No. 11, pp. 74–79, nov 2010.

67. Chen, Y., S. Zhang, S. Xu and G. Li, "Fundamental trade-offs on green wireless networks", *IEEE Communications Magazine*, Vol. 49, No. 6, pp. 30–37, jun 2011.

68. Al Haj Hassan, H., L. Nuaymi and A. Pelov, "Classification of renewable energy scenarios and objectives for cellular networks", *IEEE 24th Annual International Symposium on Personal, Indoor, and Mobile Radio Communications*, pp. 2967–2972, IEEE, sep 2013.

69. Pamuklu, T. and C. Ersoy, "Reducing the total cost of ownership in radio access networks by using renewable energy resources", *Wireless Networks*, Vol. 26, No. 3, pp. 1667–1684, apr 2020.

70. Peng, C., S.-B. Lee, S. Lu, H. Luo and H. Li, "Traffic-driven power saving in operational 3G cellular networks", *Proceedings of the 17th annual international conference on Mobile computing and networking - MobiCom '11*, p. 121, ACM

Press, New York, USA, 2011.

71. Poikselka, M., H. Holma, J. Hongisto, J. Kallio and A. Toskala, *Voice over LTE (VoLTE)*, John Wiley \& Sons, 2012.

72. Marsan, M. A. and M. Meo, "Energy efficient management of two cellular access networks", *ACM SIGMETRICS Performance Evaluation Review*, Vol. 37, No. 4, pp. 69–73, mar 2010.

73. Hossain, M. F., K. S. Munasinghe and A. Jamalipour, "A protocooperation-based sleep-wake architecture for next generation green cellular access networks", *2010 4th International Conference on Signal Processing and Communication Systems*, Dp 1096276, pp. 1–8, IEEE, dec 2010.

74. Oh, E., K. Son and B. Krishnamachari, "Dynamic Base Station Switching-On/Off Strategies for Green Cellular Networks", *IEEE Transactions on Wireless Communications*, Vol. 12, No. 5, pp. 2126–2136, may 2013.

75. ITU-R, *Guidelines for evaluation of radio interface technologies for IMTadvanced*, Tech. rep., 2009, `https://www.itu.int/pub/R-REP-M.2135`.

76. Shannon, C., "The zero error capacity of a noisy channel", *IEEE Transactions on Information Theory*, Vol. 2, No. 3, pp. 8–19, sep 1956.

77. Auer, G., V. Giannini, C. Desset, I. Godor, P. Skillermark, M. Olsson, M. Imran, D. Sabella, M. Gonzalez, O. Blume and A. Fehske, "How much energy is needed to run a wireless network?", *IEEE Wireless Communications*, Vol. 18, No. 5, pp. 40–49, oct 2011.

78. Yang, J., X. Zhang and W. Wang, "Two-stage base station sleeping scheme for green cellular networks", *Journal of Communications and Networks*, Vol. 18, No. 4, pp. 600–609, aug 2016.

79. Hassan, H. A. H., L. Nuaymi and A. Pelov, "Renewable energy in cellular networks: A survey", *IEEE Online Conference on Green Communications*, pp. 1–7, IEEE, oct 2013.

80. Valerdi, D., Q. Zhu, K. Exadaktylos, S. Xia, M. Arranz, R. Liu and D. Xu, "Intelligent energy managed service for green base stations", *IEEE Globecom Workshops*, pp. 1453–1457, IEEE, dec 2010.

81. Parkinson, G., *Citigroup: solar + battery storage "socket" parity in years*, 2014, `http://reneweconomy.com.au/`, accessed in may 2020.

82. National Renewable Energy Laboratory, *PVWatts*, 2020, `http://pvwatts.nrel.gov/`, accessed in may 2020.

83. Piro, G., M. Miozzo, G. Forte, N. Baldo, L. A. Grieco, G. Boggia and P. Dini, "HetNets Powered by Renewable Energy Sources: Sustainable Next-Generation Cellular Networks", *IEEE Internet Computing*, Vol. 17, No. 1, pp. 32–39, jan 2013.

84. Eller, A. and A. Dehamna, *Energy Storage Tracker 1Q16*, Tech. rep., Navigant Research, 2016, `https://www.navigantresearch.com/`.

85. Badawy, G. H., A. A. Sayegh and T. D. Todd, "Energy Provisioning in Solar-Powered Wireless Mesh Networks", *IEEE Transactions on Vehicular Technology*, Vol. 59, No. 8, pp. 3859–3871, oct 2010.

86. Lacey, S., *Stem CTO: Lithium-Ion Battery Prices Fell 70% in the Last 18 Months*, 2016, `http://www.greentechmedia.com/articles/read/stem-cto-weve-seen-battery-prices-fall-70-in-the-last-18-months`, accessed in may 2020.

87. Irmer, R., H. Droste, P. Marsch, M. Grieger, G. Fettweis, S. Brueck, H.-P. Mayer, L. Thiele and V. Jungnickel, "Coordinated multipoint: Concepts, performance,

and field trial results", *IEEE Communications Magazine*, Vol. 49, No. 2, pp. 102–111, feb 2011.

88. Karp, R. M., "Reducibility among Combinatorial Problems", *Complexity of Computer Computations*, pp. 85–103, Springer US, Boston, MA, 1972, `http://link.springer.com/10.1007/978-1-4684-2001-2{\_}9`.

89. Gurobi Optimization LLC, *Gurobi Optimizer Reference Manual*, 2020, `https://www.gurobi.com/documentation/9.0/refman/`, accessed in may 2020.

90. Peng, C., S.-B. Lee, S. Lu and H. Luo, "GreenBSN: Enabling Energy-Proportional Cellular Base Station Networks", *IEEE Transactions on Mobile Computing*, Vol. 13, No. 11, pp. 2537–2551, nov 2014.

91. Munsell, M., *Solar PV Prices Will Fall Below $1.00 per Watt by 2020*, 2016, `http://www.greentechmedia.com/articles/read/solar-pv-prices-to-fall-below-1.00-per-watt-by-2020`, accessed in may 2020.

92. Energysage, *Is residential electricity price going up or down?*, 2015, `http://news.energysage.com/residential-electricity-prices-going-up-or-down/`, accessed in may 2020.

93. Nvidia, *DGX-1*, 2020, `https://www.nvidia.com/en-us/data-center/dgx-1/`, accessed in may 2020.

94. Pamuklu, T., C. Cavdar and C. Ersoy, "Renewable Energy Assisted Function Splitting in Cloud Radio Access Networks", *Mobile Networks and Applications*, 2020.

95. Maeder, A., M. Lalam, A. De Domenico, E. Pateromichelakis, D. Wubben, J. Bartelt, R. Fritzsche and P. Rost, "Towards a flexible functional split for cloud-RAN networks", *European Conference on Networks and Communications (EuCNC)*, pp. 1–5, IEEE, jun 2014.

96. 3GPP TR 38.801, *Study on new radio access technology: Radio access architecture and interfaces*, Tech. Rep. Release 14, 3GPP, 2017, https://portal.3gpp.org/desktopmodules/Specifications/SpecificationDetails.aspx?specificationId=3056.

97. EPDK, *Energy Prices*, 2018, http://www.epdk.org.tr/, accessed in may 2020.

98. Energysage, *How much do solar panels cost in the U.S. in 2019?*, 2019, https://news.energysage.com/how-much-does-the-average-solar-panel-installation-cost-in-the-u-s/, accessed in may 2020.

99. Logan Goldie-Scot, *A Behind the Scenes Take on Lithium-ion Battery Prices*, 2019, https://about.bnef.com/blog/behind-scenes-take-lithium-ion-battery-prices/, accessed in may 2020.

100. Fixr, *How much does it cost to maintain your solar panels?*, 2019, https://www.fixr.com/costs/solar-panel-maintenance, accessed in may 2020.

101. Zhang, S., S. Xu, G. Y. Li and E. Ayanoglu, "First 20 Years of Green Radios", *IEEE Transactions on Green Communications and Networking*, Vol. 4, No. 1, pp. 1–15, mar 2020.

102. Group, I. . W., *Next Generation Fronthaul Interface*, 2020, https://sagroups.ieee.org/1914/, accessed in may 2020.

103. Pamuklu, T. and C. Ersoy, "GROVE: A Cost-Efficient Green Radio over Ethernet Architecture for Next Generation Radio Access Network", pp. 1–11, 2020.

104. Alabbasi, A., M. Berg and C. Cavdar, "Delay Constrained Hybrid CRAN: A Functional Split Optimization Framework", *IEEE Globecom Workshops*, pp. 1–7, IEEE, dec 2018.

105. Liu, Q., T. Han, N. Ansari and G. Wu, "On Designing Energy-Efficient Hetero-

geneous Cloud Radio Access Networks", *IEEE Transactions on Green Communications and Networking*, Vol. 2, No. 3, pp. 721–734, sep 2018.

106. Deruyck, M., D. Renga, M. Meo, L. Martens and W. Joseph, "Accounting for the Varying Supply of Solar Energy When Designing Wireless Access Networks", *IEEE Transactions on Green Communications and Networking*, Vol. 2, No. 1, pp. 275–290, mar 2018.